

Supernova remnants and γ -ray sources*

Diego F. Torres^{1,2†}, Gustavo E. Romero³, Thomas M. Dame⁴, Jorge A. Combi³, and Yousaf M. Butt⁴

June 22, 2019

¹Lawrence Livermore Laboratory, 7000 East Ave. L-413, Livermore, CA 94550, USA

²Physics Department, Princeton University, NJ 08544, USA

³Instituto Argentino de Radioastronomía, C.C.5, 1894 Villa Elisa, Buenos Aires, Argentina

⁴Harvard-Smithsonian Center for Astrophysics, 60 Garden Street, Cambridge, MA 02138, USA

Abstract

A review of the possible relationship between γ -ray sources and supernova remnants (SNRs) is presented. Particular emphasis is given to the analysis of the observational status of the problem of cosmic ray acceleration at SNR shock fronts. All positional coincidences between SNRs and unidentified γ -ray sources listed in the Third EGRET Catalog at low Galactic latitudes are discussed on a case by case basis. For several coincidences of particular interest, new CO(J=1-0) and radio continuum maps are shown, and the mass content of the SNR surroundings is determined. The contribution to the γ -ray flux observed that might come from cosmic ray particles (particularly nuclei) locally accelerated at the SNR shock fronts is evaluated. We discuss the prospects for future research in this field and remark on the possibilities for observations with forthcoming γ -ray instruments.

Keywords: gamma-rays: observations, gamma-rays: theory, ISM: supernova remnants, ISM: clouds, cosmic rays.

*To be submitted to the Physics Reports

†e-mail: dtorres@igpp.ucllnl.org

Contents

1	Introduction	3
2	Simple model for the hadronic γ-ray emission in SNRs and their environs	7
3	Relativistic Bremsstrahlung	10
4	Diffusion of CRs and γ-ray spectral evolution	12
5	Sample and correlation analysis	15
6	SNRs coincident with γ-ray sources	18
7	Pulsars within the EGRET error boxes	19
8	Variability	22
9	Observations and data analysis	25
9.1	CO data	25
9.2	Radio continuum data and diffuse background filtering	26
10	Case by case analysis	26
10.1	γ -ray source 3EG J0542+2610 – SNR G180.0-1.7	26
10.2	γ -ray source 3EG J0617+2238 – SNR G189.1+3.0 (IC443)	27
10.3	γ -ray source 3EG J0631+0642 and 3EG J0634+0521 – SNR G205.5+0.5 (Monoceros nebula)	30
10.4	γ -ray source 3EG J1013-5915 – SNR G284.3-1.8 (MSH 10-53)	32
10.5	γ -ray source 3EG J1102-6103 – SNR G290.1-0.8 (MSH 11-61A)/289.7-0.3	34
10.6	γ -ray source 3EG J1410-6147 – SNR G312.4-0.4	37
10.7	γ -ray source 3EG J1639-4702 – SNR G337.8-0.1/338.1+0.4/338.3+0.0	38
10.8	γ -ray source 3EG J1714-3857 – SNR G348.5+0.0/348.5+0.1/347.3-0.5	40
10.9	γ -ray source 3EG J1734-3232 – SNR G355.6+0.0	43
10.10	Near the Galactic Center: γ -ray source 3EG J1744-3011 – SNR G359.0-0.9/359.1-0.5 and γ -ray source 3EG J1746-2851 – SNR G0.0+0.0/0.3+0.0	45
10.11	γ -ray source 3EG J1800-2338 – SNR G6.4-0.1 (W28)	46
10.12	γ -ray source 3EG J1824-1514 – SNR G16.8-1.1	49
10.13	γ -ray source 3EG J1837-0423 – SNR G27.8+0.6	50
10.14	γ -ray source 3EG J1856+0114 – SNR G34.7-0.4 (W44)	50
10.15	γ -ray source 3EG J1903+0550 – SNR G39.2-0.3	53
10.16	γ -ray source 3EG J2016+3657 – SNR G74.9+1.2 (CTB 87)	54
10.17	γ -ray source 3EG J2020+4017 – SNR G78.2+2.1 (γ -Cyg Nebula, W66)	56
10.18	An example beyond $ b > 10$: γ -ray source 3EG J0010+7309 – SNR G119.5+10.2 (CTA 1)	58
11	SNRs discovered by their likely associated high-energy radiation	58
12	SNRs and their neighborhoods as TeV sources	60
12.1	Future TeV telescopes and their look at SNRs - Adapted from Petry (2001)	62
13	Concluding remarks	65
14	Appendix: Reviewing the prospects for the forthcoming GeV satellites	67
14.1	INTEGRAL	67
14.2	AGILE	68
14.3	GLAST	69

1 Introduction

Gamma-ray astronomy has unveiled some of the most exotic and energetic objects in the universe: from supermassive black-holes in distant radio galaxies to exotic radio-quiet pulsars and the still enigmatic gamma-ray bursts. However, it has been conspicuously less successful in achieving one of its original goals of shedding light on the sources of Galactic cosmic ray nuclei. In this report we focus on the remnants of galactic supernovae, and their possible association with discrete sources of (> 70 MeV) γ -rays, as seen by the Energetic Gamma-ray Experiment Telescope (EGRET). In doing so, we attempt to lay a framework in which the long-standing question of the supernova remnant origin of Galactic cosmic rays may be addressed.

The first firm detection of celestial high-energy γ -rays was achieved by Clark, Garmire and Kraushaar using the Orbiting Solar Observatory (OSO-3), when they discovered that the plane of the Galaxy was a source of photons with $E > 70$ MeV (Clark, Garmire & Kraushaar 1968; Kraushaar et al. 1972). Higher spatial resolution studies made with the SAS-2 satellite, launched in 1972, revealed individual sources of γ -rays from the Vela pulsar (Thompson et al. 1975), and confirmed the high-energy emission from the Crab (Kniffen et al. 1974). The long life of ESA's COS-B satellite (1975-1982) produced another major breakthrough in γ -ray astronomy: for the first time a significant number of new γ -ray sources were seen which could not be identified with objects known at other wavelengths (see Bignami & Hermsen 1983, for a review of COS-B results). Figure 1 shows the region surveyed by COS-B and the point sources discovered, as reported in the second COS-B Catalog (Hermsen 1981, Swanenburg et al. 1981).

In 1991, the EGRET telescope was launched onboard the Compton Gamma-Ray Observatory (see Gehrels & Shrader 2001, for a recent review). The Compton satellite (1991-2000), the heaviest orbital scientific payload at the time of its launch, had three other experiments apart from EGRET. All of them have contributed to our understanding of the γ -ray sky, although we shall particularly focus on EGRET results in this report. The Third EGRET (3EG) Catalog, whose point-like detections are shown in Figure 2, is now the latest and most complete source of information on high-energy γ -ray sources. It contains 271 detections with high significance, including 5 pulsars, 1 solar flare, 66 blazar identifications, 1 radio galaxy (Cen A), 1 normal galaxy (LMC), and almost two hundred unidentified sources, ~ 80 of them located at low galactic latitudes (see Grenier 2001 and Romero 2001 for recent reviews).

The detection of pulsed high-energy emission from some γ -ray sources, on one hand, and the identification of Geminga as a radio quiet pulsar, on the other, have prompted several authors to explore the possibility that all unidentified low-latitude sources contained in earlier versions of the EGRET Catalog (i.e. the Second EGRET -2EG- Catalog, Thompson et al. 1995, 1996) could be pulsars as well (excepting a small extragalactic and isotropic component which should be seen through the disc of the Galaxy). In particular, Kaaret & Cottam (1996) used OB associations as pulsar tracers, finding a significant positional correlation with 2EG unidentified sources. A similar study, including SNRs and HII regions (considered as tracers of star forming regions and, hence, of possible pulsar concentrations) has been carried out by Yadigaroglu & Romani (1997), who also concluded that the pulsar hypothesis for the unidentified 2EG sources was consistent with the available information.

However, spectral analysis by Merck et al. (1996) and Zhang & Cheng (1998) showed that several 2EG sources were at odds with the pulsar explanation; the spectra of many sources are too different from what is expected from outer or polar gap models of pulsar emission. Time variability in the γ -ray flux of many sources (discussed below) also argued against a unique population behind the unidentified galactic γ -ray sources.

Figure 1: Plot of source locations (galactic coordinates) in the COS-B catalog. The undashed region of the sky was surveyed by the satellite. Most of the sources had fluxes higher than 1.3×10^{-6} photons $\text{cm}^{-2} \text{s}^{-1}$ above 100 MeV. From Bignami & Hermsen (1983). Astro-ph arXiv file: cosb-jpg.

Most likely, the unidentified γ -ray sources at low galactic latitudes are related to several different galactic populations (e.g. Grenier 1995, 2000; Gehrels et al. 2000; Romero 2001). Among them there are surely several new γ -ray pulsars (e.g. Kaspi et al. 2000, Zhang, Zhang & Cheng 2000, Torres, Butt & Camilo 2001, Camilo et al. 2001, D'Amico et al. 2001, Mirabal et al. 2000, Mirabal & Halpern 2001, Halpern et al. 2002). Pulsars remain as the only confirmed low-latitude population, since pulsed γ -ray radiation has been already detected for at least six different sources (Thompson et al. 1999, Thompson 2001). Other populations might include X-ray transients (Romero et al. 2001), persistent microquasars (Paredes et al. 2000, Grenier 2001, Kaufman-Bernadó et al. 2002), massive stars with strong stellar winds (Benaglia et al. 2001), isolated and magnetized stellar-size black holes (Punsly 1998a,b; Punsly et al. 2000), and middle-mass black holes (Dermer 1997). Finally, there is a possibility that some γ -ray sources could be generated by supernova remnants (SNRs), especially those interacting with, or located close to, molecular clouds (e.g. Montmerle 1979; Dorfi 1991, 2000; Aharonian, Drury & Völk 1994; Naito & Takahara 1994, Combi & Romero 1995; Aharonian & Atoyan 1996; Sturner, Dermer & Mattox 1996; Esposito et al. 1996; Combi et al. 1998, 2001; Butt et al. 2001). This review is devoted to discuss this latter possibility in light of recent observations.

SNRs are thought to be the main source of both cosmic ray (CR) ions and electrons with energies below the knee in the galactic CR spectrum, at $\sim 10^{15}$ eV – however, see Plaga (2002) for alternate theories. The particle acceleration mechanism in individual SNRs is usually assumed to be diffusive shock acceleration, which naturally leads to a power-law population of relativistic particles. In the standard version of this mechanism (e.g. Bell 1978), particles are scattered by magnetohydrodynamic waves repeatedly through the shock front. Electrons suffer synchrotron losses, producing the non-thermal emission from radio to X-rays usually seen in shell-type SNRs. The maximum energy achieved depends on the shock speed and age as well as on any competing loss processes. In young SNRs, electrons can easily reach energies in excess of 1 TeV, where they produce X-rays by synchrotron mechanism (see, for example, Reynolds 1996, 1998). Non-thermal X-ray emission associated with shock acceleration has been clearly observed in at least 11 SNRs, and this number seems to be steadily increasing with time. In the case of the very nearby remnant

Figure 2: Plot of source locations (galactic coordinates) in the Third EGRET Catalog. Different populations are marked in different grades of light colours. The size of the dots gives a qualitative idea of the detected flux. From Hartman et al. (1999). Astro-ph arXiv file: 3EG.jpg.

RX J0852.0-4622 (also known as Vela Jr.) the discovery was originally made at X-rays (Aschenbach 1998) and only then the source was detected at radio wavelengths (Combi, Romero & Benaglia 1999).

As early as 1979, Montmerle suggested that SNRs within OB stellar associations, i.e. star forming regions with plenty of molecular gas, could generate observable γ -ray sources. Montmerle himself provided statistical evidence for a correlation between COS-B sources and OB associations. Pollock (1985) presented further analysis of some COS-B sources in the same vein. Statistical correlation studies of EGRET sources and SNRs have been presented by Sturner & Dermer (1995), Sturner et al. (1996), Yadigaroglu & Romani (1997), and Romero et al. (1999a). These studies show that there is a high-confidence correlation between remnants and γ -ray sources. Figure 3 shows the distribution of the SNRs in Green's Catalog (2000) along with the 3EG unidentified sources. Some of the coincident pairs that are studied in this report are marked.

SNRs can produce high-energy γ -rays through nucleus-nucleus interactions leading to π^0 -production and subsequent γ -decays. The resulting γ -ray luminosity will depend on the local enhancement of the CR energy density as well as on the density of the ambient media. GeV γ -rays (and also TeV photons, see e.g. Pohl 1996) can be produced too by electrons through relativistic Bremsstrahlung and inverse Compton upscattering of cosmic microwave background photons, diffuse Galactic infrared/optical radiation, and/or the radiation field of the remnant itself (e.g. Mastichiadis 1996, de Jager & Mastichiadis 1997). Gaisser et al. (1998) modeled these processes in detail in order to fit the observational data for the SNRs IC 443 and γ -Cyni. Sturner et al. (1997) and Baring et al. (1999) also modeled IC 433 with synchrotron emission in the radio band and relativistic Bremsstrahlung in γ -rays. De Jager & Mastichiadis (1997) included inverse Compton scattering in their model of SNR W44. Bykov et al. (2000) have recently analyzed the non-thermal emission from a SNR interacting with a molecular cloud, modeling it as a highly inhomogeneous structure consisting of a forward shock of moderate Mach number, a cooling layer, a dense radiative shell, and an interior region filled with hot tenuous plasma. Particularly for SNRs with mixed morphology (remnants which are shell-like in radio and dominated by central emission in X-rays, Rho & Petre 1998),

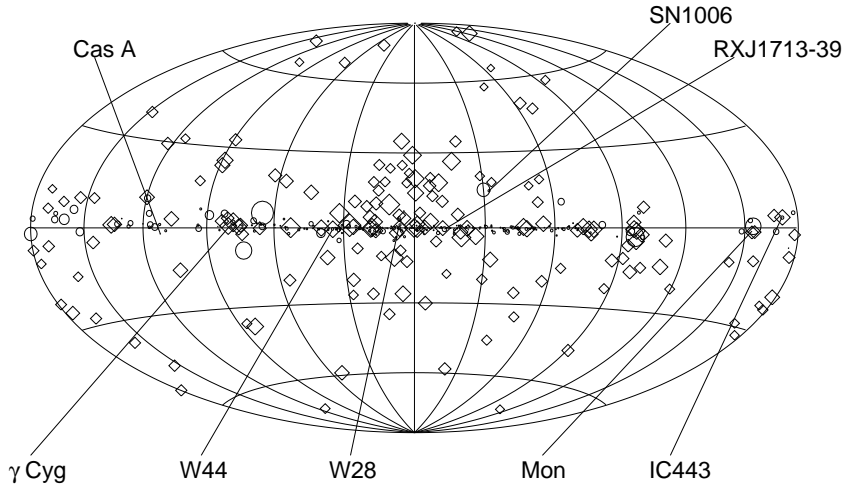


Figure 3: Distribution of the Green's SNRs (circles) together with EGRET unidentified sources (diamonds), shown in galactic coordinates. Some of the coincident pairs that are studied in this report are marked. The top marks are SNRs for which TeV radiation has been detected. From Mori (2001).

they found that Bremsstrahlung, synchrotron, and inverse Compton radiation of the relativistic electron population produce multiwavelength photon spectra in quantitative agreement with radio and high-energy observations. These are only some of the works devoted to high-energy emission from SNRs published in recent years. Differentiating the γ -ray emission produced by ions from that originating in leptons is crucial for determining the origin of cosmic-ray nuclei (for some recent reviews and more references the reader is referred to Völk 2001, 2002; Drury et al. 2001; Kirk & Dendy 2001; and Plaga 2001).

After introducing a simple theoretical model for evaluating the possible hadronic γ -ray emission from SNRs and nearby clouds, we characterize the sample to be investigated, discuss the γ -ray flux variability of the sources, and study the possibility that pulsars might be possible counterparts. For each SNR-EGRET source pair we review and analyze the different scenarios proposed as an explanation of the γ -ray emission. We present CO($J=1-0$) mm wavelength observations to evaluate whether there are molecular clouds in the vicinity of the SNRs and estimate the γ -ray flux that would be produced in each case via π^0 -decays. Some new radio continuum maps are also presented. These latter maps have been processed to eliminate, as far as possible, the galactic contaminating diffuse emission.

Our aim with this review is to provide a quantitative basis to analyze the possible γ -ray production in SNRs, providing the reader with useful information to guide future studies. Specifically, the role of INTEGRAL, AGILE, and GLAST satellites, and the Čerenkov telescopes HESS, VERITAS, MAGIC, and CANGAROO III is discussed. Several target candidates for observations with all these telescopes and satellites are mentioned. As an example, in the GeV band, the Gamma-ray Large Area Telescope (GLAST), which will be launched in a few years, is expected to detect $\sim 10^4$ high-energy γ -ray sources, thousands of them belonging to our Galaxy (see Figure 4). A technical Appendix quotes the main features of GLAST, as well as its predecessors, AGILE and INTEGRAL, for quick reference. It is also important to clarify what this review is not about. Many authors have studied the evolution of SNRs or their emission properties from very sophisticated numerical modeling points of view, during the last years. We shall not particularly focus on those, except briefly when dealing with the case by case analysis for specific SNR-EGRET source pairs.

Figure 4: Expected distribution of source locations (Galactic coordinates) for one year survey of the LAT experiment onboard GLAST. Courtesy of the GLAST Science Team and NASA. Astro-ph arXiv file: lat.jpg.

The rest of this work is organized as follows. In the next Section we introduce a simple model to account for the hadronic γ -ray emission in SNRs and their neighborhoods. Section 3 refers to Relativistic Bremsstrahlung as a competing process. Section 4 analyzes the spectral changes that diffusion could produce on the observed γ -ray spectrum. The general characteristics of the SNR sample that we shall analyze and the possible pulsar counterparts are presented in Sections 5, 6, and 7. The variability in the γ -ray emission for the Third EGRET sources under study is assessed in Section 8. Section 9 gives a brief account of the observations and data extraction techniques used in this review. A case by case analysis of all coincident pairs between SNRs and γ -ray sources is given in Section 10. Some particular cases in which SNRs were discovered by their high energy emission are discussed in Section 11. The TeV-emission properties and the prospects for new observations using new TeV-telescopes are discussed in Section 12. Finally, Section 13 presents a very brief overview and some concluding remarks.

2 Simple model for the hadronic γ -ray emission in SNRs and their environs

We first present a simple model for the hadronic γ -ray emission from “bare” SNRs, and those interacting with molecular clouds. Further details can be obtained from Dorfi (1991, 2000), Drury et al. (1994), Aharonian et al. (1994), and Aharonian & Atoyan (1996). We shall partially follow Morfill et al. (1984) and Combi & Romero (1995) in our presentation. Our intention is not to arrive at the most precise theoretical model for an individual SNR, but rather to have a simple, straightforward and robust, albeit crude, method of obtaining and inter-comparing γ -ray fluxes due to nucleus-nucleus interactions in interacting SNRs.

Let us consider the expansion of a SNR in a homogeneous medium. If this expansion is adiabatic, we can use the Sedov’s solutions (1959), which give the time since the explosion and the velocity of the shock front, respectively, as

$$t \sim 1.5 \times 10^3 n_{-1}^{1/2} E_{51}^{-1/2} R_1^{5/2} \text{yr}, \quad (1)$$

$$v_s \sim 21.6 \times 10^2 n_{-1}^{-1/2} E_{51}^{1/2} R_1^{-3/2} \text{ km s}^{-1}. \quad (2)$$

Here, E_{51} is the energy of the SN explosion in units of 10^{51} erg, R_1 is the SNR radius in units of 10 pc, and n_{-1} is the medium density in units of 0.1 cm^{-3} . The CR energy per time unit incoming to the SNR is

$$\dot{E}(t) = k_s \epsilon_{\text{CR}} 4\pi R_s(t)^2 v_s(t), \quad (3)$$

where the dot means derivative with respect to time, R_s is the SNR time-dependent radius, ϵ_{CR} is the background CR ambient density ($\sim 1 \text{ eV cm}^{-3}$ in the solar neighborhood), and k_s is the enhancement factor due to re-acceleration by Fermi mechanism at the shock front (see Jones 2001 for a recent review and references on acceleration details). If we assume equipartition, i.e. that the energy flux from the unshocked medium is converted in equal parts into electromagnetic energy, thermal energy, and CR enhancement (Morfill et al. 1984), we can write the previous expression as

$$\dot{E} \sim \frac{4\pi}{3} \frac{1-\xi}{1-2\mu n v_s^3} R_s^2, \quad (4)$$

where ξ is the downstream to upstream ratio of kinetic energy flux in the shock frame ($\xi \sim 0.06$ for strong shocks), μ is the mean molecular weight, and n is the unshocked particle density. This expression states that the power available for accelerating CRs is 1/3 of the mechanical energy flux across the shock.

When the SNR expands from a radius comprising a volume $V(t_1)$ to a volume $V(t_2)$, the energy decreases accordingly as

$$\frac{E(t_2)}{E(t_1)} = \left(\frac{V(t_1)}{V(t_2)} \right)^{\gamma-1}, \quad (5)$$

with the adiabatic index being $\gamma = 4/3$. Using the previous equations, the CR energy in the SNR between times t_1 and t_2 is

$$E_{\text{CR}}(t_1, t_2) = \frac{2\pi\mu n(1-\xi)}{3R_s(t_2)^{3(\gamma-1)}} \int_{t_1}^{t_2} dt v_s^3 R_s(t)^{3(\gamma-1)}. \quad (6)$$

Through the Sedov solutions, this leads to a ratio

$$\theta = \frac{E_{\text{CR}}}{E_{\text{SN}}} \sim \frac{\pi}{5} \left(1 - \left(\frac{t_1}{t_2} \right)^{2/5} \right). \quad (7)$$

We shall adopt t_2 as the actual age of the SNR, estimated from observational data and the Sedov solutions, and we shall assume the initial time t_1 as that obtained when the SNR has swept about $5M_\odot$ of interstellar material, starting then the Sedov phase (Lozinskaya 1992, pp. 205ff). The radius at which this happens is $R_s = (3 \cdot 5M_\odot / 4\pi\mu m_H n_0)^{1/3}$, and typical values for t_1 are in the range 200-2000 years.

In simplified models of SNRs, the remnant is divided into three regions: an interior region filled with hot gas and accelerated particles but very little mass, an immediate post shock region where most of the matter is concentrated, and a shock precursor region where the accelerated particles diffusing ahead of the shock affect the ambient medium. Following Drury et al. (1994) the production rate of γ -rays per unit volume can be written as

$$Q_\gamma = \mathcal{E}_\gamma n = q_\gamma n E_{\text{CR}}, \quad (8)$$

where n is the number density of the gas, E_{CR} is the CR energy density, and q_γ is the γ -ray emissivity normalized to the CR energy density, $q_\gamma = \mathcal{E}_\gamma / E_{\text{CR}}$. The total gamma-ray luminosity is given by $\int q_\gamma n E_{\text{CR}} d^3r$, which can be written as $q_\gamma (M_1 E_{\text{CR}1} + M_2 E_{\text{CR}2})$, where M_1 is the total mass in the precursor region, M_2 that in the immediate post-shock region, and $E_{\text{CR}1,2}$ are the corresponding CR energy densities. Since

particle diffusion occurs across the shock front, we have $E_{\text{CR}1} = E_{\text{CR}2}$. This value is also probably not very different from $E_{\text{CR},3}$, the energy density in the interior of the remnant, because of two reasons. First, there is diffusive coupling between the acceleration region around the shock and the interior of the remnant (Drury et al. 1994). Second, if the acceleration is efficient, CRs provide a substantial, if not the dominant, part of the interior pressure and the interior of the remnant has, for dynamical reasons, to be in pressure equilibrium. It follows that, to order of magnitude, the CR energy density throughout the remnant and in the shock precursor can be taken as $E_{\text{CR}1} = E_{\text{CR}2} \approx E_{\text{CR}3} \approx 3\theta E_{\text{SN}}/4\pi R^3$, where θ is, again, the fraction of the total supernova explosion energy, E_{SN} , converted to CR energy and R is the remnant radius. Thus, the γ -ray luminosity results

$$L_\gamma = q_\gamma (M_1 + M_2) \frac{3\theta E_{\text{SN}}}{4\pi R^3} \approx \theta q_\gamma E_{\text{SN}} n \approx 10^{38} \theta \left(\frac{E_{\text{SN}}}{10^{51} \text{erg}} \right) \left(\frac{n}{1 \text{cm}^{-3}} \right) \text{ph s}^{-1}, \quad (9)$$

where n is the ambient density. The exact value of θ depends on the details of the model, for which Eq. (7) gives an example. For different plausible injection models, θ is roughly constant throughout the Sedov phase with only a moderate dependence on external parameters such as the ambient density (Markiewicz et al. 1990). If the SNR is located at a distance d , the hadronic γ -ray flux is

$$F(> 100 \text{MeV})_{\text{SNR}} \sim 4.4 \times 10^{-7} \theta \left(\frac{E_{\text{SN}}}{10^{51} \text{erg}} \right) \left(\frac{d}{\text{kpc}} \right)^{-2} \left(\frac{n}{\text{cm}^{-3}} \right) \text{ph cm}^{-2} \text{s}^{-1}, \quad (10)$$

where d is the distance to the remnant. Only for very high densities can the usually observed γ -ray sources can be due to the remnant itself. In general, the flux provided by the previous equation is far too low to produce a detectable EGRET source (Drury et al. 1994), at typical galactic distances.

However, stronger emission can be produced if there are molecular clouds in the vicinity of the SNR where the locally accelerated protons interact with target ions, producing pions and hence enhancing the γ -ray flux (eg. Montmerle 1979; Dorfi 1991, 2000; Aharonian et al. 1994). The expected total flux is

$$F_\gamma = \frac{1}{4\pi d^2} \int_{V_0} n(\bar{r}) q_\gamma(\bar{r}) d^3 r. \quad (11)$$

Neglecting all possible gradients within the cloud, this equation reduces to

$$F_\gamma = \frac{M_{\text{cl}}}{m_p} \frac{q_\gamma}{4\pi d^2}, \quad (12)$$

where M_{cl} is the mass of the cloud. In particular, we may write

$$F(> 100 \text{MeV})^{\text{cloud}} \sim 10^{-9} M_3 \left(\frac{d}{\text{kpc}} \right)^{-2} q_\gamma(> 100 \text{MeV}) \text{ ph cm}^{-2} \text{s}^{-1}, \quad (13)$$

where M_3 is the mass of the target cloud in units of $10^3 M_\odot$, and q_γ is the γ -emissivity in units of $10^{-25} \text{s}^{-1} (\text{H-atom})^{-1}$. The factor q_γ will be enhanced in comparison with its normal value because of the local CR source. In a passive giant molecular cloud exposed to the same proton flux measured at the Earth, the γ -ray emissivity above 100 MeV is equal to $1.53 \eta q_{-25} (\geq 100 \text{MeV})(\text{H-atom})^{-1} \text{s}^{-1}$, where the parameter $\eta \simeq 1.5$ takes into account the contribution of nuclei both in CRs and in the interstellar medium (Dermer et al. 1986; Aharonian 2001). In clouds near CR accelerators, it may be much higher than this value. If the shape of the CR spectrum in the cloud does not differ much from that existing near the Earth, we can approximate

$$\frac{q_\gamma}{q_{\gamma,0}} \sim \frac{\epsilon_{\text{CR}}}{\epsilon_{\text{CR},0}} \sim k_s. \quad (14)$$

Following Morfill & Tenorio Tagle (1983), we can use Eq. (6) to obtain

$$k_s = \frac{3}{20} \frac{E_{\text{SN}}}{R_s(t_2)^3} \left(1 - \frac{R_s(t_1)}{R_s(t_2)}\right) \frac{1}{\epsilon_{\text{CR}}}. \quad (15)$$

The Sedov solutions for each of the SNRs considered below should be used in this latter expression to obtain k_s , and thus $F(E > 100\text{MeV})^{\text{cloud}}$. One immediate test of energetic consistency is to check that $E_{\text{CR}} = k_s \epsilon_{\text{CR}} / (4/3)\pi R^3 < E_{\text{SN}}$, for the obtained value of k_s and the assumed value of E_{SN} . If the previous inequality is not valid, one or more of the simplifying assumptions of the model are not correct for the particular case under analysis.

The expected γ -ray flux in the TeV region by a SNR is (Aharonian et al. 1994)

$$F_\gamma(> E) = f_\Gamma 10^{-10} \left(\frac{E}{\text{TeV}}\right)^{-\Gamma+1} A \text{ cm}^{-2}\text{s}^{-1}, \quad (16)$$

where the factor A is

$$A = \theta \left(\frac{E_{\text{SN}}}{10^{51}\text{erg}}\right) \left(\frac{d}{\text{kpc}}\right)^{-2} \left(\frac{n}{\text{cm}^3}\right) \text{ ph cm}^{-2}\text{s}^{-1}, \quad (17)$$

n is the medium density, and f_Γ is a function of the index in the differential power-law proton spectrum (Γ), equal to 0.9, 0.43, and 0.19 for $\Gamma=2.1$, 2.2, and 2.3, respectively. This estimate, however, usually exceeds that obtained when the GeV spectral index is extrapolated up to TeV energies. When that is the case, the extrapolated flux (with the same spectral index) will be considered a safer estimate. To extrapolate the GeV flux up to TeV energies we assume (Thompson et al. 1996)

$$\frac{dN}{dE} = K \left(\frac{E}{E_0}\right)^{-\Gamma}, \quad (18)$$

where K is a constant, E is given in MeV, and E_0 is a reference energy. This constant can be obtained simply by integrating the flux,

$$K \equiv F_{\text{ph}} / \int_{100\text{MeV}}^{10\text{GeV}} \left(\frac{E}{E_0}\right)^{-\Gamma} dE, \quad (19)$$

where F_{ph} is the observed total flux (that quoted in the 3EG Catalog, for instance). Once K is known, the flux in any given energy interval $E_1 - E_2$ is just,

$$F(E_1, E_2) = K \int_{E_1}^{E_2} \left(\frac{E}{E_0}\right)^{(-\Gamma+1)} dE. \quad (20)$$

We are extrapolating, then, the measured spectral index at MeV-GeV energies assuming that there is no spectral change at higher energies. Actually, this assumption is a simplification not compatible with TeV observations of several sources (see below). In any case, this extrapolation will always provide an upper bound to the high-energy photon flux.

3 Relativistic Bremsstrahlung

Since relativistic electron Bremsstrahlung and nucleus-nucleus induced pion-decay are competing processes in the generation of γ -rays from molecular clouds exposed to a nearby CR accelerator, it is necessary to assess the relative weight of each contribution if we are to quantitatively address the question of the possible SNR origin of nucleonic CRs.

The γ -ray emissivity at a given energy E from relativistic Bremsstrahlung is (e.g. Longair 1994, p.267-269)

$$q_B(E) = \frac{10^{-21}}{p-1} n_{\text{m}^{-3}} K E^{-p} \text{ m}^{-3} \text{ s}^{-1} \text{ GeV}^{-1}, \quad (21)$$

where it is assumed an electron power-law distribution, $N_e(E) = KE^{-p}$. We are interested in the γ -ray radiation above 100 MeV, so we integrate the previous expression to obtain

$$q_B(E > 0.1\text{GeV}) = \frac{10^{-21}}{p-1} n_{\text{m}^{-3}} K \int_{0.1\text{GeV}}^{\infty} E^{-p} dE \text{ m}^{-3} \text{ s}^{-1}, \quad (22)$$

or,

$$q_B(E > 0.1\text{GeV}) = \frac{10^{-21}}{(p-1)^2} n_{\text{m}^{-3}} K 0.1^{-(p-1)} \text{ m}^{-3} \text{ s}^{-1}. \quad (23)$$

This same population of relativistic electrons will also radiate at radio wavelengths, via the synchrotron mechanism. The synchrotron spectrum of a power-law electron energy distribution is (Longair 1994, p. 261)

$$\begin{aligned} J(\nu) &= 2.344 \times 10^{-25} a(p) B^{(p+1)/2} K \left(\frac{1.253 \times 10^{37}}{\nu} \right)^{(p-1)/2} \text{ W m}^{-3} \text{ Hz}^{-1} \\ &= 23.44 a(p) B^{(p+1)/2} K \left(\frac{1.253 \times 10^{37}}{\nu} \right)^{(p-1)/2} \text{ Jy m}^{-1}, \end{aligned} \quad (24)$$

where B is the magnetic field measured in Tesla, and

$$a(p) = \frac{\sqrt{\pi}}{2} \frac{\Gamma(\frac{p}{4} + \frac{19}{12}) \Gamma(\frac{p}{4} - \frac{1}{12}) \Gamma(\frac{p}{4} + \frac{5}{4})}{(p+1) \Gamma(\frac{p}{4} + \frac{7}{4})}, \quad (25)$$

is a numerical coefficient depending on the spectral index. Then, the ratio between the γ -ray flux emitted by relativistic Bremsstrahlung and the synchrotron emission results

$$R = \frac{q_B(E > 100\text{MeV})}{J(\nu)} = \frac{F(E > 100\text{MeV})}{F_{\nu}[\text{Jy}]} = \frac{4.3 \times 10^{-21}}{b(p)} n_{\text{cm}^{-3}} B_{\mu\text{G}}^{-(1+p)/2} \nu_{\text{Hz}}^{(p-1)/2} \text{ Jy}^{-1} \text{ cm}^{-2} \text{ s}^{-1}, \quad (26)$$

where we have defined

$$b(p) = 10^{-5(1+p)} (3.2 \times 10^{15})^{(p-1)/2} (p-1)^2 a(p), \quad (27)$$

and converted units to the cgs system.

If $F(E > 100 \text{ MeV})$ is known, estimating the right hand side of Eq. (26) for the measured spectral photon index and the derived density and magnetic field, the expected value of $F_{\nu}[\text{Jy}]$ can be obtained. This is the radio emission that *should be observed if the γ -rays are from relativistic Bremsstrahlung*. If the γ -ray source is not superposed with the bulk of the synchrotron radio/X-ray emission from the SNR, this tends to favor a nucleus-nucleus origin of the high-energy flux, rather than a electron Bremsstrahlung scenario.

In general, at the high densities found in molecular clouds, inverse Compton scattering can be ruled out as the main mechanism contributing to the γ -ray emission (e.g. Gaisser et al. 1998). Above 100 MeV, the relevant cross sections and estimates of the electron-nucleon density ratio show that relativistic Bremsstrahlung dominates over inverse Compton processes (see, for instance, Stecker's 1977, Figure 1 and 2). In particular, de Jager & Mastichiadis (1997) have shown that for molecular densities above 10 cm^{-3}

γ -ray fluxes above 70 MeV are dominated by Bremsstrahlung when electrons are considered (see their Figure 4). In what follows, since we shall mainly consider high-density scenarios, relativistic Bremsstrahlung will be the main alternative to nucleonic interactions in evaluating the origin of the observed γ -ray flux in the MeV-TeV energy range.

4 Diffusion of CRs and γ -ray spectral evolution

The spectrum of γ -rays generated through π^0 -decay at a source of proton density n_p is

$$F_\gamma(E_\gamma) = 2 \int_{E_\pi^{\min}}^{\infty} \frac{F_\pi(E_\pi)}{\sqrt{E_\pi^2 - m_\pi^2}} dE_\pi, \quad (28)$$

where

$$E_\pi^{\min}(E_\gamma) = E_\gamma + \frac{m_\pi^2}{4E_\gamma}, \quad (29)$$

and

$$F_\pi(E_\pi) = 4\pi n_p \int_{E_p^{\min}}^{E_p^{\max}} J_p(E_p) \frac{d\sigma_\pi(E_\pi, E_p)}{dE_\pi} dE_p. \quad (30)$$

Here, $d\sigma_\pi(E_\pi, E_p)/dE_\pi$ is the differential cross-section for the production of π^0 -mesons of energy E_π by a proton of energy E_p in a $p - p$ collision. If the proton spectrum $J_p(E_p)$ at the γ -ray production site is

$$J_p(E_p) = KE_p^{-\Gamma}, \quad (31)$$

we can also expect a power-law spectrum at γ -rays:

$$F_\gamma(E_\gamma) \propto E_\gamma^{-\Gamma}. \quad (32)$$

However, the spectrum given by Eq. (31) is not necessarily the same proton spectrum at the acceleration site. If there is diffusion, we shall have, instead

$$J_p(E_p, r, t) = \frac{c}{4\pi} f, \quad (33)$$

where $f(E_p, r, t)$ is the distribution function of protons at an instant t and distance r from the source. The distribution function satisfies the well-known diffusion equation (Ginzburg & Syrovatskii 1964):

$$\frac{\partial f}{\partial t} = \frac{D(E_p)}{r^2} \frac{\partial}{\partial r} r^2 \frac{\partial f}{\partial r} + \frac{\partial}{\partial E_p} (Pf) + Q, \quad (34)$$

where $P = -dE_p/dt$ is the continuous energy loss rate of the particles, $Q = Q(E_p, r, t)$ is the source function, and $D(E_p)$ is the diffusion coefficient, for which we assume here no dependency on r or t , i.e. the particles diffuse through an homogeneous, quasi-stationary medium.

We assume that $D(E_p) \propto E_p^\delta$ and $f \propto E_p^{-\Gamma}$ with continuous injection given by $Q(E_p, t) = Q_0 E_p^{-\Gamma} q(t)$, which is appropriate for a supernova remnant (Aharonian & Atoyan 1996). Further simplicity can be achieved assuming that the source is constant after turning on at some instant, i.e. $q(t) = 0$ for $t < 0$ and $q(t) = 1$ for $t \geq 0$. Atoyan et al. (1995) have found a general solution for Eq. (34) with arbitrary injection spectrum, which with the listed assumptions leads to:

$$f(E_p, r, t) = \frac{Q_0 E_p^{-\Gamma}}{4\pi D(E_p)r} \left(\frac{2}{\sqrt{\pi}} \right) \int_{r/R_{\text{diff}}}^{\infty} e^{-x^2} dx. \quad (35)$$

In this expression, $R_{\text{diff}} = R_{\text{diff}}(E_p, t)$ is the diffusion radius which corresponds to the radius of the sphere up to which the particles of energy E_p propagate during the time t after the injection. Now, for $D(E_p) = aD_{28}E_p^\delta$, where $D_{28} = D/10^{28} \text{ cm}^2 \text{ s}^{-1}$, and for $R_{\text{diff}} \gg r$, i.e. when the target is well immerse into the cosmic ray flux, Eq. (35) reduces to

$$f(E_p, r) = \frac{Q_0 E_p^{-(\Gamma+\delta)}}{4\pi a D_{28} r}, \quad (36)$$

and then, from Eq. (33), we get:

$$J_p(E_p, r) = \frac{c Q_0 E_p^{-(\Gamma+\delta)}}{(4\pi)^2 a D_{28} r}. \quad (37)$$

Hence, as has been emphasized by Aharonian & Atoyan (1996), the observed γ -ray flux $F_\gamma(E_\gamma) \propto E_\gamma^{-(\Gamma+\delta)}$ can have a significantly different spectrum from that expected from the particle population at the source (the SNR). Standard diffusion coefficients $\delta \sim 0.3 - 0.6$ can explain γ -ray spectra as steep as $\Gamma \sim 2.3 - 2.6$ in sources with particles accelerated to a power-law $J_p(E_p) \propto E^{-2}$ if the target is illuminated by the π^0 -decays are at sufficient distance from the accelerator. This can explain observed discrepancies in the particle spectral indices inferred from SNR at different frequencies, *even if all particles, leptons and hadrons, are accelerated to the same power-law in the source*.

CRs with total energy W_p and injected in the interstellar medium by some local accelerator reach a radius $R(t)$ at instant t . Their mean energy density is $w_p \approx 0.5 (W_p/10^{50} \text{ erg})(R/100 \text{ pc})^{-3} \text{ eV cm}^{-3}$. Thus, in regions up to 100 pc around a CR accelerator with $W_p \sim 10^{50} \text{ erg}$, the density of relativistic particles may significantly exceed the average level of the “sea” of galactic CRs, $w_{\text{GCR}} \sim 1 \text{ eV/cm}^3$. In Figure 5, the differential flux of protons at distances $R = 10, 30, \text{ and } 100 \text{ pc}$ from an “impulsive” accelerator, with total energy $W_p = 10^{50} \text{ erg}$ are shown. The spectrum of CRs at the given time and spatial location can differ significantly from the source spectrum. The diffusion coefficient in this figure is assumed in a power-law form, $D(E) \propto E^{0.5}$ above 10 GeV, and constant below 10 GeV. The commonly adopted value at 10 GeV is about $10^{28} \text{ cm}^2 \text{ s}^{-1}$, however smaller values, e.g. $10^{26} \text{ cm}^2 \text{ s}^{-1}$, cannot be excluded, especially in active star forming regions (Aharonian 2001). The existence of massive gas targets like molecular clouds in these regions may result in γ -ray fluxes detectable by EGRET, if $(W_{50} \cdot M_5)/d_{\text{kpc}}^2 \geq \sim 0.1$, where M_5 is the mass of the cloud in units of $10^5 M_\odot$ (Aharonian 2001). In the case of energy-dependent propagation of CRs, large variety of γ -ray spectra is then expected, depending on the age of the accelerator, duration of injection, the diffusion coefficient, and the location of the cloud with respect to the accelerator.

The comparison of γ -ray fluxes from clouds located at different distances from an accelerator may provide unique information about the CR diffusion coefficient $D(E)$. Similar information may be obtained from a *single* γ -ray emitting cloud, but in different energy domains. For the energy-dependent propagation of CRs the probability for simultaneous detection of a cloud in GeV and TeV γ -rays is not very high, because the maximum fluxes at these energies are reached at different epochs (see Figure 6). The higher energy particles propagate faster and reach the cloud earlier, therefore the maximum of GeV γ -radiation appears at the epoch when the maximum of the TeV γ -ray flux is already over. In the case of energy-independent propagation (e.g. due to strong convection) the ratio $F_\gamma(\geq 100 \text{ MeV})/F_\gamma(\geq 100 \text{ GeV})$ is independent of time, therefore the clouds that are visible for EGRET at GeV energies would be detectable also at higher energies, provided that the spectral index of the accelerated protons be $\Gamma \leq 2.3$.

Summing up, special care must be taken in analyzing the a priori expectations for the SNR-cloudy medium scenario: when particles diffuse into the ISM before reaching the cloud, a quite different spectrum

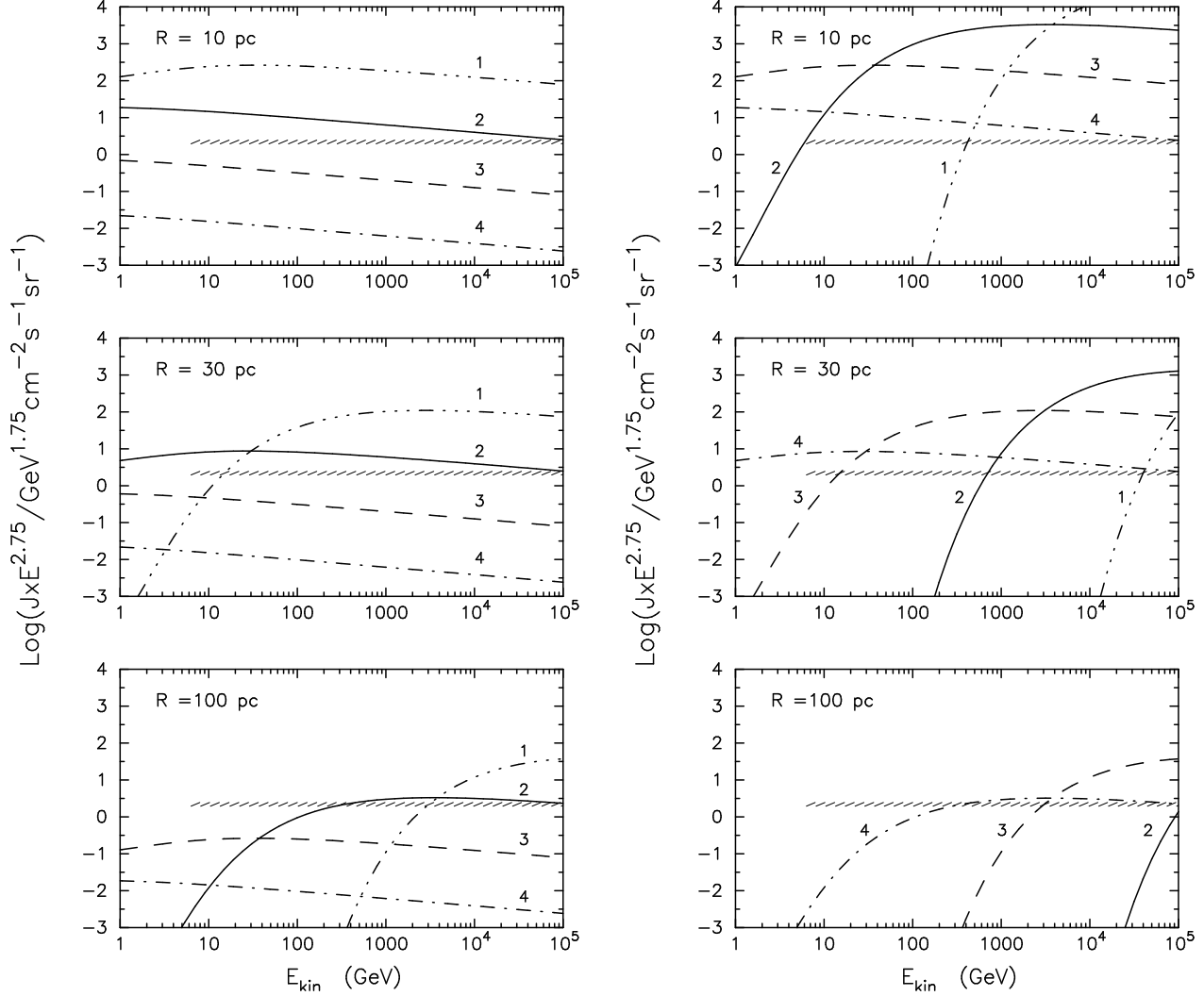


Figure 5: Temporal and spectral evolution of CR fluxes at different (10 pc, 30 pc, and 100 pc) distances from an *impulsive* proton accelerator. A power-law proton spectrum with $\Gamma = 2.2$ and total energy $W_p = 10^{50}$ erg are assumed. Curves 1, 2, 3, and 4 correspond to an age of the source of $t = 10^3$ yr, 10^4 yr, 10^5 yr, and 10^6 yr, respectively. An energy-dependent diffusion coefficient $D(E)$ with power-law index $\delta = 0.5$ is adopted. The left panel presents results for $D = D_{28} \text{ cm}^2 \text{s}^{-1}$, whereas the right panel corresponds to $D = 10^{-2} D_{28} \text{ cm}^2 \text{s}^{-1}$. The hatched curve shows the local (directly measured) flux of CR protons. More details are given in Aharonian & Atoyan (1996) and Aharonian (2001).

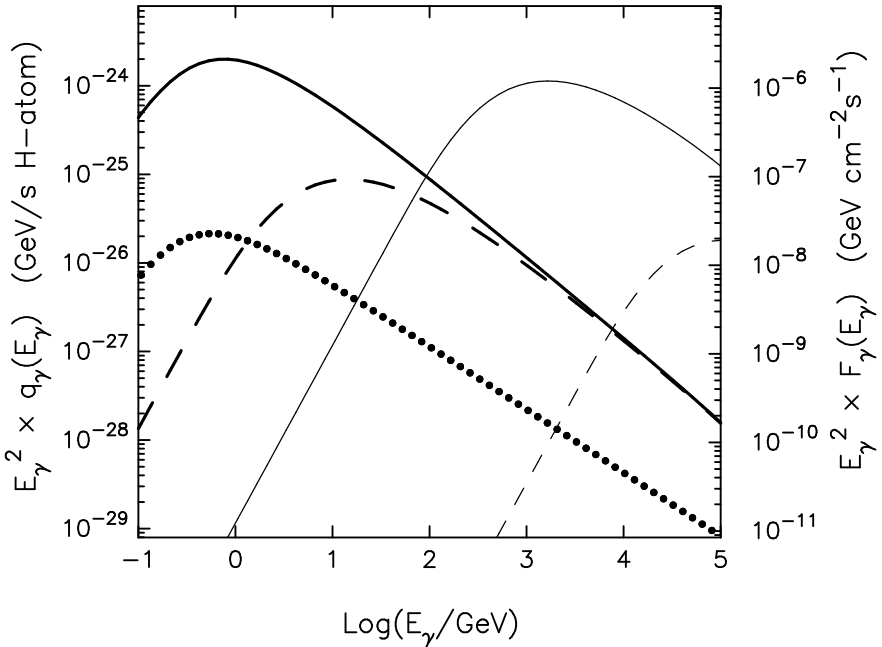


Figure 6: Gamma-ray emissivities in terms of $E_\gamma^2 \times q_\gamma(E_\gamma)$ at different times t and distances R from a proton accelerator. The right hand side axes shows the γ -ray fluxes, $E_\gamma^2 \times F_\gamma(E_\gamma)$, which are expected from a cloud with parameter $M_5/d_{\text{kpc}}^2 = 1$. The thin and bold curves correspond to times $t = 10^3$ and 10^5 yr, respectively. Fluxes at distances $R = 10$ and 30 pc are shown by solid and dashed lines. The power-law index, the total energy of protons, and the diffusion coefficient are the same as in the right panel of Figure 5. The curve shown by full dots corresponds to the γ -ray emissivity (and flux) calculated for local CR protons. In order to take into account the contribution of nuclei, all curves should be increased by a factor of $\eta \approx 1.5$. More details can be found in Aharonian & Atoyan (1996) and Aharonian (2001).

from that of the injecting source can finally emerge, depending on the distance to the cloud and the diffusion index. Even when molecular clouds are overtaken by the expanding shell of the SNR and there is clear evidence of interaction, a strong magnetic field could produce differences in the spectra.

5 Sample and correlation analysis

Table 1 shows those 3EG sources that are positionally coincident with SNRs listed in the latest version of Green's Catalog (2000). From left to right, columns are for the γ -ray source name, the measured flux in the summed EGRET phases P1234 (in units of $10^{-8} \text{ ph cm}^{-2} \text{ s}^{-1}$), the photon spectral index Γ , the EGRET class of source (em for possibly extended and C for confused), the variability indices I (as in Torres et al. 2001a,c) and $\tau_{\text{lower limit}}^{\text{upper limit}}$ (as in Tompkins 1999), information about coincidences with radio pulsars ("y" stands for a pulsar within the error box), the SNR identification (including other usual names when available), the angular distance between the center of the γ -ray source position and the center of the remnant (in degrees), the size of the remnant (in arcmin), and finally the SNR type T (S for shell-like emission, F for filled-centre or plerionic remnant, and C for composite). A separate section below analyzes the possible pulsar associations. All remnants were considered as circles with a radius equal to the major axis of the ellipse that better fits their shape, when such is given in Green (2000). It is interesting to see that many of the 3EG sources involved in the associations are classified as extended, and all of them as confused. Also,

Table 1: Positional coincidences between supernova remnants quoted in Green's Catalog (2000), and unidentified 3EG EGRET sources. See text for the meaning of the different columns.

γ -source	F_γ	Γ	Class	I	τ	P?	SNR	Other name	$\Delta\theta$	Size	T
0542+2610	14.7 ± 3.2	2.67 ± 0.22	em C	3.16	$0.70_{-0.34}^{+1.40}$		G180.0–1.7		2.04	180	S
0617+2238 ^{1,2}	51.4 ± 3.5	2.01 ± 0.06	C	1.68	$0.26_{-0.15}^{+0.38}$		G189.1+3.0	IC443	0.11	45	S
0631+0642 ^{1,3}	14.3 ± 3.4	2.06 ± 0.15	C	1.52	$75.8_{-7.89}^{\infty}$		G205.5+0.5	Monoceros	1.97	220	S
0634+0521	15.0 ± 3.5	2.03 ± 0.26	em C	1.02	$72.0_{-5.15}^{\infty}$		G205.5+0.5	Monoceros	2.03	220	S
1013–5915	33.4 ± 6.0	2.32 ± 0.13	em C	1.63	$0.22_{-0.00}^{+0.46}$	y	G284.3–1.8	MSH 10-53	0.65	24	S
1102–6103	32.5 ± 6.2	2.47 ± 0.21	C	1.86	$0.00_{-0.00}^{+0.90}$		G290.1–0.8	MSH 11-61A	0.12	19	S
							G289.7–0.3		0.75	18	S
1410–6147 ⁴	64.2 ± 8.8	2.12 ± 0.14	C	1.22	$0.33_{-0.16}^{+0.55}$	y	G312.4–0.4		0.23	38	S
1639–4702	53.2 ± 8.7	2.50 ± 0.18	em C	1.95	$0.00_{-0.00}^{+0.38}$	y	G337.8–0.1	Kes 41	0.07	9	S
							G338.1+0.4		0.65	15	S
							G338.3+0.0		0.57	8	S
1714–3857	43.6 ± 6.5	2.30 ± 0.20	em C	2.17	$0.15_{-0.00}^{+0.38}$	y	G348.5+0.0		0.47	10	S
							G348.5+0.1	CTB 37A	0.50	15	S
							G347.3–0.5		0.85	65	S
1734–3232 ⁵	40.3 ± 6.7	–	C	2.90	$0.00_{-0.00}^{+0.24}$		G355.6+0.0		0.16	8	S
1744–3011	63.9 ± 7.1	2.17 ± 0.08	C	1.80	$0.38_{-0.20}^{+0.62}$		G359.0–0.9		0.41	23	S
							G359.1–0.5		0.25	24	S
1746–2851 ⁶	119.9 ± 7.4	1.70 ± 0.07	em C	2.00	$0.50_{-0.36}^{+0.69}$		G0.0+0.0		0.12	3.5	S
							G0.3+0.0		0.19	16	S
1800–2338 ^{1,7}	61.3 ± 6.7	2.10 ± 0.10	C	1.60	$0.03_{-0.00}^{+0.32}$	y	G6.4–0.1	W28	0.17	42	C
1824–1514	35.2 ± 6.5	2.19 ± 0.18	C	3.00	$0.00_{-0.00}^{+0.51}$	y	G16.8–1.1		0.43	30	–
1837–0423	<19.1	2.71 ± 0.44	C	5.41	$12.0_{-2.17}^{\infty}$	y	G27.8+0.6		0.58	50	F
1856+0114 ⁸	67.5 ± 8.6	1.93 ± 0.10	em C	2.92	$0.80_{-0.50}^{+1.51}$	y	G34.7–0.4	W44	0.17	35	S
1903+0550 ⁴	62.1 ± 8.9	2.38 ± 0.17	em C	2.28	$0.35_{-0.18}^{+0.60}$	y	G39.2–0.3	3C396, HC24	0.41	8	S
2016+3657	34.7 ± 5.7	2.09 ± 0.11	C	2.06	$0.37_{-0.08}^{+0.75}$		G74.9+1.2	CTB 87	0.26	8	F
2020+4017 ^{1,9}	123.7 ± 6.7	2.08 ± 0.04	C	1.12	$0.07_{-0.00}^{+0.18}$?	G78.2+2.1	W66, γ -Cyg	0.15	60	S

¹ Association proposed by Sturmer & Dermer (1995) and Esposito et al. (1996). ² GeV J0617+2237 ³ GeV J0633+0645. ⁴ Association proposed by Sturmer & Dermer (1995). ⁵ GeV J1732–3130. ⁶ GeV J1746–2854. ⁷ GeV J1800–2328. ⁸ GeV J1856–0115. ⁹ GeV J2020+4023. GeV sources compiled in the GeV ASCA Catalog (Roberts et al. 2001a).

Table 2: Evolution of the number of positional coincidences between SNRs and unidentified EGRET sources. In the last row, 6 likely artifacts are disregarded in the 3EG Catalog.

Catalog EGRET	Unidentified detections	Real coincidences	Number of SNRs in Green's catalog	Significance (statistical)
First EGRET Catalog ^a	37	13 (35%)	182	1.8σ
2EG ^b	32	7 (22%)	194	?
2EG ^c	32	5 (16%)	14 ^g	?
2EG ^d	33	10 (30%)	194	h
3EG ^e	81	22 (27%)	220	5.7σ
3EG ^f	75	19 (25%)	220	4.8σ

a: Sturner & Dermer (1995). b: Sturner, Dermer & Mattox (1996). c: Esposito, Hunter, Kanbach & Sreekumar (1996). d: Yadigaroglu & Romani (1997). e: Romero, Benaglia & Torres (1999). f: Torres et al. (2001b). g: Only radio-bright SNRs, flux at 1 GHz greater than 100 Jy, were considered. h: Computed for pairs.

it was already noted (Romero et al. 1999a) that in the 3EG catalog not all the positional coincidences with SNRs are SNOBs (SNRs in OB associations), as it was the case in the studies by Montmerle (1979) and Yadigaroglu & Romani (1997) using previous samples.

The adoption of the 2000 edition¹ of Green's Catalog (2000) does not produce any substantial statistical difference with respect to the previous edition of 1998. Only 5 SNRs were added. However, there is a notable particular difference in the case of the EGRET source 3EG J1714-3857, which now coincides with three supernova remnants instead of two. One of these SNRs (the new one in Green's catalog, G347.3-0.5) appears to be amongst the strongest cases for SNR shock/ γ -ray/nucleonic cosmic-ray source associations known to date (Butt et al. 2001, see below). In addition, 2EG J1801-2312 shifted its position half a degree when converting into 3EG J1800-2338, also affecting previous positional coincidences. The evolution in the number of coincidences between SNRs and EGRET sources since the First EGRET Catalog until the current situation is shown in Table 1 (Torres et al. 2001b).

The Poisson probability for the 19 coincidences to be a chance effect is 1.05×10^{-5} , i.e., there is an a priori 0.99998 probability that at least one of the positional associations in Table 1 is physical. This expected chance association was computed using thousands of simulated sets of EGRET sources, by means of a numerical code described elsewhere (Romero et al. 1999a,b, Sigl et al. 2001). Figure 7 shows the result of numerical simulations for these random populations of γ -ray sources. Figure 8 shows the distribution of the γ -ray photon spectral index for the sample of 3EG sources coincident with SNRs. Some cases of possible physical associations mentioned in the literature and discussed in the next sections are indicated.

If some SNRs interact, as expected, with nearby massive clouds producing enhanced γ -ray emission through hadronic/Bremsstrahlung interactions, cases in which there is just a marginal coincidence between the center-points of the SNRs and the centers of the EGRET sources should be also considered, since the peak γ -ray emissivity will likely be biased towards the adjacent cloud. So we have also looked at the positional coincidences between unidentified EGRET sources and the region just around the SNRs. We have done so by artificially enlarging the size of the SNR by half a degree. We found that there are 26 coincidences of this kind, including those in Table 1. Then, there are 7 new cases perhaps worthy of further study. These cases are shown in Table 1. Interestingly, the expected chance coincidence in this case is at

¹A new edition –2001– of the catalog has recently appeared. The results presented herein are not changed when the 2001 edition is considered.

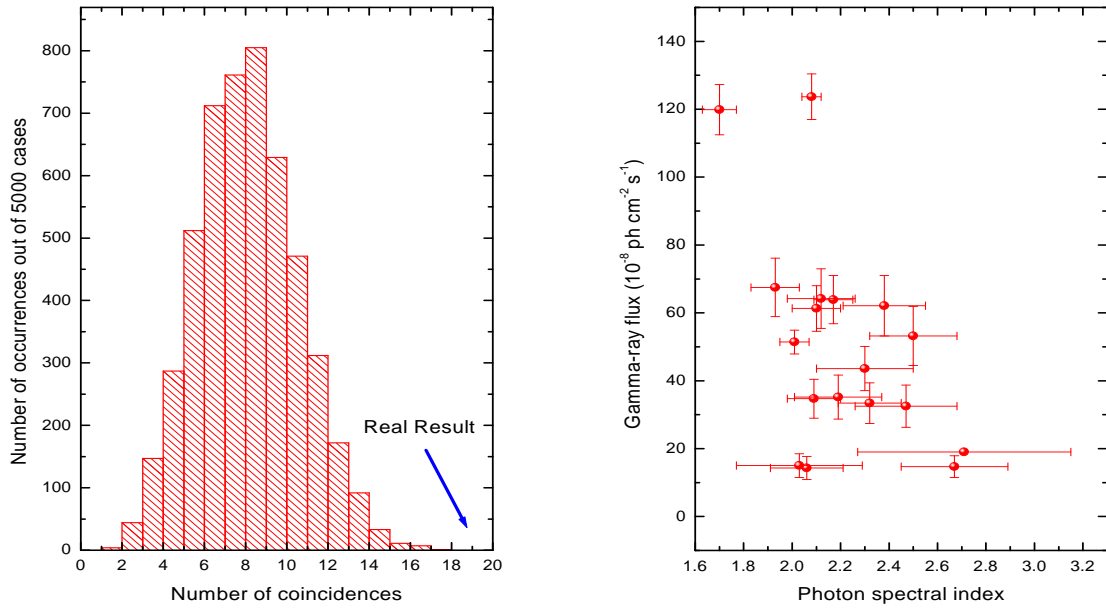


Figure 7: Left: Statistical results for the random association between SNRs and EGRET sources at low-latitudes. Right: Distribution of the γ -ray fluxes as a function of the photon spectral index. Two sources seem to differentiate from the rest. One of these sources (see below) has been recently identified with a blazar.

the level of 14.8 ± 3.14 , still 4σ lower than the real result, implying a probability of 2.5×10^{-3} for the real result to be a random (Poisson) fluctuation. In order to quantify the role played by the 7 new sources in this result new simulations were carried out, now considering only these sources. The chance result is 2.3 ± 1.2 , again 4σ below the real number of coincidences. In the present review, however, we shall focus only on those SNRs that present positional correlation with γ -ray sources, i.e. only the cases listed in Table 1.

6 SNRs coincident with γ -ray sources

We now analyze the sample of SNRs in Table 1 in more detail. Table 4 presents the radio fluxes of the SNRs, together with their spectral index and known distance estimates (with the corresponding references). Distances are only approximate since several different values for the same SNR can be found in the literature. When no direct determination is available, estimates can be made using the radio surface brightness-to-diameter relationship, known as $\Sigma - D$ (Clark & Caswell 1976, Milne 1979, Case & Bhattacharya 1998). For these cases, marked with a star in Table 4, the distances given by the new $\Sigma - D$ introduced by Case & Bhattacharya (1998) will -unless otherwise noted- be adopted. A double star symbol means that neither a distance determination nor an estimate is available. There is only one such case in Table 4, for which the distance to a coincident OB association was assumed. Thus, distances in Table 4 marked with one or two stars are, respectively, more uncertain than the others.

Using the estimated distance to each remnant in Table 4, we have calculated the approximate intrinsic γ -ray luminosity of the putative region producing the high-energy source in the energy range 100 MeV–10

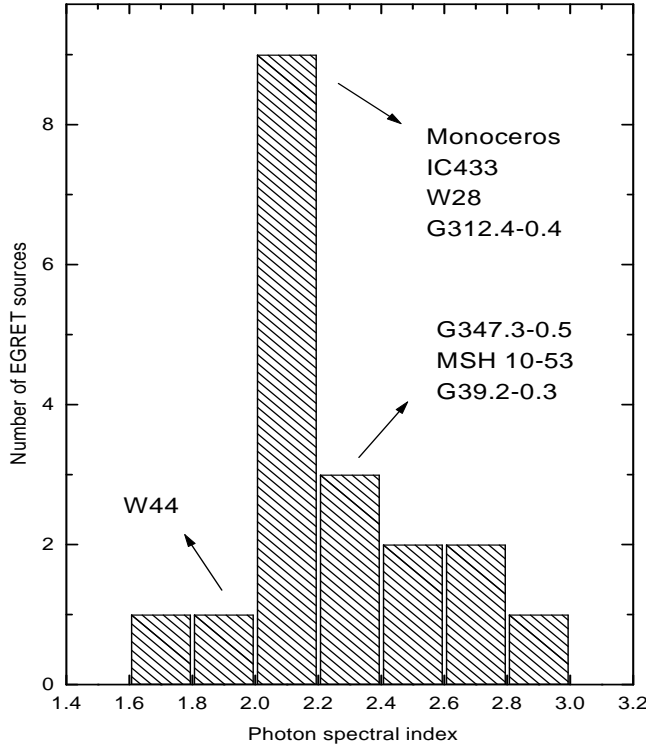


Figure 8: Distribution of the γ -ray photon spectral index. Some SNR-3EG coincidences for which the physical association has been suggested in the literature are indicated.

GeV using the observed EGRET flux and photon indices (see Table 1), assuming isotropic emission. We have also re-ordered Green's Catalog according to descending radio flux, and the rank in this list is given for each remnant. It is interesting that from the first 20 SNRs with the highest radio fluxes, only 6 appear to be correlated with EGRET sources. Sturner & Dermer (1996) have noted that SNRs not correlated with 2EG sources were either more distant than γ -Cyg (G78.2+2.1) and IC 433 (G189.1+3.0), or presenting a far smaller radio flux. This trend is not observed now with the larger 3EG sample.

squares stand

7 Pulsars within the EGRET error boxes

Since both molecular clouds and pulsars can produce γ -rays, and because both often lie close to SNRs, it is important to explore the possible origin of the high-energy flux in neighboring pulsars.

In order to firmly identify a pulsar as the origin of the γ -rays from an EGRET source, γ -ray pulsations must be detected at the pulsar period. However, this is not always possible because of the usually low photon counts observed in most cases. There are only 6 high-energy γ -ray pulsars that are already confirmed,

Table 3: Supernova remnants and nearby (but not coincident) unidentified 3EG.

γ -source	F_γ	Γ	Class	I	τ	SNR	$\Delta\theta$	Size	T	Other
0229+6151	39.9 ± 6.2	2.29 ± 0.18	C	1.3	$0.37_{0.16}^{0.74}$	G132.7+1.3	1.50	82	S	Of/OB
1736–2908	51.5 ± 9.1	2.18 ± 0.12	C	2.4	$0.66_{0.40}^{1.09}$	G359.1+0.9	0.73	12	S	–
1741–2050	24.1 ± 3.9	2.25 ± 0.12	C	2.1	$0.41_{0.14}^{0.70}$	G6.4+4.0	1.00	31	S	–
1823–1314 ^{a,b}	102.6 ± 12.5	2.69 ± 0.19	C	2.9	$0.72_{0.40}^{1.37}$	G18.8+0.3	0.88	17	S	OB
1826–1302	66.7 ± 10.1	2.00 ± 0.11	C	2.6	$0.75_{0.49}^{1.28}$	G18.8+0.3	0.88	17	S	OB
1928+1733	157.0 ± 36.9	2.23 ± 0.32	em C	3.9	$0.82_{0.43}^{2.01}$	G54.1+0.3	1.21	1.5	F?	–
1958+2909 ^c	26.9 ± 4.8	1.85 ± 0.20	em C	1.6	$0.43_{0.15}^{0.98}$	G65.1+0.6	1.36	90	S	–

a : Association proposed by Sturner & Dermer (1995), and Esposito et al. (1996). *b* : GeV J1825–1310. *c* : GeV J1957–8859.

5 of them have associated γ -ray sources in the 3EG Catalog. We give their properties in Table 5. Other candidates are usually judged by comparison with the properties of the known EGRET pulsars.

The results of a correlation analysis between the 3EG sources superposed to SNRs (Table 1) and pulsars are presented in this Section. The latter were extracted from the Princeton Catalog (Taylor et al. 1993, available on line at <http://pulsar.princeton.edu/ftp/pub/catalog/>) and from the recently -partially- released Parkes Multibeam Survey (Manchester et al. 2001, <http://www.atnf.CSIRO.AU/research/pulsar/pmsurv/>). Adding up both surveys, there are more than 1000 known pulsars.

Table 7 presents the results of the correlative 3EG-radio pulsar spatial coincidence analysis: name of the 3EG source, name of the pulsar found within the error box, their angular separation, and the size of the 95% confidence contour of the 3EG source. We provide also the available information about the pulsar: its galactic coordinates, distance, characteristic time $\tau = P/2\dot{P}$, with P and \dot{P} the period and period derivative, respectively, spin-down energy release $\dot{E} = 4\pi^2 I \dot{P}/P^3$ (assuming a neutron star moment of inertia $I = 10^{45} \text{ g cm}^2$), and the efficiency in converting the spin-down luminosity into γ -rays, if the pulsar alone were responsible for generating the 3EG source flux.

The γ -ray efficiency was estimated as

$$\eta \equiv L_\gamma/\dot{E} = f 4\pi d^2 F_\gamma/\dot{E}, \quad (38)$$

where F_γ is the observed γ -ray flux between 100 MeV and 10 GeV, and f is the γ -ray beaming fraction ($0 < f \leq 1$). This fraction is essentially unknown (see, e.g., Yadigaroglu & Romani 1995, Romero 1998), but it is common practice to assume $f \equiv 1/4\pi$ (e.g. Thompson 2001, Kaspi et al. 2000, D’Amico et al. 2001, Torres et al. 2001d). These efficiencies are uncertain also because they suffer (quadratically) the imprecise knowledge of the distance to the pulsar.

For the confirmed γ -ray pulsars, the observed efficiencies are in the range $\eta \in (\sim 0.01\%, \sim 3\text{--}19\%)$, where the interval of upper limits is caused by the different estimates of the distance to PSR B1055–52 (see Ögelman & Finley 1993, Combi et al. 1997, Romero 1998). It could be considered reasonable that a pulsar generates γ -rays with efficiencies in the range $\eta \in (\sim 0.01\%, \sim 10\%)$. For higher values the pulsar would be too close to the so-called death line, where the high-energy emission is quenched (Usov 1994).

Table 4: Properties of the SNRs coincident with 3EG sources. The distances quoted are reported or discussed in the cited references. Radio fluxes and spectral indices (α , such that $S_\nu \propto \nu^\alpha$) are taken from Green's (2000) Catalog.

γ -source	SNR	d kpc	Ref.	F_{radio} Jy	α	Rank	L_γ erg s $^{-1}$
0542+2610	G180.0-1.7	0.8-1.6	1	65	varies	24	$9.65 \cdot 10^{33}$
0617+2238	G189.1+3.0	1.5	2	160	0.36	11	$1.01 \cdot 10^{35}$
0631+0642	G205.5+0.5	0.8-1.6	3	160	0.5	12	$1.70 \cdot 10^{34}$
0634+0521	G205.5+0.5	0.8-1.6	3	160	0.5	12	$1.85 \cdot 10^{34}$
1013-5915	G284.3-1.8	2.9	4	11	0.3?	91	$1.71 \cdot 10^{35}$
1102-6103	G290.1-0.8	7	5	42	0.4	34	$8.46 \cdot 10^{35}$
	G289.7-0.3	8.2	*	6.2	0.2?	123	$1.11 \cdot 10^{36}$
1410-6147	G312.4-0.4	1.9-3.1	6	45	0.26	32	$3.06 \cdot 10^{35}$
1639-4702	G337.8-0.1	12.3	7	18	0.5	67	$4.17 \cdot 10^{36}$
	G338.1+0.4	9.9	*	4?	0.4	153	$2.70 \cdot 10^{36}$
	G338.3+0.0	8.6	*	7?	?	121	$2.04 \cdot 10^{36}$
1714-3857	G348.5+0.0	11.3	8	9	0.4?	96	$3.47 \cdot 10^{36}$
	G348.5+0.1	11.3	8	72	0.3	21	$3.47 \cdot 10^{36}$
	G347.3-0.5	6.3	9	?	?	?	$1.07 \cdot 10^{36}$
1734-3232	G355.6+0.0	12.6	*	3?	?	170	—
1744-3011	G359.0-0.9	6	10	23	0.5	54	$1.65 \cdot 10^{36}$
	G359.1-0.5	8.5-9.2	8-11	14	0.4?	81	$3.56 \cdot 10^{36}$
1746-2851	G0.0+0.0	8.5	8	100?	0.8?	18	$1.20 \cdot 10^{37}$
	G0.3+0.0	8.5	12	22	0.6	55	$1.20 \cdot 10^{37}$
1800-2338	G6.4-0.1	1.6-4.2	13	310	varies	6	$4.04 \cdot 10^{35}$
1824-1514	G16.8-1.1	1.48	**	2?	?	186	$5.42 \cdot 10^{34}$
1837-0423	G27.8+0.6	2	14	30	varies	44	$3.40 \cdot 10^{34}$
1856+0114	G34.7-0.4	2.5	15	230	0.30	7	$4.14 \cdot 10^{35}$
1903+0550	G39.2-0.3	7.7-9.6	15	18	0.6	68	$2.12 \cdot 10^{36}$
2016+3657	G74.9+1.2	10	15	9	varies	104	$2.75 \cdot 10^{36}$
2020+4017	G78.2+2.1	1.7	16	340	0.5	5	$3.20 \cdot 10^{35}$

1. Anderson et al. (1996)
2. Fesen (1984)
3. Jaffe et al. (1997) and Hensberge et al. (2000)
4. Ruiz & May (1986)
5. Kaspi et al. (1997)
6. Caswell & Barnes (1985), Case & Bhattacharya (1999)
7. Koralesky et al. (1998)
8. Green et al. (1997), see also Reynoso & Mangum (2000)
9. Slane et al. (1999)
10. Bamba et al. (2000)
11. Uchida, Morris & Yusef-Zadeh (1992)
12. Kassim & Frail (1996)
13. Frail et al. (1993) and Clark & Caswell (1976)
14. Reich, Furst & Sofue (1984)
15. Green (2000) and Caswell et al. (1975)
16. Lozinskaya et al. (2000)

* From the $\Sigma - D$ relationship presented by Case & Bhattacharya (1998)
** Distance assumed equal to a coincident OB association, Romero, Benaglia & Torres (1999).

Table 5: Properties of the γ -ray pulsars detected by EGRET. Pulsar parameters and distances are taken from Kaspi et al. (2000), except PSR B1055–52, for which a smaller value of distance was also considered (Ögelman & Finley 1993, Combi et al. 1997), and Vela (Caraveo et al. 2001 and references therein). $\tau = P/2\dot{P}$, and $\dot{E} = 4\pi^2 I \dot{P}/P^3$, with $I = 10^{45}$ g cm 2 . The “P1234” γ -ray fluxes and spectral indices are from the 3EG catalog (Hartman et al. 1999).

Pulsar/3EG source	P (ms)	τ (kyr)	\dot{E} (erg s $^{-1}$)	d (kpc)	$F_{\gamma}^{3EG} [\times 10^{-8}]$ (ph cm $^{-2}$ s $^{-1}$)	γ^{3EG}	η (100MeV – –10GeV)
Crab/0534–2200	33	1.2	5.0×10^{38}	2.0	226.2 ± 4.7	2.19 ± 0.02	0.01%
Vela/0834–4511	89	12.5	6.3×10^{36}	0.25	834.3 ± 11.2	1.69 ± 0.01	0.08%
B1951+32/–	39	100.0	3.7×10^{36}	2.4	–	–	0.3%
B1706–44/1710–4439	102	15.8	3.1×10^{36}	1.8	111.2 ± 6.2	1.86 ± 0.04	1%
Geminga/0633+1751	237	316.2	3.1×10^{34}	0.16	352.9 ± 5.7	1.66 ± 0.01	3%
B1055–52/1058–5234	197	501.1	3.1×10^{34}	0.5/1.5	33.3 ± 3.8	1.94 ± 0.10	2/19%

Two of the pulsars in Table (7), PSR J1800-2343 and PSR J1902+0615, lack a confident determination of the period Derivative; for these it is impossible to assess their expected efficiencies. Based on the required efficiencies and derived spin-down luminosities of the other members of the group shown in the first (Princeton) panel, none of the positional associations seem likely except that between 3EG 1856+0114 and PSR J1856+0113. For this case, the pulsar should have an efficiency of 13% in converting rotational energy into γ -rays. PSR J1856+0113 was already mentioned as possibly associated with the EGRET source by de Jager & Mastichiadis (1996).

The bottom panel of Table (7) contains data that were analyzed elsewhere (Torres et al. 2001d); here are the main conclusions. 1. The physical association between 3EG J1013-5915 and PSR J1016-5857 is possible, as first noted by Camilo et al. (2001). 2. The source 3EG J1410-6147 and either PSR J1412-6145 or J1413-6141 might be physically associated if either of the latter lie closer than their dispersion measure distances, say at the estimated distance to G312.4-0.4 (2-3 kpc). 3. The pulsar PSR J1637-4642 could contribute part of the high-energy budget of the source 3EG J1639-4702.

8 Variability

If SNRs, molecular clouds, or pulsars are responsible for some EGRET sources, we would expect them to be non-variable on the time scale of EGRET observations, i.e. from weeks to a few years. Hence, variability analysis of the γ -ray emission is an important tool to test the original hypothesis, in the sense that variable sources could be ruled out as being produced by SNRs (or pulsars).

Three variability indices for EGRET sources have been introduced in the literature so far. The first of them, dubbed V , was presented by MacLaughlin et al. (1996), who computed it for the sources contained in the Second EGRET Catalog. This method was later used, also, for short timescale studies by Wallace et al. (2000, 2002). The basic idea behind V is to find χ^2 from the measured fluxes, and to compute $V = -\log Q$, where Q is the probability of obtaining such a χ^2 if the source were constant. Several critiques have been mentioned concerning this procedure, among them, that the scheme gets complicated when the fluxes are just upper limit detections. It can be shown that sources which have upper limits included in the analysis will have a lower V than what is implied by the data (Tompkins 1999). In addition, a source can have a large value of V because of intrinsic reasons or because of small error bars in the flux measurements. Similarly, a small value of V can imply a constant flux or big error bars. Each value of V is obtained

Table 6: Positional coincidences between 3EG unidentified sources superposed to SNRs and pulsars in the Princeton Catalog and in the recently -partially- released Parkes Multibeam Survey. We show measured and derived pulsar parameters as well. See text for details. In the case of 3EG J1410-6147, second and third values of efficiency are given for two different estimates of the distance to G312.4-0.4, 1.9 kpc and 3.1 kpc, respectively. All efficiencies are based on the new data of the 3EG Catalog (Hartman et al. 1999).

3EG J	PSR J	$\Delta\theta$ deg	θ deg	(l, b) deg	d kpc	τ kyr	P ms	\dot{P} 10^{-15}	\dot{E} erg s $^{-1}$	η (%) (beamed)
Princeton										
1013-5915	1012-5857	0.29	0.72	283.7,-2.1	10.1	741	820	17.69	1.2×10^{33}	> 100
1639-4702	1640-4715	0.29	0.56	337.7,-0.4	7.2	188	518	42.02	1.3×10^{34}	$\gg 100$
1800-2338	1800-2343	0.12	0.32	6.1,-0.1	4.8	—	1030	—	—	—
1824-1514	1825-1446	0.46	0.52	16.8,-1.0	5.4	195	279	22.68	4.1×10^{34}	> 100
1837-0423	1836-0436	0.28	0.52	27.1,1.1	4.6	33	354	1.66	1.5×10^{33}	$\gg 100$
1856+0114	1856+0113	0.05	0.19	34.5,-0.5	3.3	10	267	208.408	4.3×10^{35}	13
1903+0550	1902+0556	0.26	0.64	39.5,0.2	3.9	912	746	12.896	1.2×10^{33}	$\gg 100$
	1902+0615	0.48	—	39.8,0.3	10.1	—	673	—	—	—
Parkes										
1013-5915	1016-5857	0.16	0.72	284.1,-1.9	3.0	21	107	0.806	2.6×10^{36}	0.5
	1013-5934	0.31	—	284.1,-2.6	11.3	12561	442	0.557	2.5×10^{32}	$\gg 100$
1410-6147	1412-6145	0.15	0.36	312.3,-0.3	9.3	50	315	98.7	1.2×10^{35}	> 100/12/30
	1413-6141	0.28	0.36	312.4,-0.3	11.0	13	286	333.4	5.7×10^{35}	80/3/6
1639-4702	1637-4642	0.46	0.56	337.8,+0.3	5.8	41	154	59.2	6.4×10^{35}	12
	1640-4648	0.37	—	338.1,-0.2	6.1	3501	178	0.806	5.6×10^{33}	$\gg 100$
	1637-4721	0.45	—	337.3,-0.1	5.9	4160	1165	4.44	1.1×10^{32}	$\gg 100$
1714-3857	1713-3844	0.30	0.51	348.1,0.2	6.5	143	1600	177.41	1.7×10^{33}	$\gg 100$
	1715-3903	0.23	—	348.1,-0.3	4.8	117	278	37.688	6.9×10^{34}	72
1837-0423	1838-0453	0.50	0.52	27.1,+0.7	8.2	52	381	115.7	8.3×10^{34}	< 55

disregarding those of a control population. Then, there could be pulsars with very high values of V , or variable AGNs with very low ones. Hence, the use of V to classify the variability of γ -ray sources seems not to produce confident results. Two other indices have been computed for all γ -ray sources: the I index and the τ index (Torres et al. 2001a; Tompkins 1999, respectively). See Torres et al. (2001c) for a comparison among the results obtained with them. The idea behind the index I is to carry out a direct comparison of the flux variation of any given source with that shown by pulsars, which is considered as instrumental. It basically establishes how variable a source is with respect to the pulsar population. Contrary to Tompkins' index, the I -scheme uses only the publicly available data of the 3EG Catalog, and is defined as follows. Firstly, a mean weighted value for the EGRET flux is computed as

$$\langle F \rangle = \left[\sum_{i=1}^{N_{vp}} \frac{F(i)}{\epsilon(i)^2} \right] \times \left[\sum_{i=1}^{N_{vp}} \frac{1}{\epsilon(i)^2} \right]^{-1}. \quad (39)$$

Here N_{vp} is the number of single viewing periods for each γ -ray source, $F(i)$ is the observed flux in the i^{th} -period, whereas $\epsilon(i)$ is the corresponding error in the observed flux. These data are taken directly from the 3EG Catalog. A fluctuation index, μ , is defined as (e.g. Romero et al. 1994):

$$\mu = 100 \times \sigma_{\text{sd}} \times \langle F \rangle^{-1}, \quad (40)$$

where σ_{sd} is the standard deviation of the flux measurements. This fluctuation index is also computed for the confirmed γ -ray pulsars in the 3EG Catalog, and then the averaged statistical index of variability, I ,

is introduced by

$$I = \frac{\mu_{\text{source}}}{\langle \mu \rangle_{\text{pulsars}}}. \quad (41)$$

We refer the reader to the work by Torres et al. (2001a,c) for details on the error estimates.

Since the I -scheme is a relative classification, a result like $I = 3.0$ says that the flux evolution is three times more variable than (equivalently, 4σ above) the mean flux evolution for pulsars. Torres et al. (2001c) mentioned that in order to get more reliable results under the I -scheme at low-latitudes it seems safer to consider a restrictive criterion. For instance, a source will be considered very variable only when $I - \delta I > [I_p] + 3\sigma_{p,I}$. Here $\delta I \sim 0.5I$, $[I_p]$ is the mean value of I for pulsars, $\sigma_{p,I}$ is their standard deviation, and $[I_p] + 3\sigma_{p,I} = 2.5$. Rephrasing the previous constraints just in terms of I , a source will be very variable if $I > 5$. This represents a deviation of 8σ from the mean I -value for pulsars. With this criterion, 3EG J1837-0423, with $I = 5.41$, is a very variable source. We have 7 non-variable sources, those having $I < 1.7$ in Table 1. The rest of the sources listed there are dubious under this classification scheme.

Tompkins (1999) used the 145 marginal sources that were detected but not included in the final official 3EG list, and, simultaneously, all the detections within 25 deg of the source of interest. The maximum likelihood set of source fluxes was then re-computed. From these fluxes, a new statistic measuring the variability was defined as $\tau = \sigma/\mu$, where σ is the standard deviation of the fluxes and μ their average value. The final result of Tompkins' analysis is a table listing the name of the EGRET source and three values for τ : a mean, a lower, and an upper limit (68% error bars).

The mean value of τ for pulsars -again an assumed non-variable population- is very low, 0.09, but the mean of the upper limits is ~ 0.2 . So pulsars are consistent with having values of τ up to 0.2. The deviation for the mean value of pulsars is 0.08. A source will be likely variable under the τ scheme when the lower limit is at least 0.6, 3σ above the mean value of the τ upper limit for pulsars. A source will be considered non-variable when the upper limit for τ is below that threshold. Sources not fulfilling either classification will be considered as dubious. This is also consistent with the fact that the mean τ value for the known population of AGNs is 0.9. Using this scheme, too, 3EG J1837-0423 is a variable source. In addition, 3EG J0631+0642 and 3EG J0634+0521 are also variable under τ . However, Tompkins (1999) adds a word of caution for these two sources: the fitted flux for them is zero. Such sources are most likely variable, but unknown instrument systematics or numerical problems within the τ scheme could conceivable change these results. Also important is to note that many sources have a dubious classification: within the 68% error bars on τ , they can be as variable as an AGN, or as non-variable as a pulsar. This is, unfortunately, a common situation for many of the sources. For those ones, in particular, the I -index scheme can provide some additional information.

Based on the variability of the γ -ray flux, then, it is highly unlikely that 3EG J1837-0423 is caused by SNR G27.8+0.6, or by the pulsars PSR J1836-0436 (from Princeton Catalog) and PSR J1838-0453 (from Parkes Catalog). In addition, the spectral index for this 3EG source is very steep, possibly arguing against the pulsar hypothesis (Fierro et al. 1993), although it should be noted that Halpern et al. (2001) have recently presented a strong argument for the association of PSR J2229+6114 with 3EG J2227+6122, which a relatively soft index of 2.24 ± 0.14 .

Out of 19 sources in Table 1, 12 have the same classification under the two schemes; in Table 2, 6 out of 7 have the same classification. This confirms, for these sources, that the schemes are statistically correlated and that it is safe to consider both indices to smooth out any particular problem with singular

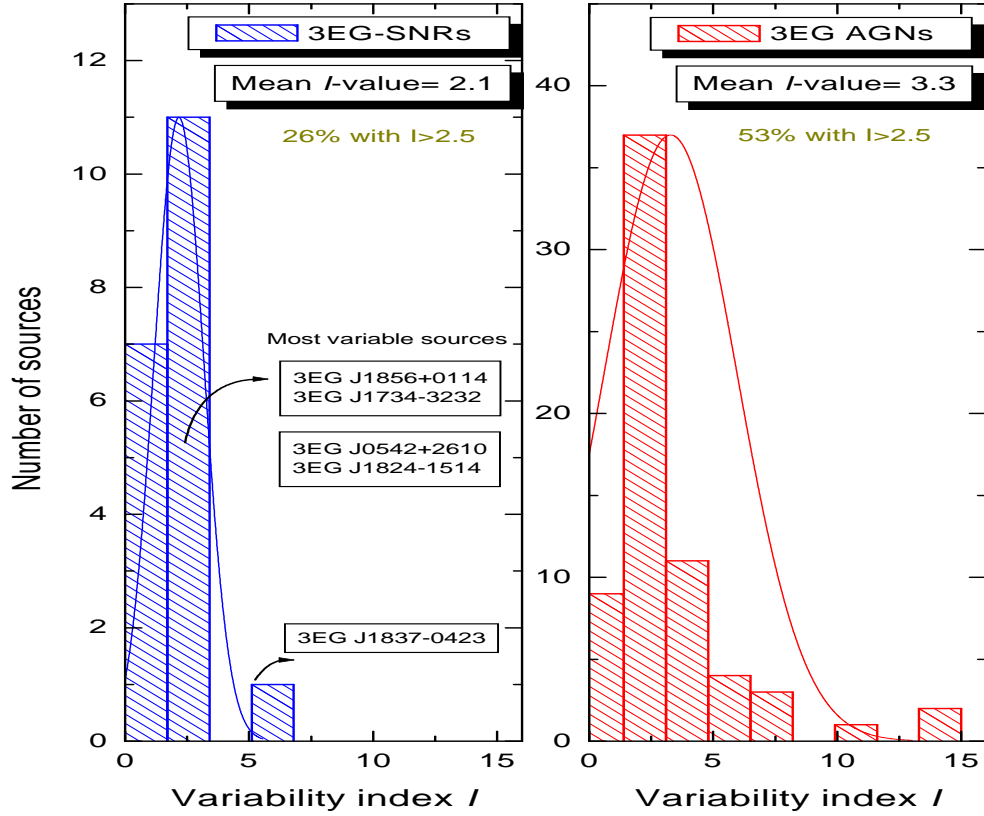


Figure 9: Comparison of the variability indices of the 3EG sources superposed with SNRs and identified 3EG AGNs.

sources, as apparently is the case for 3EG J0631+0642 and 3EG J0634+0521.

Figure 9 presents a comparison between the variability indices for those 3EG sources superposed to SNRs and the set of ‘A’ AGNs identified in the same catalog. The distributions are quite different, showing a more non-variable population in the case of the sources herein investigated. The most variable sources in the set are identified for reference.

9 Observations and data analysis

9.1 CO data

CO is a polar molecule with strong dipole rotational emission in the mm waveband, and is considered a reliable tracer of molecular hydrogen, H_2 , which, though much more abundant, has only a weak quadrupole signature. Throughout this paper, molecular gas masses are derived from observations of the $J=1-0$ rotational transition of CO at 115 GHz, assuming a proportionality between velocity-integrated CO intensity, W_{co} , and molecular hydrogen column density $N(H_2)$. Specifically, we adopt

$$N(H_2)/W_{\text{co}} = 1.8 \times 10^{20} \text{ cm}^{-2}\text{K}^{-1}\text{km}^{-1}\text{s}^{-1},$$

the value derived by Dame, Hartmann, & Thaddeus (2001) from an intercomparison of large-scale far-infrared, 21 cm, and CO surveys. To estimate total nucleon densities in molecular clouds, we account for elements heavier than hydrogen by assuming a mean molecular weight per H_2 molecule of 2.76.

All CO(1-0) data presented here are from the whole-Galaxy survey of Dame, Hartmann, & Thaddeus (2001). This survey is a composite of 37 separate CO surveys carried out over the past 20 years with two nearly identical 1.2 meter telescopes, one located at the Harvard-Smithsonian Center for Astrophysics in Cambridge, Massachusetts, and the other at the Cerro Tololo Interamerican Observatory in Chile. The angular resolution of the composite survey is ~ 8.5 arcmin and the velocity resolution ~ 1 km s $^{-1}$. Many of the 37 separate surveys have been published previously and, where appropriate, the earlier papers are cited instead of, or in addition to, Dame, Hartmann, & Thaddeus (2001).

In a few cases, observations of the CO(J=2-1) transition at the same angular resolution, obtained with the Tokyo-NRO 60 cm Survey Telescope (Sakamoto et al. 1995), are used to search for enhancements of the CO(J=2-1)/CO(J=1-0) ratio as an indicator of SNR-molecular cloud interaction (e.g., Seta et al. 1998).

9.2 Radio continuum data and diffuse background filtering

In general, the diffuse radio emission of the Galaxy hampers the detection of weak and extended sources with low surface brightness, like SNRs. This large-scale diffuse emission can be removed through different techniques for astronomical data analysis. These techniques can range from detailed modeling of the non-thermal emission in the Galaxy to model-independent filtering algorithms. In this work, many of the radio continuum maps have been cleaned of background diffuse contamination using the method originally introduced by Sofue & Reich (1979). Basically, the technique consists of convolving the continuum map with a Gaussian filtering beam, producing a new map with a different brightness temperature T_0^1 . A new temperature distribution is computed as $T_0'^1 = T - \Delta T^1$, for $\Delta T^1 > 0$ and $T_0'^1 = T$ for $\Delta T^1 < 0$. In these expressions, T is the temperature distribution of the original map, and $\Delta T^1 = T - T_0^1$ are the residuals between the original and the convolved maps. The procedure is repeated, now convolving the $T_0'^1$ map in order to obtain T_0^2 , ΔT^2 and finally $T_0'^2$. After n iterations, the difference $|T_0^n - T_0^{n-1}|$ becomes smaller than the rms noise, and a map of residuals $\Delta T^n = T - T_0^n$ is obtained where all diffuse emission with size scales larger than the original filtering beam has been removed. The result is completely independent of the original mechanism that produced the large-scale emission. In the following sections we apply this technique to Effelsberg 100m-telescope data and to the MOST Galactic plane survey in order to get images of the SNRs as clean as possible at low galactic latitudes.

10 Case by case analysis

10.1 γ -ray source 3EG J0542+2610 – SNR G180.0-1.7

The possible counterparts of this γ -ray source were explored in detail in a recent paper (Romero et al. 2001). No known radio pulsar coincides with this source (see Table 3). Additionally, a radio-quiet Geminga-like pulsar origin is disfavored a priori because of the high variability and the steep spectral index that this source presents ($\Gamma = 2.67 \pm 0.22$, Hartman et al. 1999). We have searched the EGRET location error box for other compact radio sources. Although 29 point-like radio sources were detected, none of them is strong enough to be considered a likely counterpart (Romero et al. 2001). The strongest of the sources detected have a radio flux one order of magnitude less than those presented by known γ -ray blazars detected by EGRET. Moreover, the absence of an X-ray counterpart to this source suggest that it is not an accreting

Please see the jpg file attached.

Figure 10: CO distribution around the remnant IC443 (G189.1+3.0). The 3EG γ -ray source J0617+2238 is superposed. Note the positional coincidence of the contours of the latter with part of the most dense regions of the CO distribution. The optical boundary of the SNR is superposed as a black contour. The optical emission seems to fade in regions where CO emission increases, this indicates that the molecular material is likely located on the foreground side of the remnant, absorbing the optical radiation. Optical contours are from Lasker et al. (1990). Astro-ph arXiv file: GIC433.jpg.

source, like a microquasar.

Some of us suggested that the only object within the 95% error box capable of producing the required γ -ray flux is the X-ray transient A0535+26. This Be/accreting pulsar, not detected at all in the radio band, can produce variable hadronic γ -ray emission through the mechanism originally proposed by Cheng & Ruderman (1989, 1991). See Romero et al. (2001) for further details.

On the basis of results discussed in that paper we conclude that 3EG J0542+2610 and G180.0-1.7 are most likely unrelated. An interesting comparison between this case and one of the EGRET sources coincident with the Monoceros Loop is made below.

10.2 γ -ray source 3EG J0617+2238 – SNR G189.1+3.0 (IC443)

A detailed description of SNR IC443 was given by Chevalier (1999). We have recently reviewed the spatially-resolved multiwavelength spectrum of IC443 and argued that the morphology and spectrum of the γ -ray emission make it a likely hadronic cosmic-ray accelerator (Butt et al. 2002b).

Seta et al.(1998) have provided an analysis of the CO environment of this remnant. They concluded,

Please see the jpg file attached.

Figure 11: Hard energy band (3–10 keV) of the IC443 nebula. Most of the thermal emission associated with IC443 is not present in this band. The image shows several point sources, besides the plerion nebula itself. The nebula can be represented by an ellipse of 8 arcmin \times 5 arcmin. The 95% confidence EGRET error circle for 3EG J0617+2238 is also shown. From Bocchino & Bykov (2001). Astro-pharXiv file: ic443-2.jpg.

as was previously reported by Scoville et al. (1977) and Cornett et al. (1977), that IC433 is interacting with several ambient molecular clouds with a total mass of about $10^4 M_\odot$. They also analyzed the ratio $R=CO(J=2-1)/(J=1-0)$ in the environs of IC443 and concluded that parts of the clouds presented an abnormally high value, consistent with shock interaction. The detected value of R exceeds 3 (the average galactic value is ~ 0.6) in some regions. Interestingly, the peak of the $CO(J=2-1)/(J=1-0)$ ratio is coincident with the location of the newly discovered pulsar wind nebula by Olbert et al. (2001), which may indicate an alternate way of exciting molecular gas. Dickman et al. (1992) has estimated that the total perturbed molecular gas has a mass of 500–2000 M_\odot .

In recent years, X-ray observations of IC443 have been carried out. IC443 was a target for X-ray observations with HEAO 1 (Petre et al. 1988), Ginga (Wang et al. 1992), ROSAT (Asaoka & Aschenbach 1994), ASCA (Keohane et al. 1997), and more recently, with Chandra and Beppo-SAX; we discuss the latter in more detail below. IC443 was believed to be mostly thermal in the X-ray band (Petre et al. 1988, Asaoka & Aschenbach 1994), although it has been discovered to emit hard X-ray emission (Wang et al. 1992). Keohane et al. (1997) later found that the hard X-ray emission was localized and non-thermal. They concluded that most of the 2–10 keV photons came from an isolated emitting feature and from the South East elongated ridge of hard emission. Even more recently, Preite Martínez et al. (1999) and Bocchino & Bykov (2000) reported a hard component detected with the Phoswich Detector System (PDS) on BeppoSAX and two compact X-ray sources corresponding to the ASCA sources detected with the BeppoSAX Medium-Energy Concentrator Spectrometer (MECS) (1SAX J0617.1+2221 and 1SAX J0618.0+2227). 1SAX J0617.1+2221 has also been observed with the Chandra satellite by Olbert et al.

2001, who also obtained VLA observations at 1.46, 4.86 and 8.46 GHz and a polarization measurement. The hard radio spectral index, the amount of polarization, and the overall X-ray and radio morphology led them to suggest that the source is a plerion nebula containing a point source whose characteristic cometary shape is due to supersonic motion of the neutron star. Bocchino & Bykov (2001) have, in addition, recently observed IC443 with XMM-Newton Observatory (see Figure 11). They resolve the structure of the nebula into a compact core with a hard spectrum of photon index $\gamma = 1.63_{-0.10}^{+0.11}$ in the 2–10 keV energy range, and found that the nebula also has an extended (~ 8 arcmin \times 5 arcmin) X-ray halo, much larger than the radio emission extension. The photon index softens with distance from the centroid, a behavior also found in other X-ray plerions such as 3C58 and G21.5-0.9. Bocchino & Bykov (2001) also looked for periodic signals from the NS but found none with 99% confidence level in the $10^{-4} - 6.5$ Hz range. Assuming that $L_X/\dot{E} \sim 0.002$, the spin-down luminosity of the central object results in $\dot{E} = 1.3 \times 10^{36}$ erg s $^{-1}$. If the power-law spectrum of the nebula core region were extrapolated up to the GeV regime, it would provide a flux of $2.0 (0.4-15.2) \times 10^{-7}$ ph cm $^{-2}$ s $^{-1}$, which is consistent with the EGRET flux from the IC443 region (see Table 1). However, the fact that the nebula lies outside the 95% confidence circle of the source argues against an association. Further, the EGRET source luminosity would require a substantial fraction of the estimated spin-down power.

The H₂ mass near SNR IC443 that we report here, $1.1 \times 10^4 M_\odot$, is the total molecular mass in the IC443 velocity range, $v = -40$ to $+20$ km s $^{-1}$, within a rectangle enclosing the main clump coincident with the SNR: $l=188.75$ to 189.5 , $b=2.5$ to 3.375 , see Figure 10. The average density of that region is about 840 nucleons cm $^{-3}$.

Assuming that the energy of the explosion was $E_{51} = 0.27$, and an unshocked density of 0.21 cm $^{-3}$ (from a 2D dynamic model by Hnatyk and Petruk 1998), we found that the hadronic flux would be 4.7×10^{-6} photons cm $^{-2}$ s $^{-1}$. Indeed, just 10% of the ambient mass is necessary to produce the observed flux of 3EG J0617+2238.

The energy of the explosion and the unshocked density yield a CR enhancement factor, $k_s \sim 600$ within the SNR, which appears to be unusually high. However, computation of the energy transformed into cosmic rays by the direct product $k_s \epsilon_{\text{CR}} (4/3\pi R^3)$ gives $0.4E_{51}$, a value compatible with that obtained for θ (the efficiency of SN energy conversion to CRs) in the Morfill et al. (1984) prescription discussed above. Alternatively, by direct use of Eq. (13), and using the mass considered above and the observed γ -ray flux, we can obtain an estimate of the enhancement factor k_s of 66. The difference between the CR enhancement factor of the cloud ($k_s = 66$) and the SNR ($k_s = 600$) could be explained in a variety of ways: most simply, that the CR enhancement predicted by the Morfill et al. (1984) prescription for SNRs overestimates the value within the adjacent cloud. Particularly if the cloud abuts the remnant, its enhancement will naturally be smaller than that calculated for the SNR interior. As Figure 10 shows, the optical emission seems to fade in regions where CO emission increases, which perhaps indicates that the molecular material is absorbing the optical radiation, abutting the remnant on the near side. The report by Cornett et al. (1977) also argues that the molecular mass is located between us and the SNR. In any case, we remark that the previous estimations of the CR enhancement factors assume that the explosion proceeds in an homogeneous medium, something which we know is not true in this case (Chevalier 1999).

We note that an electronic bremsstrahlung hypothesis for the origin of the GeV flux (eg. Bykov et al. 2000) is difficult to reconcile with the fact that the radio synchrotron emission is concentrated towards the rims of the remnant, whereas the GeV source is centrally located (Figure 10).

It is clear that IC443 will continue to be a primary target for future satellites missions and telescopes.

Please see the jpg file attached.

Figure 12: Left: CO contours (white) on a background image from the Digital Sky Survey. The map covers a somewhat larger region than the left panel Figure, and shows the HII region and young cluster NGC 2244 producing a hole in the cloud. Most of the Monoceros Loop is also seen faintly. EGRET sources contours are marked in black. Right: CO emission plus contours (black) of 1.4 GHz emission to mark the Rosette Nebula. The peak of the CO emission is near 3EG J0634+0521. The position of the X-ray source SAX J0635+0533 is marked with a star. White lines are the confidence levels of the EGRET sources. Astro-ph arXiv files GMon1.jpg and GMon2.jpg.

A better localization of the EGRET sources, by AGILE, or GLAST, as well as the already approved INTEGRAL observations could help much in determining the ultimate nature of 3EG J0617+2238. The reader is referred to Butt et al. (2002b) for further analysis of the likely hadronic origin of the γ -ray emission.

10.3 γ -ray source 3EG J0631+0642 and 3EG J0634+0521 – SNR G205.5+0.5 (Monoceros nebula)

The large SNR G205.5+0.5 (Monoceros Loop nebula, 220 arcmin in size) has been thoroughly studied in the past. Various papers have proposed that the Monoceros Loop SNR is interacting with the Rosette Nebula (e.g., Odegard 1986). A recent study of the stars in NGC 2244, the cluster within the Rosette, finds a distance of 1.39 ± 0.1 kpc (Hensberge et al. 2000); we assume this distance in the following computations. In the left panel of Figure 12, we show an overlay of the CO contours on an image from the Digital Sky Survey (Lasker et al. 1990). It shows very nicely the HII region and young cluster apparently carving a hole in the cloud. Most of the Monoceros Loop is also seen very faintly. This justifies the distance adopted, under the assumption that the Nebula and the Monoceros Loop are equally distant from Earth. Bloemen et al. (1997) presented COMPTEL observations of the Monoceros region, and found excessive 3-7 MeV emission which they attributed to nuclear deexcitation lines at 4.44 and 6.13 MeV from accelerated ^{12}C and ^{16}O nuclei.

Monoceros was already suggested by Esposito et al. (1996) as a source of γ -rays, and it was also mentioned by Sturner and Dermer (1995) and Sturner, Dermer and Mattox (1996) as a possible case of γ -rays production by hadronic interactions. The age of the remnant is not well determined, $3\text{--}20\ 10^4$ yrs. A study of Einstein IPC data (Leahy et al. 1986) shows diffuse X-ray thermal emission in a region corresponding to the detection of optical filaments (Odegard 1986). This is only possible if the gas is sufficiently hot, and thus if the remnant is sufficiently young. This would be in contradiction with the age one obtains from the homogeneous Sedov solutions, which would give an age in excess of 100,000 yrs. One direct interpretation of this discrepancy (Leahy et al. 1986) is that the expansion of the remnant proceeds in a non-homogeneous multi-component medium, where the homogeneous Sedov solutions are not valid.

A large region covering the spatial extent of both 3EG sources was studied by Jaffe et al. (1997): ($198 < l < 214$, and $-6 < b < 8$). They presented an image reconstruction of the region around the Rosette Nebula and Monoceros using high-energy (>100 MeV) γ -ray data from EGRET. The resulting image showed a 7σ extended feature in excess of the expected diffuse emission located at the point-source position listed in the EGRET catalog (2EG at that time). These authors proposed that this excess could be evidence of an interaction between the Monoceros remnant and the Rosette nebula. They concluded that if the γ -ray emission arises solely in the interaction between the two nebulae then the cosmic-ray enhancement would be around $k_s=300$. This value appears to be excessively high in this case, should the enhancement be the same for all the SNR region. The energy in cosmic-rays, computed using $k_s\epsilon_{\text{CR}}(4/3\pi R^3)$ together with the size of the Monoceros remnant (~ 60 pc), imply an energy of the explosion about one order of magnitude larger than the assumed $E_{51} \sim 1$. This may indicate that the hadronic origin of the γ -rays in the interaction of the Monoceros SNR and the Rosette Nebula (i.e. 3EG 3EG J0634+0521) cannot be responsible for the entire observed flux.

Indeed, within the 95% contour of 3EG J0634+0521 there exists an X-ray source SAX J0635+0533, and a Be-star/neutron-star X-ray binary pulsar, probably with a relatively short orbital period (Kaaret et al. 1999, Cusumano et al. 2000, Nicastro et al. 2000). The hard X-ray source SAX J0635+0533 shows pulsations at a period of 33.8 ms but no radio flux was detected at the Be-star position (see below). SAX J0635+0533 might be, as in the case of A0535+26 mentioned above, a source of γ -rays through hadronic processes. Kaaret et al. (1999) suggested that SAX J0635+0533 and 3EG J0634+0521 are related. One fact favoring this physical association is that the SAX satellite has not detected extended emission in the region of 3EG J0634+0521, as would be the case if the bulk of the radiation were produced in a SNR shock. Additionally, the probability for chance positional coincidence between a Be/X-ray binary and an EGRET source is less than 4% (Kaaret et al. 1999).

The situation, however, is far from resolved. The EGRET source, for instance, is non-variable as it would be expected for a binary with eccentric orbit. Recent results reported by Kaaret et al. (2000), comparing observations obtained with BeppoSAX and RXTE separated in time by 2 years, showed that the period derivative of the pulsar has a lower bound equal to 3.8×10^{-13} . This value is 30 times larger than values found from accreting neutron stars (Bildsten et al. 1997), and it implies a mass accretion rate of $6 \times 10^{-7} M_\odot \text{ yr}^{-1}$ (Kaaret et al. 2000, Bildsten et al. 1997), which far exceeds the expected mass capture rate of a neutron star $\sim 10^{-11} M_\odot \text{ yr}^{-1}$, and is even slightly larger than the average mass loss rate of Be-stars (Kaaret et al. 2000). Apparently, this would indicate that the X-ray luminosity does not originate in the accretion disk, and argues in favor of SAX J0635+0533 being a rotation powered pulsar. In this case, the value of \dot{P} would imply a characteristic age of only 1400 years and a high spin-down luminosity of $5 \times 10^{38} \text{ erg s}^{-1}$, out of which less than 0.05% could make a noticeable contribution to the observed γ -ray flux (assuming a distance of 4 kpc, Kaaret et al. 1999). Additionally, arguing against an accretion

origin of the radiation, the derived X-ray luminosity ($7.7 \times 10^{34} (d_{\text{kpc}}/4 \text{ kpc})^2 \text{ erg s}^{-1}$) and magnetic field strength ($\sim 10^9 \text{ G}$) are too low in comparison to other Be-X-ray binaries such as A0535+26 (Cusumano et al. 2000).

Very recently, Monoceros was the target of the HEGRA Čerenkov telescopes (see Lucarelli et al. 2001). HEGRA observed the Monoceros-Rosette region for about 120 hours, with an energy threshold of 500 GeV and an angular resolution of 0.1 deg, and mapped a $2 \times 2 \text{ deg}^2$ region centered in the source SAX J0635+0533. The EGRET source 3EG J0634+0521 is also within the field of view. Although the flux and spectrum have not yet been officially reported, HEGRA found a tentative excess of counts in four different pixels ($0.2 \times 0.2 \text{ deg}^2$) within the 3EG contours; interestingly, none of them coinciding with SAX J0635+0533 (Lucarelli et al. 2001). It is possible that TeV emission coming from the binary is being re-absorbed in its neighborhood, as in the case studied by Romero et al. (2001).

What HEGRA observations seem to imply is that the marginally significant TeV radiation has an extended origin, different from that producing GeV photons in the binary system SAX J0635+0533, but this remains to be confirmed.

In the right panel of Figure 12 we show the CO emission plus contours of 1.4 GHz continuum emission marking the Rosette. Using the standard CO-to- H_2 mass conversion and a mean molecular weight per H_2 molecular of 2.76, we calculate a total H_2 mass for the associated cloud (in the region $l = 205$ to 209 , $b = -3$ to -1 , and velocity range $v = -5$ to 30 km s^{-1}) of $1.2 \times 10^5 M_\odot$. We have calculated the molecular masses in small rectangles enclosing the two 3EG sources near the Rosette. Using a distance of 1.39 kpc we get the following results: In the case of 3EG J0634+0521 the region considered is $l = 205.5$ to 206.875 and $b = -2.125$ to -0.375 , and the mass is $2.0 \times 10^4 M_\odot$. For 3EG J0631+0643, in the region $l = 204.25$ to 205.5 and $b = -2.125$ to -0.75 , the mass is $4.7 \times 10^4 M_\odot$. In both cases, the velocity range considered is $v = -5$ to 30 km s^{-1} and the formal error on these masses, based on the instrumental noise, is $\sim 0.2 \times 10^3 M_\odot$.

Because of uncertainties on the nature of this SNR (for instance, the controversy on the SNR age) Mорfill et al.'s method is unreliable for estimating the SNR GeV-flux. However, using directly Eq. (13) and the observed flux (Table 1), we can estimate the value of k_s needed to generate the observed flux, resulting in $k_s \sim 6.5$ for 3EG J0634+0521. Because of the high molecular density, just a modest enhancement of the cosmic-ray density can explain a substantial part of the detected γ -ray flux. We suggest, then, that 3EG J0634+0521 might be a composite source: SAX J0635+0533 might be responsible for part of the GeV flux, as well as the bulk of the emission at X-ray energies. The interacting SNR and Rosette Nebula might also contribute to the flux in the GeV range, and would provide the bulk of the possibly detected TeV emission from the region. One direct way to test this scenario would be through an analysis of the spectrum from GeV to TeV. In the case of a composite source, there should be a break in the spectrum between GeV and TeV energies, the latter corresponding only to the accelerated particles in the SNR remnant.

In the case of 3EG J0631+0643, a CR enhancement value of just $k_s \sim 3$ can explain the observed GeV flux. New high-sensitivity radio measurements of the region would be of great value in determining the relative importance of hadronic and leptonic γ -ray emission.

10.4 γ -ray source 3EG J1013-5915 – SNR G284.3-1.8 (MSH 10-53)

For this 3EG source, a natural candidate to generate a significant part of the γ -ray emission seems to be the recently discovered pulsar PSR J1013-5915; see Table 3 (Camilo et al. 2001). This pulsar has a

Please see the jpg file attached.

Figure 13: (a) Longitude-velocity map of CO integrated over 1 degree of Galactic latitude roughly centered on the SNR G284.3-1.8 (MSH 10-53), $b = -2.5$ to -1.5 . The longitude of the SNR is indicated by the dotted vertical line. (b) Spatial map of CO integrated over the velocity range -22 to 3 km s^{-1} . The plus sign marks the center position of the SNR G284.3-1.8, whose size is 25 arcmin. The dotted circle is the 95% confidence radius about the position of 3EG J1013-5915 (Hartman et al. 1999). Note that the longitude range (x axis) of both maps is the same. Astro-ph arXiv file: G284.jpg.

characteristic age of $\tau = 21$ kyr and a spin-down luminosity of $\dot{E} = 2.6 \times 10^{36}$ erg s $^{-1}$. If only the pulsar is considered, the efficiency required for converting spin-down luminosity into γ -rays is $\eta \sim 0.5\%$ (Camilo et al. 2001), well within the range of efficiencies for previously confirmed γ -ray pulsars detected by EGRET.

Another Parkes' pulsar, PSR J1013–5934, is also coincident with 3EG 1013–5915, but it can be ruled out on the basis of energetic arguments. So also the Princeton pulsar PSR J1012-5857 (Table 3), which requires an efficiency of about 100% in the generation of the γ -ray emission from the spin-down losses. It is also interesting to note that 3EG J1013–5915 has a photon spectral index softer than typical for pulsars: $\Gamma = 2.32 \pm 0.13$.

The remnant is located in the near side of the Carina spiral arm, in a region with a high density of molecular clouds. Ruiz & May (1986) found filamentary optical emission associated with the remnant. These authors also found clear evidence of at least three small CO clouds interacting with G284.3-1.8. Other small clouds could have been disrupted by the supernova blast wave and are now forming the shell. Their CO(J=1-0) mm line data shows sudden changes with position in radial velocity, and the presence of broad asymmetric lines with peak-shoulder profiles, both of which indicate a shock wave disruption of the CO clouds. Since Ruiz & May (1986) gave only an upper limit for the mass of the shell, we have re-analyzed the gas content for this region. As the longitude-velocity map in Figure 13a shows, nearly all CO emission in the general direction of the 3EG source and the SNR G284.3-1.8 lies in the velocity range -22 to 3 km s $^{-1}$. A CO map integrated over this range is shown in Figure 13b. The mean velocity of the emission is ~ -9 km s $^{-1}$, which is consistent with the terminal velocity in this direction, suggesting a distance of approximately 2.1 kpc. However, since radial velocity changes very slowly with distance in this direction, the uncertainty on the kinematic distance is large, approximately ± 1 kpc. We adopt a distance of 2.9 kpc, the value inferred by Ruiz & May (1986) based on optical observations of the SNR filaments, the $\Sigma - D$ distance, as well as the CO kinematics.

There is no CO detected at any velocity toward the nominal center of the 3EG source ($l = 283.93$, $b = -2.34$), although the total molecular mass within the 95% confidence radius of the 3EG source (dotted circle in Figure 13b) is $5.9 \times 10^4 M_{\odot}$. Most of this mass does not coincide with the SNR, which is completely included within the 3EG source. Since this emission does not form a single well-defined cloud, it's possible that it arises from gas spread over quite a large distance along the line of sight, perhaps 1 – 2 kpc. If so, the gas density near the SNR could be quite low. Our study therefore reinforces the idea that it is most likely the pulsar, and not the hadronic or bremsstrahlung emission from the SNR neighborhood, that is responsible for 3EG J1013-5915.

In the TeV regime no observations of this southern remnant have yet been made. For the ~ 25 arcmin diameter of the SNR, the sensitivity of HESS is expected to be $\sim 1.5 \times 10^{-12}$ erg cm $^{-2}$ s $^{-1}$ at 100 GeV and $\sim 2.5 \times 10^{-13}$ erg cm $^{-2}$ s $^{-1}$ at 1 TeV (a 5σ detection with at least 10 detected photons in 50 hours).

10.5 γ -ray source 3EG J1102-6103 – SNR G290.1-0.8 (MSH 11-61A)/289.7-0.3

Sturner & Dermer (1995) proposed that this γ -ray source, in its 2EG J1103-6106 incarnation, may have been related to SNR G291.0-0.1. However, the more precise localization in the 3EG catalog shifted the source's position such that it is no longer superposed with that SNR.

Zhang & Cheng (1998) argued against a newly discovered young radio pulsar, PSR J1105-6107 (Kaspi et al. 1997), as the source of the observed high-energy γ -ray emission. Its age ($\sim 6.3 \times 10^4$ yr) also seems high for a Vela-like pulsar. In addition, the photon spectral index is very soft, $\Gamma = 2.47 \pm 0.21$, though

Please see the jpg file attached.

Figure 14: CO integrated over the velocity range of the far Carina arm, 0 to 45 km s^{-1} . Contours: 843 MHz continuum from the MOST Galactic plane survey (Green 1997); the survey has been smoothed to a resolution of 3 arcmin to highlight extended sources. The contour interval is 0.04 Jy/beam, starting at 0.04 Jy/beam. The dotted circle is the 95% confidence radius about the position of 3EG 1102-6103 (Hartman et al. 1999). G290.1-0.8 is the SNR MSH 11-61A (Kirshner & Winkler 1979). Both HII regions are in the catalog of Georgelin & Georgelin (1970) and have recombination line velocities in rough agreement with that of the complex. The component clouds A and B are discussed in the text. Astro-ph arXiv file: G290.jpg.

this in itself does not disqualify a possible pulsar origin, as seen in the case of PSR J2229+6114/3EG J2227+6122 (Halpern et al. 2001b).

The line of sight to 3EG 1102-6103 intersects both the near and far sides of the Carina spiral arm, at velocities near -20 km s^{-1} and $+20 \text{ km s}^{-1}$ respectively. There is a distinct gap in the near side of the Carina arm in the direction of the 3EG source, with almost no molecular gas within $\sim 1 \text{ deg}$ of the source direction (see, e.g., Figure 2 of Dame, Hartmann, & Thaddeus 2001). On the other hand, as Figure 14 shows, there is a very massive molecular complex in the far Carina Arm overlapping the direction of the 3EG source; this complex is No. 13 in the Carina Arm cloud catalog of Grabelsky et al. (1988). There is little doubt that the two component clouds labeled A and B in Figure 14 are part of the same complex, since they have approximately the same velocity of 22 km s^{-1} , and are connected smoothly by weaker emission, also at the same velocity. Also, the HII regions are evidence of abundant on-going star formation in this molecular complex which additionally supports the association of the SNR. Assuming a flat rotation curve beyond the solar circle, the kinematic distance of the complex is 8.0 kpc and its total molecular mass is $2.1 \times 10^6 M_\odot$.

It is worth noting that the composite CO line profile of cloud B is very broad and complex, suggesting

possible interaction with SNR G290.1-0.8. In the case of cloud A, its radius (~ 48 pc) and composite linewidth (17 km s^{-1} FWHM) are roughly consistent with the radius-linewidth relation found for large molecular complexes by Dame et al. (1986). For cloud B, however, its linewidth ($\sim 27 \text{ km s}^{-1}$) is about a factor of 3 too large compared to its radius (~ 28 pc). We can also see that the coinciding SNR G289.7-0.3 is far from Cloud B, in a region of low molecular density. It is extremely unlikely that this SNR is related with the 3EG source in question. The only remaining candidate is, then G290.1-0.8. The total molecular mass within the 95% confidence radius of the 3EG source (dotted circle in Figure 14) is $7.7 \times 10^5 M_\odot$ and most of it is localized in Cloud B ($4.5 \times 10^5 M_\odot$).

Assuming typical values for the energy of the explosion ($E_{51}=1$) and the unshocked ambient density ($n = 0.1 \text{ cm}^{-3}$) we obtain a CR enhancement factor of ~ 250 . Assuming that the same CR enhancement is applicable to the cloud overpredicts the EGRET flux by about a factor of 10. Thus, it is likely that the average CR enhancement factor within the cloud is ten times lower than within the SNR, a reasonable result. It is possible, then, that 3EG J1102-6103 and SNR G290.1-0.8 are indeed related. Note that Bremsstrahlung, which we have neglected here, will contribute still more to the predicted flux from SNR-cloud interactions. If the outlined scenario is correct, GLAST and AGILE ought to observe a strong, compact γ -ray source coincident with the position of Cloud B.

An alternative, and promising, hypothesis for explaining the high-energy emission is stellar winds collisions, as developed by Eichler & Usov (1993). Recently, Contreras et al. (1997) have provided convincing evidence for non-thermal radio emission from the colliding winds region in the stellar system Cygnus OB2 No 5. The position of their radio-imaged shocked region is consistent with the inferred location of the contact discontinuity of the wind-wind interaction of the constituent stars. Benaglia et al. (2001) have argued that the source 3EG J2033+4118 could be mainly due to inverse Comptonization of the stellar photons by the locally accelerated electrons. Similarly, in the present case, 3EG J1102-6103 might be the result of γ -ray production by the stellar winds of the early-type stars WR37, WR38, WR38B and WR39, all located within the 95% confidence contour of the γ -ray source and at 2 kpc from the Sun. In particular, WR39 presents an unusually strong wind with a terminal velocity of about 3600 km s^{-1} (Romero et al. 1999a and references therein). Non-thermal radio emission at the mJy level has been recently detected at ~ 3 arcsec from the optical position of the star by Chapman et al. (1999). This emission is a clear indication of the existence of a population of relativistic electrons in the region. Chapman et al. (1999) have suggested that particle acceleration could be occurring at the region where the wind of WR39 collides with the wind of the neighboring Wolf-Rayet star WR38B. This hypothesis is supported by the fact that synchrotron radiation is located between both stars (2 arcsec from WR38B). The relativistic electrons should interact with UV photons from the star, producing IC γ -rays that could explain part of the emission of 3EG J1102-6103.

Fortunately, the peak of the spectral energy distribution should be in the IBIS energy range, the imager on-board INTEGRAL. Using Benaglia et al.'s (2001) model with a spectral index of -2 , we get an integrated flux for the energy interval 100 keV - 200 keV of $1.2 \times 10^{-4} \text{ ph s}^{-1} \text{ cm}^{-2}$. For the entire IBIS energy range (20 keV-10 MeV) the expected value is $1.2 \times 10^{-3} \text{ ph s}^{-1} \text{ cm}^{-2}$. In addition to this wind-wind contribution, single stars might also be sources of γ -rays in the IBIS energy band through the IC emission of electrons locally accelerated in shocks at the base of the winds. These shocks are produced by line-driven instabilities (see Chen & White 1991 for a discussion of γ -ray emission from single stars, and Benaglia et al. 2001 for a particular application).

Consequently, further study of the possible association of 3EG J1102-6103 with the SNR G290.1-0.8 (MSH 11-61A) is of the utmost importance, since there are at least two scenarios (aside from the pulsar possibility) that might well contribute to the observed γ -ray flux.

Please see the jpg file attached.

Figure 15: CO integrated over the velocity range of the Centaurus arm, -75 to -35 km s^{-1} . Contours: 843 MHz continuum from the MOST Galactic plane survey (Green et al. 1999); the survey has been smoothed to a resolution of $3'$ to highlight extended sources. The contour interval is 0.01 Jy/beam, starting at 0.01 Jy/beam. The dotted circle is the 95% confidence radius about the position of 3EG J1410-6147 (Hartman et al. 1999). Many of the other radio sources in the map are unrelated HII regions discussed by Caswell & Barnes (1985). Astro-ph arXiv file: G312.jpg.

10.6 γ -ray source 3EG J1410-6147 – SNR G312.4-0.4

Although there is no correlated Princeton pulsar within the contours of 3EG J1410-6147, there are two Parkes pulsars near the γ -ray source (see Table 3 above). Both of them require an unreasonable efficiency, at their dispersion-measure distances, to explain the observed γ -ray flux. Both pulsars are located (at least in projection) well within the boundaries of the incomplete shell of SNR G312.4-0.4 (Caswell & Barnes 1985), to which Yadigaroglu & Romani (1997) estimate a $\Sigma - D$ distance of 1.9 kpc, whereas Case & Bhattacharya (1999) find 3.1 ± 1.0 kpc. At either of these distances, the required efficiencies would be substantially smaller. The photon spectral index of the γ -ray source, $\Gamma = 2.12 \pm 0.14$, seems to be in the range of other pulsar cases. More recently, Doherty et al. (2002) have provided important new HI absorption measurements toward SNR G312.4-0.4 which indicate that it may be much further away, 8.1 kpc (see below).

Case & Bhattacharya (1999) have made an in depth study of the possible association between the rem-

nant and the γ -ray source and concluded that the γ -ray data alone cannot at present provide conclusive evidence to decide whether the γ -ray emission from 2EG J1412-6211 is due to a pulsar or SNR-molecular cloud interaction, or both. They suggested that CO observations of the environment surrounding G312.4-0.4 would help in determining whether a molecular cloud of sufficient mass is present in the right location to produce the observed γ -ray intensity. Such observations are presented here.

The CO emission toward 3EG 1410-6147 is extremely bright and complex, arising mainly from the tangent region of the Centaurus spiral arm at $v < -30 \text{ km s}^{-1}$. The line of sight also intersects the near side of the Carina arm at less negative velocities and the far side of Carina at positive velocities. The cloud in the general direction of the 3EG source is also by far the most massive and dense. This cloud, with a velocity of -49 km s^{-1} , is labeled A in Figure 15. The near and far kinematic distances of the cloud are 3.3 kpc and 8.1 kpc respectively (Clemens 1985); we will adopt the far kinematic distance since it agrees with the HI absorption measurements of Doherty et al. (2002) towards SNR G312.4-0.4.

The mass of Cloud A is quite uncertain owing to the fact that molecular gas in both the near and far sides of the Centaurus arm probably contribute to the CO emission at the cloud velocity; the high-velocity limit of the cloud is also uncertain owing to blending with emission at higher (less negative) velocities. If we assume that all of the emission in the velocity range of Figure 15 (-75 to -35 km s^{-1}) arises from cloud A at 8.1 kpc, the total molecular mass within the 95% confidence radius of the 3EG source (dotted circle in Figure 15) is $3.3 \times 10^5 M_\odot$; given the uncertainties just discussed, the actual mass might be as much as a factor of 2 lower.

Even at such a distance, the large quantity of molecular material is sufficient to explain a significant part of the γ -ray flux observed. As in the case of 3EG 1102-6103, with the usual assumptions, a CR enhancement factor of ~ 100 is necessary to explain the bulk of the γ -ray emission from 3EG J1410-6147. It is most likely, however, that this EGRET source is a composite. New X-ray observations could be used to study the pulsars and evaluate their γ -ray emissivities. An extrapolation of the GeV spectrum to the TeV regime, if there is no break, would give a flux of $1 \times 10^{-10} \text{ erg cm}^{-2} \text{ s}^{-1}$, which is above the HESS sensitivity in the range 500 GeV–10 TeV. Even with a substantial break in the spectrum the 3EG source should be observable by HESS (see the study on SNR TeV observability below, Section 12.1).

10.7 γ -ray source 3EG J1639-4702 – SNR G337.8-0.1/338.1+0.4/338.3+0.0

Figure 16 shows the relative positions of these SNRs within the large location contours of 3EG J1639-4702. One Princeton pulsar is within the contour of 3EG 1639-4702, but it can be ruled out as a possible counterpart because of the required energetics. In addition, three Parkes pulsars coincide with the same 3EG source (see Table 3). Two of them can be immediately discarded based on the same grounds: the required efficiencies are unphysically high. However, PSR J1637-4642 seems to be a plausible candidate. Only a 12% efficiency would be needed to convert this pulsar into a plausible counterpart for the origin of the γ -ray emission. Although the spectral index, $\Gamma = 2.50 \pm 0.18$, seems quite soft in comparison with detected EGRET pulsars, the work of Halpern et al. (2001) suggests that a soft spectral index does not automatically rule out a pulsar origin of the γ -rays: they present a strong case for PSR J2229+6114 being responsible for 3EG J2227+6122, even though it has a high-energy spectral index of 2.24 ± 0.14 .

Based on HI absorption seen all the way up to the terminal velocity, Caswell et al. (1975) placed the SNR G337.8-0.1 beyond the tangent point at 7.9 kpc. Koralesky et al. (1998) detected maser emission in the SNR at -45 km s^{-1} , implying a far kinematic distance of 12.4 kpc. As Figure 17 shows, there is a very massive giant molecular cloud adjacent to the SNR in direction and close to the associated maser in

Please see the jpg file attached.

Figure 16: Relative positions of 3EG J1639-4702 (which occupies all the box) and the SNRs G333.8-0.1, G338.1+0.4, and G338.3+0.0, which are very small in comparison. The superposed grey-scaled levels show the radio emission at 843 MHz of the three SNRs as reported in the MOST Catalog prepared by Whiteoak and Green (1996). Astro-ph arXiv file: G338-1.jpg.

velocity (-56 km s^{-1}). The far kinematic distance for this giant molecular cloud is favored by (1) its likely association with both the far-side maser just mentioned and a group of far-side HII regions (group 5 in Georgelin & Georgelin 1976); (2) its location very close to the Galactic plane; and (3) the radius linewidth relation for giant molecular clouds (Dame et al. 1986). The mean velocity of the complex is -56 km s^{-1} , implying a far kinematic distance of 11.8 kpc.

The giant molecular cloud has recently been discussed by Corbel et al. (1999) because an adjacent cloud (just outside the velocity integration range of Figure 17) apparently harbors the soft γ -ray repeater SGR 1627-41. Corbel et al. suggest that collision or tidal interaction between these two giant molecular clouds may have set off the burst of star formation evident in both.

Taking the total CO luminosity of the giant molecular cloud to be that in the range $l = 337.625$ to 338.25 , $b = -0.25$ to 0.25 , and $v = -65$ to -45 km s^{-1} , the total molecular mass is $5 \times 10^6 M_\odot$; this mass may be overestimated by 10-20% owing to the inclusion of emission from gas at the same velocity at the near kinematic distance. Even with this correction, this giant molecular cloud ranks among the few most massive GMCs in the Galaxy (see, e.g., Dame et al. 1986); its composite CO linewidth of $\sim 20 \text{ km s}^{-1}$ is correspondingly very large. Adopting a mean radius of 0.31 deg, or 65 pc at 11.8 kpc, the mean nucleon density of the cloud is 176 cm^{-3} . The total mass within the 95% confidence radius of the 3EG source is $7.6 \times 10^6 M_\odot$; this mass too may be overestimated by 10-20% owing to inclusion of near-side emission.

The enhancement factor obtained from Eq. (15) is large for typical parameter values. However, since

Please see the jpg file attached.

Figure 17: CO integrated over the velocity range -65 to -45 km s⁻¹. Contours: 843 MHz continuum from the MOST Galactic plane survey (Green et al. 1999); the contour interval is 0.2 Jy/beam, starting at 0.1 Jy/beam. The dotted circle is the 95% confidence radius about the position of 3EG J1639-4702 (Hartman et al. 1999). Astro-ph arXiv file: G338.jpg.

the SNRs seems to be immersed in the molecular cloud, the Morfill et al. (1984) prescription may be an oversimplification in this case. This case is similar to that of 3EG J1903+0550 in that we have a distant SNR that we would not expect to be able to detect with EGRET in the neighborhood of a very large molecular cloud. AGILE observations, in advance of GLAST, would greatly elucidate the origin for this 3EG source, since even a factor of 2 improvement in resolution would be enough to favor or reject the SNR connection.

, where we find a far SNR, which we would expect not to be able to detect using EGRET, in the neighborhood of very large concentrations of molecular material. AGILE and GLAST observations would, of course, help much in the elucidation of the origin for this 3EG source, since even improving the resolution by a factor of just 2 could be enough to favor or reject the SNR connection.

10.8 γ -ray source 3EG J1714-3857 – SNR G348.5+0.0/348.5+0.1/347.3-0.5

The supernova remnant RX J1713.7-3946 is probably the most convincing case for a hadronic cosmic-ray accelerator detected so far in the Galaxy. Butt et al. (2001) noted the positional coincidence of the nearby γ -ray source 3EG J1714-3857 with a very massive ($\sim 3 \times 10^5 M_\odot$) and dense (~ 500 nucleons cm⁻³) molecular cloud that is clearly interacting with the SNR RX J1713.7-3946 (G347.3-0.5) (Slane et al., 1999; Butt et al., 2001). Figure 18 shows the CO(J=1-0) line intensity distribution in the vicinity of the SNR. The remnant is a strong X-ray source (Slane et al. 1999) whose ROSAT contours are indicated in the figure. Two massive clouds, which we called Cloud A and Cloud B, can be seen. The first one is coincident with the γ -ray source 3EG J1714-3857, whose location confidence contours are also superposed in the figure. The X-ray emission is produced by TeV-range electrons radiating by the synchrotron mechanism in

Please see the jpg file attached.

Figure 18: Intensity map of the CO(J=1-0) transitions in the region around RX J1713.7-3946, from Butt et al. (2002a). Two massive clouds, called Cloud A and Cloud B, are indicated. The X-ray contours of the SNR (Slane et al. 1999) are superposed in black, as well as the location confidence contours of the GeV γ -ray source 3EG J1714-3857 (coincident with Cloud A) and the significance contours of the TeV detection of the remnant by Enomoto et al. (2002), mostly coincident with the X-ray radiation. Astro-ph arXiv file: G347.jpg.

the local magnetic field. These same electrons were suggested to be responsible, through IC up-scattering of cosmic microwave background photons, for the TeV γ -ray emission detected from the NW rim of the remnant by Muraishi et al. (2000) and Butt et al (2002a).

We have previously provided measures of line intensity ratios $R = \text{CO(J=2-1)/(J=1-0)}$ for the entire region demonstrating that the SNR is likely interacting with Cloud A (Butt et al. 2001). For this cloud, $R \sim 2.4$, more than 3.5σ above the average Galactic value.

Upper limits to the continuum radio emission of Cloud A and the use of Eq. (26) above, allow us to rule out a Bremsstrahlung origin of the GeV radiation from 3EG J1714-3857 (see Figure 19): the electron flux needed to explain the GeV source in terms of bremsstrahlung emission overpredicts the radio synchrotron emission for any reasonable molecular cloud magnetic fields (Crutcher, 1988,1994,1999). The GeV γ -rays seem to be the result of π^0 -decays produced when the population of cosmic-rays accelerated at the remnant shock are injected into the dense medium of Cloud A. We estimate a cosmic-ray enhancement factor in the range $24 < k_s < 36$ given the parameters of the SNR (Slane et al. 1999).

In addition, the γ -ray spectrum of 3EG J1714-3857 (Hartman et al. 1999) is consistent with a narrow spectral bump at ~ 70 MeV that could correspond to the signature of the pion-decays resulting from an enhanced population of low energy ($E \sim 1$ GeV) protons. This apparent peak, although highly suggestive,

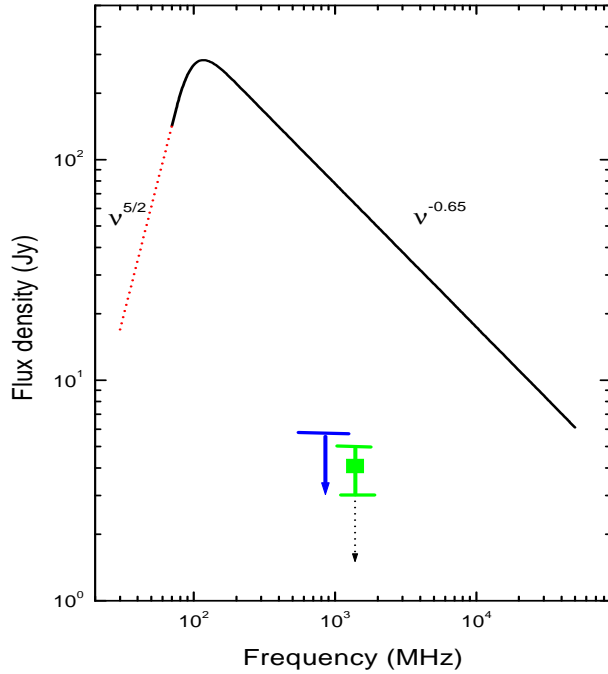


Figure 19: The radio synchrotron spectrum which would be expected from the region of the shocked molecular material located towards the NE of the remnant RX J1713.7-3946 (Cloud A), under the assumption that the observed GeV flux were due to electron/positron Bremsstrahlung. Since this spectrum violates the upper limit (dark) derived from the non-detection of the cloud in the radio band by a factor of ~ 20 at 843 MHz (Slane et al., 1999), we can rule out a predominantly leptonic origin of the GeV luminosity. Furthermore, if the GeV flux of 3EG J1714-3857 were of electronic origin, the cloud region would outshine even the radio-brightest NW rim of the remnant, which is found to be emitting only 4 ± 1 Jy at 1.36 GHz (Ellison et al. 2001), as shown by the light data point. An assumed low frequency turnover at ~ 100 MHz in the radio spectrum is shown by the red dotted line.

is not statistically significant and improved observations are needed to confirm its existence.

Uchiyama et al. (2002a) have reported the discovery of extended ($10' \times 15'$) and hard (spectral shape described by a flat power-law photon index $\Gamma = 1.0^{+0.4}_{-0.3}$) X-ray emission from the position of Cloud A, using ASCA data. This emission is interpreted as bremsstrahlung from a Coulomb-loss-flattened distribution of nonthermal low-energy protons in the cloud or mildly relativistic electrons (see also Uchiyama et al. 2002b). Uchiyama et al. (2002a) estimate that the energy content in subrelativistic protons within the cloud far exceeds that in the relativistic protons, say by a factor ~ 80 . The explanation could be that the bulk of the more energetic particles have already diffused from the cloud whereas the sub-relativistic population is captured there. Alternatively, energetic secondary leptons may also be producing low-level non-thermal X-ray and radio emission in the clouds. Higher spatial and spectral resolution measurements of this remnant in the radio and X-ray band have been made and will hopefully clarify the situation (P. Slane, personal communication).

Regarding the highest energy particles produced in the SNR, a CANGAROO re-observation of the NW-rim of RX J1713.7-3946 with a new 10-m reflector (CANGAROO II) has allowed a determination of

the TeV γ -ray spectrum, which can be fitted with a power-law of photon index $\Gamma \sim -2.8$ (Enomoto et al. 2002). Such a steep spectrum is hard to explain by IC emission and Enomoto et al. (2002) have claimed that the TeV emission is also of hadronic origin. If this were the case, however, the GeV gamma-ray flux would be much higher than observed, as recently noted independently by Reimer & Pohl (2002) and by Butt et al. (2002a). (It is conceivable that protons with a hard index of ~ 1.8 may alleviate the discrepancy but then it becomes difficult to explain how such a population of protons could produce the measured -2.8 index TeV γ -rays in the first place.)

The SNR RX J1713.7-3946 is perhaps the best natural laboratory available today for studying the acceleration and diffusion of cosmic-rays. The unique combination of a relatively close SNR and a group of well defined molecular clouds in its surroundings, none of them in front of the remnant itself, makes this source a priority target for the forthcoming generation of high-energy instruments such as HESS, AGILE, INTEGRAL, and, GLAST, as well as for infrared, radio, mm and sub-mm observatories.

10.9 γ -ray source 3EG J1734-3232 – SNR G355.6+0.0

The shell type supernova remnant G355.6+0.0 (Figure 20) was first identified in the MOST Galactic Center survey (Gray 1994) as a compact (~ 0.1 deg $\times \sim 0.1$ deg) radio source with both thermal and non-thermal emission. The western limb shows possible indications of an interaction with the ambient diffuse thermal gas present at that location. X-ray emission from this SNR has also recently been reported by the ASCA X-ray satellite under the designation AX J173518-3237 (Sugizaki et al., 2001).

The physical relation of even part of the γ -ray flux of 3EG J1734-3232 with SNR G355.6+0.0, however, is unclear because of the lack of information about both the SNR and its environs. The lack of a γ -ray spectral index for 3EG J1734-3232 (Hartman et al. 1999, see Table 1) further complicates any attempt to connect the SNR with the γ -ray emission. The γ -ray error box is also coincident with a very young open cluster, NGC 6383, $(l, b) = (355.66, 0.05)$, which is centered around the bright spectroscopic binary HD 159176 (O7V+O7V) (eg. van den Ancker et al., 2000). Together with NGC 6530 and NGC 6531, NGC 6383 belongs to the Sgr OB1 association. The nearby radio source G355.3+0.1, also within the γ -ray error box, is most likely an HII region at a distance of ~ 10 kpc (Crovisier et al. 1973).

Although the Third EGRET catalog lists GeV 1732-3130 (Lamb & Macomb 1997) as an alternate name for this source, the large positional offsets indicate that these two may be separate γ -ray sources (Roberts et al. 2001a). Interestingly, “bridging” these two sources is a “possibly variable” COS-B source, 2CG 356+00, located at $(l, b) = (356.5, +0.3)$ (Swanenburg et al. 1981), which may be related to one or both of them.

The report of a bright, transient hard X-ray source, KS/GRS 1730-312 ($l, b = 356.6, +1.06$) (Vargas et al. 1996), within the 95% error ellipse of GeV 1732-3130 may also explain part of the detected γ -ray emission from this region. It is possible that in the quiet state KS/GRS 1730-312 was actually seen in ASCA data, as “src 1” in Roberts et al. (2001). A mild indication of variability for 3EG J1734-3232 ($I = 2.9, \tau = 0.00^{0.24}_{0.00}$) appears within the I -scheme, and would support the flaring hard X-ray source being associated with it, although this is not conclusive with the data now at hand. The transient source could also be separately connected to GeV 1732-3130/2CG 356+00. 2CG 356+00 is listed as “possibly variable”, supporting such an argument (Swanenburg et al. 1981).

It is clear that no conclusive determination can be made regarding possible association among SNR G355.6+0.0, GeV 1732-3130, 2CG 356+00, and 3EG J1734-3232 until the sizes of the γ -ray error boxes

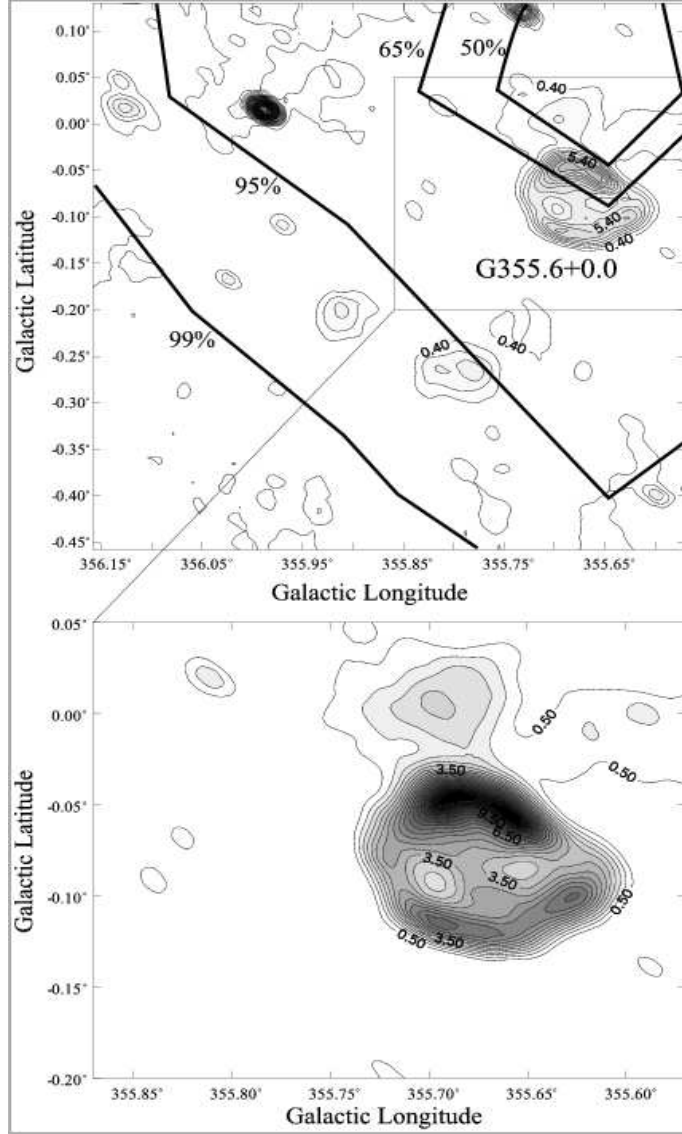


Figure 20: Upper panel: MOST image of the SNR G355.6+0.0 at 0.843 GHz (Gray 1994). The grey-scale representation ranges from 0.4×10^{-2} to 10×10^{-2} Jy beam⁻¹. Radio contours are shown in steps of 1 Jy beam⁻¹, the resolution is 43 arcsec. Part of the γ -ray probability contours of 3EG J1734-3232 are superposed. Lower panel: Detailed radio image of the SNR at the same frequency. Radio contours are shown in steps of 1×10^{-2} Jy beam⁻¹, starting from 0.5×10^{-2} Jy beam⁻¹.

are significantly reduced by future GeV telescopes. It is almost certain that many GeV sources, especially those located towards the inner Galaxy, will eventually be resolved into several separate sources.

10.10 Near the Galactic Center: γ -ray source 3EG J1744-3011 – SNR G359.0-0.9/359.1-0.5 and γ -ray source 3EG J1746-2851 – SNR G0.0+0.0/0.3+0.0

Since the 3EG sources J1744-3011 and J1746-2851 lie near the very confused Galactic Center region, an analysis of the sort we present for other SNR-EGRET source pairs is not possible in this case. Galactic Center region sources must to be considered as possibly extended (most likely composite) and confused, embedded in high and structured background, and the analysis procedures used for other sources in the EGRET catalogs may not apply (Mayer-Hasselwander et al. 1998).

A detailed discussion of the Galactic Center region is beyond the scope of this report; for this the reader is referred to Markoff et al. (1999), Yusef-Zadeh et al. (2000), Melia & Falcke (2001), as well as the book edited by Falke et al. (1999). Very recently, Goldwurm (2001) has presented a review of the high-energy emission detected from the direction of the Galactic center; the reader is referred to that paper for details on different X-rays observations of the Galactic Center region.

A complete discussion of EGRET observations of the Galactic Center region was presented by Mayer-Hasselwander et al. (1998). They found 5488 ± 516 counts above 30 MeV, representing a high significance excess. The region analyzed was larger than the position of the central EGRET sources by several degrees (see Figure 1 in Mayer-Hasselwander et al. 1998). They also re-analyzed COS-B data, showing that the COS-B observations of the region were in agreement, despite previous claims, with the more recent EGRET data. Several objects in the region are potential counterparts for the γ -ray radiation detected, including, for example, GRO 1744-28, 2S1743-2941, E1740-2942, PSR 1742-30, GRS 1736-297, GRS 1739-278, and GX 359+02. However, not all of these coincide with the positions of the 3EG sources we are considering. The γ -ray fluxes in different energy bands give only the hint of variability, which is consistent with 3EG Catalog estimates for I and τ (Table 1). The photon spectrum of the diffuse emission of the Galactic Center region shows a clear break at energies about 1 GeV, with a significant steepening thereafter (it shifts from -1.3 to -3.1). The hard spectrum at energies above 100 MeV has to be compared with the already hard values obtained with standard EGRET analysis techniques, quoted in Table 1 for the sources of interest. These hard values argue against γ -rays being produced in diffusive processes, i.e., by ambient matter–cosmic-ray interactions. However, this is yet to be confirmed.

Yusef-Zadeh et al. (2002) have suggested that the central γ -ray source may be due to the interaction of the G0.13-0.13 molecular cloud with the diffuse and filamentary X-ray features discovered using Chandra, all lying within the 95% confidence location contours of 3EG J1746-2851. The hard spectrum of the EGRET source (-1.7) seems to match the cloud spectrum at about 10 keV when extended down to X-ray energies. Electron Bremsstrahlung and inverse Compton may be responsible for the GeV emission. Pohl (1997) raised the possibility that the radio arc at the Galactic Center could be the counterpart of the high-energy γ -ray source. Existing radio data on the arc support the view that its synchrotron emission originates from cooling, initially monoenergetic electrons that diffuse and convect from their sources to the outer extensions of the arc. If the source of high-energy electrons coincides with the sickle region (G0.18-0.04), as indicated by the radio data, then the ambient far-infrared photons could be subject to inverse Compton interaction by high-energy electrons. Pohl (1997) was able to show that the predicted γ -ray emission depends mainly on the magnetic field strength in the arc and that both the flux and the spectrum of the central source could be explained by such a process.

Please see the jpg file attached.

Figure 21: Relative positions of 3EG J1800-2338 and SNR W28. Contours in step of 5 mK, starting from 15 mK, from the 2695-MHz map obtained with the Effelsberg 100-m single dish telescope (Fürst et al. 1990). Astro-ph arXiv file: G6-4.jpg

On the other hand, the starving state of accretion flow around the supermassive black hole make it a dubious counterpart for the high-energy radiation. Note, however, that from an statistical point of view the probability of such a good agreement in the positions of the Galactic Center and the 3EG source is about 10^{-4} (Mayer-Hasselwander et al. 1998). However, early scenarios were presented in which the γ -ray emission is produced by the wind accretion from the nearby IRS16 cluster (Melia 1992, Mastichiadis & Ozernoy 1994). More recently, Markoff et al. (1997) were able to reproduce the observed spectrum with a combination of synchrotron radiation and pion decay. If the γ -ray flux is directly related to the dissipation of gravitational energy, i.e. if it is produced by relativistic particles energized by a shock within the infalling plasma, Sgr A* could still be the source of the γ -rays observed. However, in a refined analysis, Markoff et al. (1999), using data from the 3EG catalog and an improved physical treatment, concluded that this was not the case.

Forthcoming satellites, particularly INTEGRAL, will scrutinize the Galactic center region and hopefully resolve the nature of this mysterious and interesting region.

10.11 γ -ray source 3EG J1800-2338 – SNR G6.4-0.1 (W28)

This EGRET-SNR positional coincidence was originally proposed by Sturner et al. (1996) and Esposito et al. (1996). However, the previous 2EG J1801-2321 source does not coincide with 3EG J1800-2338, since the new position has shifted position by about half a degree. W28 was also presented as a possible candidate for an association with a COS B source by Pollock (1985), after noticing that SNR W28 appears to be interacting with molecular clouds. Dubner et al. (2000) have made a recent study of the remnant using the VLA. They concluded that the remnant is indeed interacting with molecular clouds in the vicinity,

and observed maser emission, as earlier reported by Claussen et al. (1997, 1999). Arikawa et al. (1999) observed W28 and mapped the CO(J=3-2) and CO(J=1-0) rotational transition lines toward the remnant, and also concluded that the remnant is interacting with the clouds. The mass of the clouds was found to be $2 \times 10^3 M_\odot$. This mass, however, is with respect to the 2EG source position. A new molecular mass estimate with respect to 3EG J1800-2338 is given below.

The H-alpha filaments in W28 have a mean velocity of $18 \pm 5 \text{ km s}^{-1}$ (Lozinskaya 1974). HI absorption measurements by Radhakrishnan et al. (1972) are consistent with this velocity, since absorption features at 7.3 and 17.6 km s^{-1} are seen against the SNR continuum. As Figure 22 (lower panel) shows, there is a molecular cloud at about the same velocity ($\sim 19 \text{ km s}^{-1}$) which is most likely the birth place of the supernova progenitor. Directly toward the radio-bright rim of W28 ($l \sim 6.6 \text{ deg}$, $b \sim -0.3 \text{ deg}$), which has been proposed by Wootten (1981) and Arikawa et al. (1999) as the site of SNR-giant molecular cloud interaction, a jet-like CO feature is seen in Figure 22, extending to a smaller cloud at $\sim 7 \text{ km s}^{-1}$. Arikawa et al. (1999) proposed the 7 km s^{-1} component as the systemic velocity of W28, whereas Claussen et al. (1997) suggested that the entire 7 km s^{-1} cloud has been accelerated by the SNR from the main cloud $\sim 10 \text{ km s}^{-1}$ higher in velocity. The alignment of the 7 km s^{-1} cloud with the bright interacting rim of W28 and the jet-like feature linking it to the larger cloud at higher velocity supports the Claussen et al. proposal.

The low longitude of W28 (6.5 deg) makes both the kinematic distance and the mass of the associated molecular cloud difficult to measure. Assuming a systemic velocity of 19 km s^{-1} , the near kinematic distance is $3.7 \pm 1.5 \text{ kpc}$. If all emission in the velocity range $0 - 28 \text{ km s}^{-1}$ is associated with W28 (see Figure 22b), the total molecular mass within the 95% confidence radius of the 3EG source is $3.9 \times 10^5 M_\odot$. Owing to the severe velocity crowding at this Galactic longitude, this mass estimate may be overestimated by as much as 50%.

Even reduced by 50% for the observed EGRET flux. Ignoring bremsstrahlung, a CR enhancement factor of about $k_s \sim 20$, similar to that found in other cases, is necessary to explain the emission by hadronic interactions. This result is stable against reasonable variations in the input parameters and is compatible with consistency tests. Note that the distance used here is near the upper limit of those shown in Table 4; a smaller distance would make a physical association even more likely. Velázquez et al. (2002), in a recent analysis of large-scale neutral hydrogen around W28, adopt a distance of $\sim 1.9 \text{ kpc}$. They concluded that the SN energy was $\sim 1.6 \times 10^{50} \text{ erg}$ about 3.3×10^4 years ago.

An intriguing possibility in this case is that there are actually two (or more) γ -ray sources, each associated with a different molecular cloud in Figure 22 and/or with the pulsar PSR B1758-23 (which, coincides with the GeV source as reported in the Roberts et al. (2001) catalog). Investigation of this possibility will require the next generation of GeV and TeV-telescopes, with their improved sensitivity and angular resolution.

W28 is one of the few remnants observed with Čerenkov telescopes. Rowell et al. (2000) observed it with CANGAROO 3.8-m telescope and were able to set an upper limit on the flux (for photons with $E > 1.5 \text{ TeV}$) of a diffuse source encompassing the clouds discovered by Arikawa et al. (1999) and part of the 3EG source: $6.64 \times 10^{-12} \text{ ph cm}^{-2} \text{ s}^{-1}$. A simple extrapolation of the 3EG flux, with the same spectral index, up to TeV energies yields a value higher than this upper limit by more than an order of magnitude (see Figure 5 of Rowell et al. 2000). This implies the existence of a break in the spectrum in the GeV-TeV region. But even considering such a break (see Section 12.1 and Table 9) the 3EG J1800-2338 region could be visible to an observatory such as HESS in a matter of hours.

Please see the jpg file attached.

Figure 22: (a) CO integrated over the velocity range 0 to 28 km s⁻¹ corresponding to the distance of the SNR W28. Contours: 4850 MHz continuum from the survey of Condon et al. (1991); the lowest contour is at 0.32 Jy/beam and the contours are logarithmically spaced by a factor 2. The three labeled sources are HII regions: M20 the Trifid Nebula and M8 the Lagoon Nebula. The dotted circle is the 95% confidence radius about the position of 3EG J1800-2338 (Hartman et al. 1999). (b) CO intensity integrated over the latitude range of the molecular gas associated with W28, b = -0.5 to -0.125 deg. Astro-ph arXiv file: GW28.jpg.

Please see the jpg file attached.

Figure 23: High-resolution radio map of the nearby star LS 5039 obtained with the VLBA and the VLA in phased array mode at 6 cm wavelength. The presence of radio jets in this high- mass x-ray binary is the main evidence supporting its microquasar nature. The contours shown correspond to 6, 8, 10, 12, 14, 16, 18, 20, 25, 30, 40, and 50 times 0.085 mJy beam. From Paredes et al. (2000). Astro-ph arXiv file: ls5039.jpg.

The possibility of a leptonic origin for the γ -ray source cannot be ruled out in this case. The SNR is ranked sixth when ordered by radio flux among all entries in Green's (2000) Catalog (Table 4). With standard values of magnetic fields appropriate to molecular clouds (eg. Crutcher 1988, 1994, 1999), the radio flux that would be generated by the same electronic population producing the GeV emission would not overpredict the currently detected radio flux. A model such as the one presented by Bykov et al. (2000) could explain the EGRET source without invoking the dominance of hadronic interactions.

10.12 γ -ray source 3EG J1824-1514 – SNR G16.8-1.1

Paredes et al. (2000) proposed that the massive star LS 5039 is part of a newly discovered microquasar system, and that it can be identified with the γ -ray source 3EG J1824-1514. The detection of radio jets and strong variability at different wavelengths (including γ -rays) supports their claim. Gamma-ray emission from microquasars with high-mass companions has been recently discussed by Kaufman-Bernadó et al. (2002), who show that GeV γ -rays can result from the up-scattering of UV stellar photons by the relativistic jet (see also Georganopoulos et al. 2002). Variability is naturally produced by the changing viewing angle as the jet precesses due to tidal forces from the accretion disk.

The supernova remnant G16.8-01.1, also within the 95 % confidence contour of the γ -ray source, has been recently studied by Ribó et al. (2002). Although the radio structure of the remnant is not well-resolved because of contamination from the partially superposed HII region RCW 164 (Rodgers et al.

1960), but its size is ~ 30 arcmin and its total flux at 5 GHz is ~ 1 Jy (Ribó et al. 2002). The distance to the source is not known, but a lower limit of ~ 2 kpc has been established by Ribó et al. (2002) through H166 α line observations of the foreground HII region. HI observations by the same authors indicate that the ambient density around the remnant is ~ 5 cm $^{-3}$, with no evidence of interacting clouds. For a SN energy release $E_{51} \sim 1$ and a distance $d \sim 3$ kpc, we found that the expected pion-decay γ -ray flux from this SNR should be $F(E > 100 \text{ MeV}) \sim 10^{-7} \text{ ph cm}^{-2} \text{ s}^{-1}$ ($\theta \sim 0.5$). This is about one third of the observed flux from 3EG J1824-1514. It is possible that bremsstrahlung from SNR shell-cloud interactions could also generate a fraction of the observed γ -rays.

In addition, there is one Princeton pulsar superposed on this 3EG source, but it is not energetic enough to be a plausible alternative to the microquasar found by Paredes et al. (see Section 4). The apparent (though marginal) variability of the γ -ray source, in addition, argues weakly against a pulsar origin of the GeV flux. A variability analysis (Torres et al. 2001) suggests that 3EG J1824-1514 is marginally variable, but this is not confirmed by Tompkins's τ index, which is compatible with a steady source (although the difference between the upper and the lower limit on Tompkins' τ is large). These results are not conclusive, but it seems unlikely that most of the γ -ray flux could come from either the SNR or pulsar alone, especially when the uncertainties in distance are taken into account.

The source 3EG J1824-1514 remains the best candidate for a γ -ray emitting microquasar. Future tests of this interesting source will surely be carried out with AGILE and GLAST.

10.13 γ -ray source 3EG J1837-0423 – SNR G27.8+0.6

This source is variable between EGRET observations, which argues against a SNR or pulsar origin (see above). Indeed, 3EG J1837-0423 was detected only once, in viewing period 423.0 with 5.8σ significance level. In all other single viewing periods in which it was observed, only an upper limit to the flux could be established (see Figure 24). This behavior is compatible with objects presenting flares, such as AGNs. A microlensing model might be a plausible alternative given the absence of a strong radio emitter in the 3EG field (Torres et al. 2002a, b). Another possibility is a non-pulsating black hole of the sort discussed by B. Punsly (1998a,b and Punsly et. al. 2000). In any case, the variability clearly indicated by both the I and τ indices make 3EG J1837-0423 incompatible with a SNR or pulsar origin.

10.14 γ -ray source 3EG J1856+0114 – SNR G34.7-0.4 (W44)

The possible association of the γ -ray source 3EG J1856+0114 and SNR G34.7-0.4 (W44) has already been proposed by Esposito et al (1996) and by Dermer et al. (1997). A comprehensive review of the morphological properties of W44 at different frequencies is given by De Jager & Mastichiadis (1996). The radio emission of the SNR is shell-like, but the X-ray emission is centrally peaked (Rho et al. 1994). A pulsar is found near the center of the 3EG source, PSR B1853+01 (quoted as PSR J1856+0113 in Table 7). Frail et al. (1996) discovered a corresponding radio pulsar wind nebula, with a tail-shape pointing back to the center of W44. In addition, they found that the transverse velocity of the pulsar is compatible with the expansion speed of the radio shell. Thus, it is probable that this pulsar is the compact remnant of the supernova.

Recently, two new studies concluded that the remnant is in interaction with molecular clouds: a new radio and optical study by Giacani et al. (1997) and a complete CO study by Seta et al. (1998). In Figure 25, a map of CO(1-0) integrated over the velocity range 30 to 65 km/s is shown. There are six giant molecular clouds, with masses between 0.3 and $3 \times 10^5 M_\odot$, in the vicinity of W44. Three of them, with a

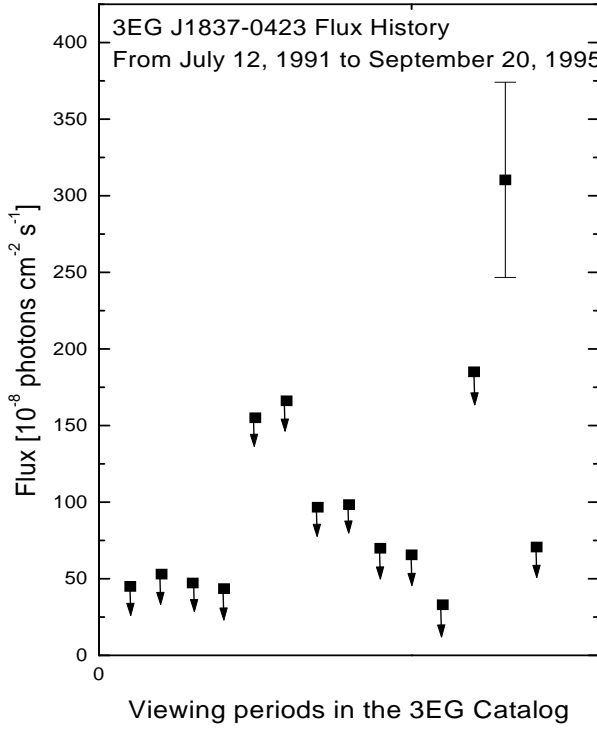


Figure 24: Flux history of the 3EG J1837-0423. Only for one viewing period 423.0, the source was undoubtedly detected, all others being only upper limits. The x-axis in the figure does not represent a linear scale of time. Rather, each point represent the measurement for a different single viewing period given in Hartman et al. (1999).

total mass of $4.1 \times 10^5 M_{\odot}$ (Seta et al. 1998) are apparently interacting with the remnant.

The total molecular mass in the vicinity of the 3EG source in W44, specifically in the region $l = 34.5$ to 34.875 , $b = -0.375$ to -0.75 , and $v = 30 - 65 \text{ km s}^{-1}$, is $6.2 \times 10^4 M_{\odot}$. Based on the Clemens (1985) rotation curve, the main clump near the 3EG source has a kinematic distance of 2.8 kpc. The molecular mass is obtained based on the usual assumption that the H₂ column density is proportional to the CO velocity-integrated intensity. The mass in the velocity-perturbed wings can be a factor ~ 100 less than the total mass of the cloud. With these values for the masses of passive targets and an CR enhancement factor of ~ 40 , the entire GeV flux could, in principle, be explained by hadronic interactions, although an additional Bremsstrahlung component will be present also in the SNR shell-cloud interactions. The enhancement factor of ~ 40 is obtained assuming $E_{51} = 0.67$ and a pre-shock ambient density $n_0 = 1$, but the conclusions are robust for reasonable variations in these parameters.

We can compute mean densities for the well-defined clumps (lighter colors in Figure 25) by assuming they are roughly spherical. However, the 3EG source contours enclose less intense emission that is spread throughout the whole W44 complex, which is about ~ 1 deg across, (49 pc at the assumed distance of 2.8 kpc). Thus it is reasonable to assume that the molecular gas enclosed by the 3EG contours is spread over about 49 pc along the line of sight as well. The mean density would then be $n \sim 6.2 \times 10^4 M_{\odot} / [\pi(9\text{pc})^2 \times 49\text{pc}] = 188 \text{ H/cm}^{-3}$; here, 9 pc is the 95% location contour of the 3EG

Please see the jpg file attached.

Figure 25: The colors are CO(1-0) integrated over the velocity range 30 to 65 km/s. The solid contours are 4.85 GHz continuum from the survey of Condon et al. (1994). The dashed contours are the 50%, 68%, 95%, and 99% confidence contours for 3EG J1856+0114. The white "+" marks the position with the highest ratio CO(2-1)/CO(1-0) as determined by Seta et al. (1998). Astro-ph arXiv file: GW44.jpg.

source. This density is 6 times larger than that used by de Jager & Mastichiadis' (1997) in computing the hadronic emission.

De Jager & Mastichiadis (1997) developed a specific model for this EGRET source (at the time, 2EG J1857+0118) and proposed that the γ -ray radiation could be accounted for by relativistic Bremsstrahlung and inverse Compton scattering. One of their main motivations was to explain the hard spectral index of the corresponding γ -ray source, ~ -1.80 , as well as the hard index of the radio source ~ -0.3 , both difficult to reconcile with the standard Fermi first order acceleration process. The model of de Jager & Mastichiadis (1997) propose the pulsar PSR B1853+01 as the source of the gamma-rays; indeed, the required efficiency to produce all the γ -ray radiation is 13%, which appears marginally plausible, given the uncertainties. However, the luminosity of the pulsar wind nebula (PWN) is negligible in comparison with the total X-ray luminosity of W44 (Harrus, Hughes, & Helfand 1996). The bulk of the X-ray emission from W44 is thermal (Jones, Smith, & Angellini 1993, Rho et al. 1994). But even though the X-ray luminosity of the PWN is negligible, the pulsar could have injected a significant amount of electrons in an earlier stage. Mastichiadis' paper Good fits of the 2EG spectrum were obtained for a range of particle density, whereas the magnetic field was required to be $\sim 10\mu$ G and the synchrotron cutoff frequency, $\nu_b \sim 10^{12.5}$ Hz. A reasonable field strength could then explain the γ -ray spectrum of W44 as originating in leptonic

Please see the jpg file attached.

Please see the jpg file attached.

Figure 26: Left: Relative positions of 3EG J1903+0550 and the SNR G39.2-0.3. Radio contours in step of 2 mK, starting from 5 mK, from the 2695-MHz map obtained with the Effelsberg 100-m single dish telescope (Fürst et al. 1990). Right: CO integrated over the velocity range of the far Sagittarius arm, 48 to 70 km s⁻¹. Contours: 4.85 GHz continuum from the survey of Condon et al. (1994). The angular resolution is 7 arcmin; the contour interval is 0.5 Jy/beam, starting at 0.3 Jy/beam. The dotted circle is the 95% radius about the central position of 3EG J1903+0550 (Hartman et al. 1999). Astro-ph arXiv files: G39.jpg and G39-2.jpg.

processes.

W44 is then a complicated case. While the γ -ray source may be due to SNR shock-cloud interactions (hadronic and leptonic), a significant part of the γ -ray flux observed – perhaps even all of it – could be due to a pulsar. Application of Eq. (26) does not allow us to discard, as in the case of SNR G347.3-0.5, a leptonic origin for the high-energy radiation. Here, then, future satellites and telescopes will play an essential role in disentangling the different possibilities. W44 was not observed to be emitting at TeV energies, where an upper limit has been imposed by the Whipple observatory at $(F(E > 250\text{GeV}) = 8.5 \times 10^{-11} \text{ cm}^{-2} \text{ s}^{-1}$, Leslard et al. 1995), implying that there is a possible break in the spectrum from GeV to TeV. This can be tested by forthcoming higher sensitivity TeV-telescopes.

10.15 γ -ray source 3EG J1903+0550 – SNR G39.2-0.3

Figure 26 shows the relative positions of 3EG J1903+0550 and the SNR G39.2-0.3. The 3EG source is also coincident with two Princeton pulsars (Table 3). One of them can be readily discarded as the origin of the γ -ray emission because of the unrealistically high value required for the efficiency. The other pulsar, PSR J1902+0615, lacks a measurement of the period derivative and so we cannot judge the likelihood of this particular association. The SNR G39.2-0.3 has been searched for OH maser emission by Koralesky et al. (1998), but none was detected, although, of course, this does not imply a lack of possible interaction. The

SNR is more than 8 kpc away, which seems to be -a priori- a problem for generating the requisite flux via shock interactions. We find, however, that the large distance may be, at least partially, compensated for by the large amount of molecular material in the neighborhood.

Caswell et al. (1975) detected HI absorption all the way up to the terminal velocity towards the SNR G39.2-0.3, with almost continuous strong absorption between 60 km s^{-1} and the terminal velocity. They therefore concluded that the remnant was certainly beyond the tangent point, and most likely at the far distance corresponding to 60 km s^{-1} , $\sim 9.6 \text{ kpc}$. Such a large distance is consistent with the high foreground hydrogen column inferred both by Becker & Helfand (1987) based on 21 cm absorption measurements with the VLA, and by Harris & Slane (1999) based on ASCA observations. A distance of 9.6 kpc would place the SNR in the far Sagittarius arm, where as Figure 26 shows, the remnant is nearly coincident with a massive molecular complex. The complex is (40,59) in the catalog of Dame et al. (1986), who assigned the far kinematic distance based on 2 associated HII regions. The mass of this complex is estimated to be $2.1 \times 10^6 M_{\odot}$. The mass within the 95% confidence radius of the 3EG source (dotted circle in Figure 26) is even higher, $3.4 \times 10^6 M_{\odot}$, because the radius also includes part of another molecular complex at higher longitude. If part of the mass contained in the molecular complex could serve as target material for the relativistic particles accelerated in the SNR shock, this 3EG detection could plausibly be produced by a combination of Bremsstrahlung and pion decay. With the mass quoted, a CR enhancement factor of less than 10 is all that is needed to produce the bulk of the observed γ -ray emission. However, it is clear that not all of the molecular mass can be illuminated by the SNR shock front. The SNR itself is less than 8 arcmin in size, while the 3EG source is ~ 1 deg in size. Only 0.1% of the molecular material need serve as a target for the particles accelerated in G39.2-0.3 in order to produce the 3EG source. In this case, however, as in the case of 3EG J1639-4702, the enhancement factor (Eq.15) is very large (~ 1000), as a result of the use of the Sedov solutions with typical values for the energy of the explosion and ambient unshocked density.

There is an additional nearby SNR, G40.5-0.5 (Downes et al. 1980), which is also associated with the same cloud complex as G39.2-0.3 and at a similar distance. Though the center of G40.5-0.5 does not coincide with the 3EG source herein analyzed, it is suggestive that the location of the 3EG source lies between the two SNRs, and could thus have a composite origin. (SNR G40.5-0.5 does not appear in Table 1 due to the high ellipticity of the confidence level contours of 3EG J1903+0550.) A large region, $-10 < b < 5$, $38 < l < 43$, comprising this latter SNR as well as the 3EG source was subject of a search for gamma-ray emission using the HEGRA system of imaging atmospheric telescopes (Aharonian et al. 2001). No evidence for emission from point sources was detected, and upper limits imposed were typically below 0.1 Crabs for the flux above 1 TeV.

10.16 γ -ray source 3EG J2016+3657 – SNR G74.9+1.2 (CTB 87)

Although it has been suggested that SNR G74.9+1.2 (CTB 87) may be interacting with ambient clouds (Huang et al. 1983, Huang and Thaddeus 1986), the coincident 3EG J2016+3657 source has been proposed as a counterpart of the blazar-like radio source G74.87+1.22 (B2013+370) (Halpern et al. 2001a, Mukherjee et al. 2000). B2013+370 is a compact, flat spectrum, 2 Jy radio source at 1 GHz. Its multiwavelength properties were compiled by Mukherjee et al. (2000), and since they resemble other blazars detected by EGRET, make B2013+370 an interesting possible counterpart for this 3EG source.

Optical photometry of B2013+370 shows that it is variable, providing additional evidence of its blazar nature (Halpern et al. 2001a). Additionally, the same authors presented a complete set of classifications for the 14 brightest ROSAT X-ray sources in the error circle of the 3EG source, of which B2013+370

Please see the jpg file attached.

Figure 27: CTB 87 region: The dashed contours are the usual EGRET 50%, 68%, 95%, and 99% confidence levels. The solid contours are taken from the 4.85 GHz continuum survey of Condon et al. (1994). The color is CO integrated over the range $v=-65$ to -50 km/s. The positions of the blazar G74.87+1.22 and of the WR-star WR138 are marked. Astro-ph arXiv file GCTB87.jpg.

remained the most likely source of the γ -rays, should these come from a point-like source. The Crab-like supernova remnant CTB 87 is located at more than 10 kpc (Green 2000), seemingly disfavoring its shell interactions as the cause of the EGRET source. There are also WR stars in the field (Romero et al. 1999), which might produce γ -ray emission. This possibility remains to be analyzed. INTEGRAL observations would help in determining if there is γ -ray emission coming from the stars.

Figure 27 shows a CO map for the CTB 87 region. One clearly defined molecular cloud appears in the map. The mean velocity of the molecular cloud is -57 km/s. Assuming a flat rotation curve beyond the solar circle, the cloud's kinematic distance is 10.4 kpc. The total molecular mass within the 95% confidence radius of the 3EG source is $1.7 \times 10^5 M_\odot$. With such a high value for the molecular mass, there is still a chance that the hadronic or leptonic γ -ray emission may be contributing to 3EG J2016+3657.

As in previous cases, only a precise determination of the γ -ray source position will disentangle the origin of this γ -ray source. Contrary to other EGRET-SNR pairs, though, this one has the particularity of enclosing a good candidate for an extra-galactic origin of the radiation.

Please see the jpg file attached.

Figure 28: The filtered radio emission at 2.7 GHz of the SNR G78.2+2.1 is shown in black. Radio contours, from the 2695-MHz map obtained with the Effelsberg 100-m single dish telescope (Fürst et al. 1990), are labeled in steps of 1 K in brightness temperature, starting at 3.0 K. The superposed white levels represent the 99%, 95%, 68%, and 50% statistical probability that a γ -ray source lies within each contour according to the EGRET catalog (Hartman et al. 1999). In the background, a CO(J=1-0) map of the region, integrated over the range $v = -20$ to 20 km s $^{-1}$, which includes all the emission in this direction except for a small amount in the range -50 to -40 km s $^{-1}$ which is probably associated with the Perseus Arm is shown. Astro-ph arXiv file: GW66.jpg.

10.17 γ -ray source 3EG J2020+4017 – SNR G78.2+2.1 (γ -Cygni Nebula, W66)

The SNR G78.2+2.1 lies in a very complex region of the sky, where more than forty HII regions and a large number of shell structures exist. Recently, Lozinskaya et al. (2000) have made an in depth analysis of the SNR, which included new optical observations and re-analysis of archival X-ray data. We refer the reader to their paper for appropriate details on the SNR structure and other features, other than those commented here, related with the possible association with the 3EG source. The main result of Lozinskaya et al. is that X-ray observations lead to a self-consistent model of a young SNR at an early stage of adiabatic expansion into a medium of relatively low density ($t = (5 - 6) \times 10^3$ yr, $n_0 = 0.14 - 0.3$ cm $^{-3}$).

The possible association between 3EG J2020+4017 (with the largest signal-to-background ratio of any of the sources in the third EGRET catalog that are positionally coincident with shell-type supernova remnants) and G78.2+2.1 was previously suggested by Pollock (1985), Sturner and Dermer (1995) and Esposito et al. (1996), each using the γ -ray catalog available at the time. Brazier et al. (1996) studied this

source (2EG 2020+4626 then) and reported the discovery of a point like X-ray source, RX J2020.2+4026, which lies close to the center of the remnant. If one is to assume that this source and the 3EG detection are related, the ratio of the gamma to X-ray fluxes is about 6000, similar to what is detected for the radio quiet Geminga-pulsar. This prompted Brazier et al. to suggest that 3EG J2020+4017 can indeed be a new Geminga-like radio quiet pulsar, something which would be in tune with the hard spectra, the low variability index, and the absence of ‘em’ classification in the 3EG Catalog (see Table 1). This possible association remains, then, very suggestive. However, Brazier et al. have reported no evidence for pulsations in the range $13.3 > f(\text{Hz}) > 2$, $\dot{F} < 10^{-11} \text{ s}^{-2}$. Also, no radio pulsar is known to be superposed to the 3EG contours (see Table 7). The absence of pulsar γ -ray radiation can well be due to a statistical limitation of the EGRET data. Analysis of GLAST (LAT) performance shows that periodicities should be detectable if present in any of the known low-latitude EGRET sources (Carramiñana 2001, Thompson et al. 2001).

In particular, Brazier et al. considered that the absence of em (i.e. extended) classification in the 3EG Catalog was definitive in disregarding the SNR as a possible site of cosmic ray acceleration: the SNR is about 1 deg in size, and it should be visible as extended by EGRET if the ambient matter were uniformly distributed. This, however, may not be the case if the shock accelerated particles interact and emit γ -rays most intensely at a localized nearby concentration of molecular material.

Yamamoto et al. (1999) have studied the possible SNR-cloud interaction here and observed a very high CO($J=2-1$)/CO($J=1-0$) intensity ratio (~ 1.5), very suggestive of an interacting cloud, is observed at $(l, b) = (78, 2.3)$. Interestingly, this position exactly coincides with that of the 3EG source (see Figure 28). After re-analyzing the same set of data used by Yamamoto et al. (1999), we agree with their result, but have also found another high ratio CO($J=2-1$)/CO($J=1-0$) at an adjacent position ($l = 77.875$, $b = 2.25$), and yet another moderately high ratio (~ 1) at another adjacent position: $(l, b) = (78.00, 2.25)$. These high ratios coincide nicely with the γ -ray source and with a fairly well-defined CO cloud, and make a good case for the interaction between the SNR and the cloud.

Assuming a distance of 1.7 kpc (Lozinskaya et al. 2000), the molecular mass of this cloud is $4700 M_{\odot}$ (calculated over the range $l = 77.75 - 78.125$ deg, $b = 2.00 - 2.375$ deg, and $v = -10$ to 0 km s^{-1}). This mass is rather uncertain since W66 lies in the so-called Cygnus X region of the Galaxy where the CO emission is very complex and strong, probably because we are viewing the Local spiral arm tangentially. It is hard to judge what amount of CO might be associated with the SNR and what amount is seen in projection. The Local arm emission is mainly in the range -20 to 20 km s^{-1} , and the Perseus Arm is seen at more negative velocities. Kinematic distances, particularly at low velocity, are very unreliable because our line of sight is almost tangent to the solar circle.

Using the data obtained for the mass of the cloud in the vicinity of the 3EG source and apparently in interaction with the SNR, as well as the mean value for the unshocked density ($n_0 = 0.22 \text{ cm}^{-3}$) and distance (from Lozinskaya et al. 2000), it is possible to explain the γ -rays by hadronic processes. The use of Eq. (26) with plausible values of the magnetic fields in molecular clouds (Crutcher 1988, 1994, 1999) rules out leptonic processes as the source of most of the radiation.

We cannot discard, however, a composite origin for the γ -rays, with part of the radiation coming from the putative γ -ray pulsar proposed by Brazier et al. (1996) and part from cloud interactions with the nucleonic component of freshly accelerated CRs.

10.18 An example beyond $|b| > 10$: γ -ray source 3EG J0010+7309 – SNR G119.5+10.2 (CTA 1)

The SNR-EGRET connection that we have explored so far was based on the sample shown in Table 1, constructed using 3EG sources within 10° of the Galactic plane. Although most SNRs fall into this latitude range, there is the possibility of finding a few nearby SNRs related with γ -ray sources at higher latitudes. An example of such is briefly described in this section.

CTA 1 is a shell-type SNR, but its shell is incomplete and broken-out towards the NW. This breakout phenomenon may be caused by more rapid expansion of the blast wave shock into a lower density region toward the NW. HI observations supported this interpretation (Pineault et al. 1993, 1997). Since CTA 1 is located at a relatively high latitude (10 deg) and is nearby (1.4 \pm 0.3 kpc, Pineault et al. 1993), it has a large angular size (90 arcmin), little foreground or background confusion, and it can be observed at exceptionally high linear resolution. The age of the SNR was estimated to be 10^4 yr by Pineault et al. (1993), but it could be younger by a factor of 2 (Slane et al. 1997). CTA 1 was subject of intense observational campaigns in the past years. There have been both ROSAT and ASCA X-ray observations (Seward et al. 1995, Slane et al. 1997), as well as optical, infrared and radio (see Pineault et al. 1997 and Brazier et al. 1998 for a review).

The ROSAT observation confirmed that CTA 1 belongs to the class of composite SNRs, which show a shell-type morphology in the radio band and are centre-filled in X-rays. Five point sources were detected with ROSAT, one of which was found to coincide with the EGRET source (at the time of the analysis, 2EG J0008+7307). ASCA data later revealed that this source, named RX J0007.0+7302, has a non-thermal spectrum, suggesting that it is the pulsar left from the supernova explosion (Slane et al. 1997). Optical observations were carried out by Brazier et al. (1998), with a 2.12-m telescope, but no object was found within the positional error box of the X-ray source. This allowed an upper limit to be set on the optical magnitude of any counterpart to the putative pulsar.

The 3EG J0010+7309 is a non-variable source under the I and τ schemes, and has a hard spectral index of 1.85 ± 0.10 , compatible with those of the Vela pulsar. This source was also detected in the Second EGRET Catalog, but with a shifted position which made it coincide with a nearby AGN – which was at the time proposed as a possible counterpart (Nolan et al. 1996). This AGN is not coincident with the 3EG source and can not be considered a plausible counterpart any longer. Based on positional coincidence, on the hard spectral index, and on physical similarities between the Vela pulsar and RX J0007.0+7302, Brazier et al. (1998) proposed that the 3EG source and this X-ray source were related. For an assumed 1 sr beaming, the observed 100-2000 MeV flux corresponds to a luminosity of 4×10^{33} erg s $^{-1}$, compatible with other γ -ray pulsar detections (see Table 5).

Although a thorough CO investigation has not yet been done for this SNR, current data from HI observations do not support the presence of very dense and massive molecular clouds in its neighborhood (Pineault et al. 1997). It seems CTA 1 and 3EG J0010+7309 might be related only through the compact object left by the latter (RX J0007.0+7302). A better localization of the γ -ray source with AGILE and GLAST will certainly test this suggestion.

11 SNRs discovered by their likely associated high-energy radiation

The SNR catalog compiled by Green (2000) is by no means complete. A large number of low surface brightness remnants remain to be discovered, hidden in the diffuse non-thermal continuum emission pro-

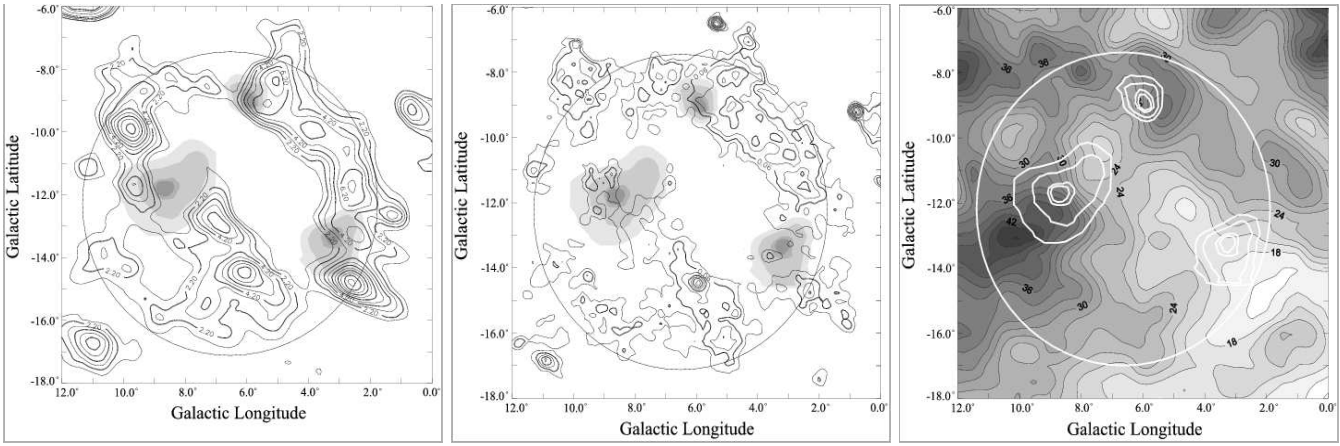


Figure 29: The Capricornus SNR uncovered by the likely associated high-energy emission. Left: Background filtered radio emission at 408 MHz (radio data from Haslam et al. 1982) of the region surrounding three 3EG sources, whose contours are marked. Middle: Radio map at 2.3 GHz (data from Jonas et al. 1998). The use of both maps shows that the SNR is a non-thermal radio source. Right: A map of the integrated column density of HI (velocity interval -3 to $+5$ km s^{-1}). Label units are 10^{19} atoms cm^{-2} . Use of this map shows that small enhancement factors could produce all three EGRET sources. From Combi et al. (2001).

duced by the diffuse component of the cosmic-ray electrons in the Galaxy. In recent years, the application of filtering techniques in radio continuum data has lead to the detection of several new SNR (e.g. Duncan et al. 1995, 1997, Jonas 1999, Combi et al. 1999, Klothes et al. 2001). The use of unidentified non-variable γ -ray sources as tracers of interacting remnants can result in new SNRs being discovered by their (plausibly associated) high-energy emission.

As it was emphasized in the previous sections, not all SNR generate observable γ -rays (say, at EGRET sensitivity) at typical Galactic distances. A second ingredient is necessary: a target, i.e., a dense medium such as a molecular cloud. If a SN explodes in a cloudy medium then more than a single cloud could be illuminated by $p - p$ collisions and thus multiple γ -ray sources can emerge. Clusters of steady unidentified γ -ray sources could trace these situations and lead to the discovery of new, very extended SNRs of low radio surface brightness.

This approach of considering EGRET sources as tracers of SNRs has been applied by Combi et al. (1998, 2001), leading to the discovery of two new SNRs. The basic technique consists of making HI line observations in the direction of clearly non-variable γ -ray sources. If some well-defined but small clouds ($M \sim 10^3 - 10^4 M_\odot$) are found within the 95% contours of the 3EG sources at velocities that correspond, according to the galactic rotation curve, to distances of less than 1 kpc, then large-scale (i.e. several degrees) radio continuum observations are carried out. These observations aim at detecting, through image filtering techniques, large SNRs of low surface brightness. Observations at more than a single frequency are necessary in order to determine if the radio spectral index is non-thermal, as expected from such remnants.

The SNR candidates discovered by this procedure are G327-12.0, located in the ARA region (Combi et al 1998) and G06.5-12.0, located in Capricornus (Combi et al 2001): see Figure 29. The first one appears to be responsible for the γ -ray source 3EG J1659-6251, whereas the second could be related to a cluster of

three 3EG sources: 3EG J1834-2803, 3EG J1847-3219, and 3EG1850-2652. HI clouds have been found at the positions of all these sources except for 3EG J1847-3219. Both remnants are thought to be so close that cosmic-ray enhancement factors in the range $5 < k_s < 45$ are sufficient to explain the γ -sources through π^0 -decays alone. Their low radio surface-brightnesses rule out electronic Bremsstrahlung as the source of the GeV flux.

We expect that the use of filtering techniques in interferometric radio observations could lead to the discovery of more such remnants in the near future (see, eg., Klothes et al. 2001), and with the improved capabilities of the next generation satellites, γ -ray emission from far more distant interacting SNRs could be detected.

12 SNRs and their neighborhoods as TeV sources

As can be seen in Table 7, several observations of SNRs such as W44, W51, γ -Cyg, W63 and Tycho's SNR, selected because of their possible association with molecular clouds and/or EGRET sources, have only produced TeV emission upper limits (Buckley et al. 1998). This, as discussed below, could indicate spectral cutoffs or breaks in the GeV-TeV energy range. For instance, the required differential source spectrum would have to steepen to $\sim E^{-2.5}$ for γ -Cyg in order to escape detection at TeV energies (Fegan 2001).

Very recently (Aharonian et al. 2002a), the HEGRA system of imaging atmospheric Cherenkov telescopes reported a survey of one quarter of the Galactic plane ($-2 < l < 85$). TeV gamma-ray emission from point sources and moderately extended sources (diameter less than 0.8 deg), including 86 known pulsars (PSR), 63 known supernova remnants (SNR) and 9 GeV sources, were searched with negative results. Upper limits range from 0.15 Crab units up to several Crab units, depending on the observation time and zenith angles covered: no TeV source was detected above 4.5σ in a total observation time of 115 h. At the same time, a search for point sources of radiation above 15 TeV has been conducted with HEGRA AIROBICC array (Aharonian et al. 2002b), but only flux upper limits of around 1.3 times the flux of Crab nebula were obtained for candidate sources (including SNRs), depending, again, on the observation time and zenith angles covered.

Positive detections, however, already exist. SN1006 (Tanimori et al. 1998) and RXJ1713.7-3946 (Muraishi et al. 2000, Enomoto et al. 2002) were detected by the CANGAROO telescopes. Observations of SN1006 in 1996 and 1997 show a significant excess from the NW rim of the SNR. The excess is consistent with the location of non-thermal X-rays detected by ASCA (Koyama et al. 1995).

Cassiopeia A and Monoceros were recently announced as TeV sources by the HEGRA collaboration (Pühlhofer et al. 2001, Lucarelli et al 2001). In the former case, 232 hours of observations yield an excess at the 4.9σ level, and a flux of $F = 5.8 \pm 1.2_{\text{stat}} \pm 2_{\text{syst}} \times 10^{-13} \text{ cm}^{-2} \text{ s}^{-1}$ at ($E > 1 \text{ TeV}$). The origin of the γ -rays has been proposed to be bremsstrahlung of radio emitting electrons (Atoyan et al. 2000a,b). Cas A has already been associated with a bright source of hard X-rays which indicates a population of non-thermal electrons with energies up to 100 TeV (Allen et al. 1999b). At the same time, Cas A is situated in a region of high ambient matter density. Nevertheless it is interesting to note that Cas A is not a 3EG source. The latter case, Monoceros, was already discussed in Section 10.3.

There have also been observations of unidentified γ -ray sources whose identifications are, perhaps, more tentative. These observations were made with the Whipple 10-m telescope (Buckley et al. 1997) Two of

Table 7: TeV Observations of SNRs. Plerions are shown in the first panel and shell-type SNRs in the second. The third panel shows results for two 3EG sources coincident with SNRs for which there have also been TeV observations. Partially adapted from Fegan (2001) and Mori (2001).

Object Name	Exposure time (hours)	Flux/Upper Limit or spectrum $10^{-11} \text{ cm}^{-2} \text{ s}^{-1}$ or $10^{-11} \text{ cm}^{-2} \text{ s}^{-1} \text{ TeV}^{-1}$
All TeV Observatories		
Crab Nebula	$\rightarrow \infty$	7.0 ($> 400 \text{ GeV}$)
CANGAROO		
PSR 1706-44	60	0.15 ($> 1 \text{ TeV}$)
Vela Pulsar	116	$0.26 (\text{E}/2 \text{ TeV})^{-2.4} \text{ TeV}^{-1}$
Durham		
PSR 1706-44	10	1.2 ($> 300 \text{ GeV}$)
Vela Pulsar	8.75	$< 5.0 (\text{E}/2 \text{ TeV})^{-2.4}$
CANGAROO		
RXJ 1713.7-3946	66	0.53 ($\geq 1.8 \text{ TeV}$)
RXJ 1713.7-3946 ^f	32	$0.53 \text{--} 1.63 \pm 0.15 \pm 0.32) E^{-2.84 \pm 0.15 \pm 0.20}$
SN1006	34	0.46 ($\geq 1.7 \text{ TeV}$)
W28	58	$< 0.88 (\text{E}/2 \text{ TeV})^a$
HEGRA		
Cas A	232	0.058 ($> 1 \text{ TeV}$) ^b
γ -Cygni	47	$< 1.1 (\text{E}/2 \text{ TeV})^c$
Monoceros	120	? ^e
Durham		
SN1006	41	$< 1.7 (\text{E}/2 \text{ TeV})^d$
Whipple		
Monoceros	13.1	$< 4.8 (\text{E}/2 \text{ TeV})^d$
Cas A	6.9	$< 0.66 (\text{E}/2 \text{ TeV})^d$
W44	6	$< 3.0 (\text{E}/2 \text{ TeV})^d$
W51	7.8	$< 3.6 (\text{E}/2 \text{ TeV})^d$
γ -Cygni	9.3	$< 2.2 (\text{E}/2 \text{ TeV})^d$
W63	2.3	$< 6.4 (\text{E}/2 \text{ TeV})^d$
Tycho	14.5	$< 0.8 (\text{E}/2 \text{ TeV})^d$
CAT		
CasA	24.4	$< 0.74 (\text{E}/2 \text{ TeV})^d$
J2016+3657	287	5.8^d
J2020+4017	513	0.990^d

^aA different definition of Energy Threshold is used. ^bEvidence for emission at the 4.9σ level (Pühlhofer et al. 2001).

^cLimits converted from Crab units using flux of Hillas et al. (1998). ^dIntegral Flux Above 400 GeV. ^eNot yet reported. ^fObservations made with CANGAROO-II (Enomoto et al. 2002).

them were related with the 3EG sources in our sample, and details are provided in Table 7.

The Crab Nebula has been detected by several Cherenkov observatories and it is often used to provide a check on the calibration of new instruments (e.g. Aharonian et al. 2000). STACEE and CELESTE, on which we comment below, have published significant detections of the Crab Nebula in an energy range lower than that obtained by others ground-based instruments, $E > 190 \pm 60$ GeV (Oser et al. 2000) and $E > 50$ GeV (De Naurois et al. 2001), respectively. The Crab's energy spectrum between 300GeV and 50TeV has been well established (see below), and it steepens with energy (Hillas et al. 1998, Aharonian et al. 2000). No pulsation has yet been seen (Gillanders et al. 1997, Burdett et al. 1999, Aharonian et al. 1999).

The CANGAROO team has detected the pulsar PSR 1706-44 in 60 hours of observations (Kifune et al. 1995). They have also detected the Vela pulsar at the 6σ level, based on ~ 120 hours of observation. Observations by the Durham group (Chadwick et al. 1997) also confirmed these detections. In the case of Vela, the VHE signal, which is offset from the location of the pulsar by 0.14° , is thought to originate from a synchrotron nebula, powered by a population of relativistic electrons which were created in the supernova explosion and which have survived since then due to the low magnetic field in the nebula.

12.1 Future TeV telescopes and their look at SNRs - Adapted from Petry (2001)

At higher and higher energies the sky appears darker and darker. There are just 57 sources detected between 1 and 10 GeV (Lamb & Macomb 1997) and higher frequencies remain largely unobserved. In order to reach the highest energy γ -rays, new ground-based telescopes are being built and older ones upgraded. A very brief description of them, and of their impact on the SNR- γ -ray source association problem is given in this section.

One approach to constructing high-energy γ -ray detectors is to use existing solar farms, which have fields of large heliostats focusing sunlight on a central tower; such facilities lie unused at night. The arrival of the Čerenkov wavefront at groups of heliostats is precisely measured, and this information is used to differentiate γ -rays from cosmic-ray primaries (Ong 1998). STACEE (Chantell et al. 1998), CELESTE (Smith et al. 1997), Solar-2 (Tümer et al. 1999), and GRAAL (Arqueros et al. 1999) are all examples of such facilities.

MILAGRO (Sinnis et al. 1995) and Tibet HD (Amenomori et al. 1999) are examples of air showers detectors. These arrays can in principle operate 24 hours a day and are expected to achieve a larger energy range, comparable to the next generation imagers discussed below.

Imaging Atmospheric Čerenkov Telescopes (IACTs) are ground-based γ -ray detectors using the atmosphere as a tracker and calorimeter and having good all-around performance, both in sensitivity and angular resolution, for sources above 100 GeV (see Figure 30). They typically have point spread functions with $\theta_{68} < 0.16^\circ$. The number of detected primary gamma-photons will typically be > 100 , and therefore source locations, computed as θ_{68}/\sqrt{N} , can reach arcmin accuracies. Generically, the possibility of separating two nearby point sources can be realized if their angular distance is $> 3\theta_{68}$. Some forthcoming IACT telescopes in the TeV regime are detailed in Table 8.

The successful introduction of stereo imaging technology in the HEGRA instrument has paved the way for bigger and more complex instruments. The unprecedented accuracy in air shower stereo reconstruction of the HESS telescopes in Namibia will allow one to obtain an angular resolution of $\sim 0.1^\circ$ with a source

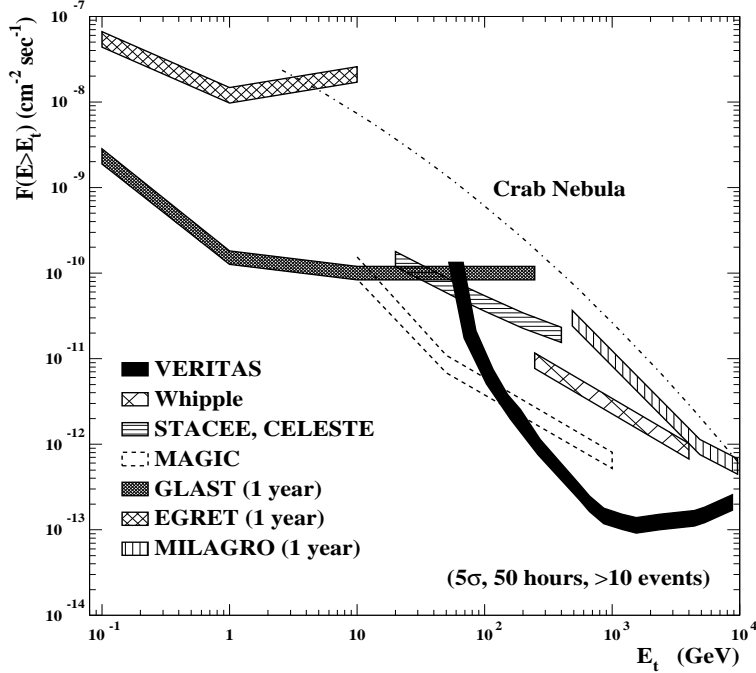


Figure 30: Comparison the sensitivity for point source detection of the very high-energy telescopes mentioned in the text. VERITAS sensitivity curve is comparable to HESS and CANGAROO III; Whipple's, to that of HEGRA, CAT, and CANGAROO-II. From Weekes et al. (2001) and Fegan (2001).

location accuracy of only 10 arcseconds (Konopelko 2001). After 50 hours of observation of a point source, HESS will detect a flux of $\sim 10^{-11} \text{ ph cm}^{-2} \text{ s}^{-1}$ at $E > 100 \text{ GeV}$. In the case of extended sources of angular size Θ , the flux detected will be $\sim (\Theta/0.1 \text{ deg}) \times 10^{-11} \text{ ph cm}^{-2} \text{ s}^{-1}$ in the same energy range. It is clear that such a powerful instrument will provide answers to many of the pending questions mentioned in this review, at least for the case of southern SNRs.

A natural next step in the development of stereo imaging arrays for TeV astronomy is to place one of these systems at high altitude, where it could detect much lower-energy gamma-rays. It has been estimated that at an altitude of 5 km, a threshold of 5 GeV might be achieved (Aharonian et al. 2001b). These systems, then, might replace orbital observatories in the GeV band in the foreseeable future.

In an attempt to establish an agenda for the new TeV telescopes, Petry (2001) and Petry & Reimer (2001) have analyzed the observational possibilities for each of the unidentified and tentatively identified EGRET sources. Several problems have to be taken into account. The first is that of the apparent spectral steepening of several 3EG sources between the GeV and the TeV band (see Reimer and Bertsch 2001). This could be why strong sources such as γ -Cyggni, IC443, W28, and CTA 1 were not observed in the TeV band (eg. Buckley et al. 1998). In order to get an estimate of the impact of this effect on any 3EG source, Petry (2001) proposed to use the same spectral steepening as that of the Crab Nebula. The differential spectral index $\Gamma_{0.1\text{GeV}}$ of the Crab Nebula at 0.1 GeV is $\Gamma_{0.1} = 2.19 \pm 0.02$ (Hartman et al. 1999) while it was measured by the Whipple telescope at 500 GeV to be $\Gamma_{500\text{GeV}} = 2.49 \pm 0.06 \pm 0.04$ (Hillas et al. 1998). The latter authors showed that the steepening towards higher energies can be described by an increase in spectral index of 0.15 per decade of energy. Petry (2001) showed that this would then imply, if a similar

Table 8: Next-generation Imaging Čherenkov Telescopes and their main characteristics. The locations of the sites chosen for these observatories and their estimated minimum energy thresholds are given. Roman numbers behind some of the project names denote the project phases. The Type refers to the number of individual telescopes and diameter of their mirror dish. The last column is the predicted energy threshold for γ -ray photons at zenith angle $\vartheta = 0^\circ$. (From Petry 2001).

Project name	latitude	longitude	altitude	Type	$E_{\text{thr}}(0^\circ)$
CANGAROO III	31° S	137° E	160 m	4×10 m	80 GeV
HESS I	23° S	17° E	1800 m	4×13 m	40 GeV
MAGIC I	29° N	17° W	2200 m	1×17 m	30 GeV
VERITAS	32° N	111° W	1300 m	7×10 m	60 GeV

situation is the case for the unidentified EGRET sources, that

$$\begin{aligned}
 F(E > x[\text{GeV}]) &= F_0 \cdot 10^{-\alpha} \cdot 10^{-(\alpha+0.15)} \cdot \left(\frac{x}{10}\right)^{-(\alpha+0.30)} \\
 &= F_0 \cdot 10^{-(\alpha-0.15)} \cdot x^{-(\alpha+0.30)} \\
 &\quad \text{for } 10 < x < 100 \\
 F(E > x[\text{GeV}]) &= F_0 \cdot 10^{-\alpha} \cdot 10^{-(\alpha+0.15)} \cdot 10^{-(\alpha+0.30)} \cdot \left(\frac{x}{100}\right)^{-(\alpha+0.45)} \\
 &= F_0 \cdot 10^{-(\alpha-0.45)} \cdot x^{-(\alpha+0.45)} \\
 &\quad \text{for } 100 < x < 1000
 \end{aligned} \tag{42}$$

where F_0 is the integrated flux above 0.1 GeV and α is the flux spectral index (obtained by subtracting 1.0 from the differential spectral index Γ , quoted for instance in Table 1) of a given source taken from the Third EGRET Catalog. An extrapolation without taking into account possible breaks in the spectrum could give a large over-estimation of the high-energy flux. Although not valid for all sources, the previous scheme can be used to give an idea of the expected flux from interesting 3EG detections (Petry 2001, Petry & Reimer 2001).

Nonetheless, not only the spectral cutoffs, but some other technical problems affect actual observation. Čherenkov telescopes typically cannot observe at zenith angles much larger than 70° . The zenith angle ϑ at the upper culmination of an astronomical object depends on the the latitude ϕ of the observatory and the declination DEC of the object according to $\vartheta = |\phi - \text{DEC}|$. Therefore, the condition $|\phi - \text{DEC}| \leq 70^\circ$ has to be imposed in the selection of observable objects.

The area perpendicular to the optical axis illuminated by the Čherenkov light at the position of the telescope is proportional to the square of the distance d to the shower maximum. d grows with ϑ as $d \propto 1/\cos(\vartheta)$. The energy threshold E_{thr} of a Čherenkov telescope is equivalent to a Čherenkov photon density threshold ρ_{thr} at the position of the telescope. ρ_{thr} is an instrumental constant determined by the trigger condition of the data acquisition system. These parameters depend on the zenith angle ϑ and the primary photon energy, and impact directly on the required flux sensitivity for an observation to be plausible. Under reasonable assumptions, $\rho(E, \vartheta) \propto E \cdot \cos^2(\vartheta)$ (Petry 2001), and then, to satisfy the trigger condition $\rho(E, \vartheta) > \rho_{\text{thr}}$, E has to increase with ϑ as $E_{\text{thr}}(\vartheta) = E_{\text{thr}}(0^\circ) \cdot \cos^{-2}(\vartheta)$, with the values for $E_{\text{thr}}(0^\circ)$ shown in Table 8. An increase in effective collection area is accompanied by a proportional increase in hadronic background rate, such that the gain in flux sensitivity is therefore only the square-root of the gain in area. If we define, $F_{5\sigma}(E_{\text{thr}})$ as the integral flux above the energy threshold E_{thr} which results

in a 5σ detection after 50 h of observation time,

$$F_{5\sigma}(E_{\text{thr}}(\vartheta), \vartheta) = F_{5\sigma}(E_{\text{thr}}(0^\circ), 0^\circ) \cdot \cos^{-1}(\vartheta). \quad (43)$$

The last main ingredient that has to be considered is the needed observation time itself. It can be computed as (Petry 2001)

$$T_{5\sigma}(E_{\text{thr}}) = \left(\frac{F(E_{\text{thr}})}{F_{5\sigma}(E_{\text{thr}})} \right)^{-2} \cdot 50\text{h}. \quad (44)$$

Objects requiring much more than 50-100 hours will probably be excluded from the first years of operation of the next generation IACTs, since, typically, the maximum expected duty cycle for these telescopes will be about 1000 hours yr^{-1} .

Taking these considerations into account it is possible to determine which of the 3EG sources analyzed here might be detected by the next generation IACTs. 12 out of the 19 SNR-EGRET cases listed in Table 1 can be considered likely candidates, from a practical point of view. The complete results for all 3EG sources superposed to SNRs that might be detected in less than 50 hours is compiled in Table 9. Columns are as follows: 3EG name, radius of the 95% confidence contour, spectral index at 0.1 GeV, all from Hartman et al. (1999), minimum zenith angle, IACTs minimum energy threshold, expected flux at the minimum energy threshold, the integral spectral index at the IACTs minimum energy threshold for this source, the observation time to obtain a detection with 5σ significance (in brackets are the corresponding data if the spectrum at 0.1 GeV was steeper by one standard deviation). A ‡-mark indicates that the detection is photon flux limited: the observation time was increased such that 100 photons are detected.

Many of the SNR-EGRET pairs studied will be primary candidates for one or several of the forthcoming IACTs. A combination of TeV and GeV observations, together with an understanding of the molecular material distribution of the region, will be crucial in determining the nature of several of the unidentified EGRET sources analyzed here.

13 Concluding remarks

The coming years will be exciting times again for γ -ray astronomy – after the unfortunate and premature forced demise of the Compton Observatory. INTEGRAL, AGILE and the new stereo-IACTs should be on-line soon; and in the longer term, GLAST will surely bring about another revolution, answering existing questions, such as the one reviewed here, and posing further challenges.

Ultimately, it will take a sensitive and high spatial-resolution MeV-GeV detector such as GLAST working in close consort with the ground-based TeV and radio telescopes to address the Galactic cosmic ray origin problem: the single most definitive test that SNRs (or any other putative sources) are accelerating CR nuclei would be the statistically significant detection of the signature neutral pion γ -ray hump centered at 67.5 MeV (in $\log E_\gamma$), as has been seen already by EGRET in the diffuse γ -ray background (Hunter et al. 1997). Though such a detection, by itself, only proves the existence of lower energy (~ 1 GeV/n) nuclei, the detection allows one to immediately normalize the hadronic vs. electronic contributions in a model-independent fashion at those ‘lower’ energies. Thus, such a detection together with the extension of the spectrum into the TeV regime, and a multiwavelength spectrum inconsistent with an electronic origin, ought to be sufficient evidence to conclude that nuclei are being accelerated by SNRs. It remains to be seen if this will be borne out by the data.

Table 9: TeV observability of EGRET-SNR pairs, adapted from Petry (2001).

object name	θ_{95} [°]	α	ϑ_{\min} [°]	E_{thr} [GeV]	$F(E_{\text{thr}})$ [cm $^{-2}$ s $^{-1}$]	$\alpha(E_{\text{thr}})$	$T_{5\sigma}$ [h]
3EG		CANGAROO III					
0617+2238	0.13	1.01 ± 0.06	54	228	5.13×10^{-11} (3.22×10^{-11})	1.46(1.52)	22(55)
0631+0642	0.46	1.06 ± 0.15	38	128	4.12×10^{-11} (1.41×10^{-11})	1.51(1.66)	19(161)
0634+0521	0.67	1.03 ± 0.26	36	123	5.39×10^{-11} (8.47×10^{-12})	1.48(1.74)	11(430)
1410-6147	0.36	1.12 ± 0.14	31	108	8.78×10^{-11} (3.30×10^{-11})	1.57(1.71)	3.51(25)
1714-3857	0.51	1.30 ± 0.20	8	82	2.70×10^{-11} (7.06×10^{-12})	1.60(1.80)	28(409)
1744-3011	0.32	1.17 ± 0.08	1	80	9.72×10^{-11} (5.70×10^{-11})	1.47(1.55)	2.86 ‡ (6.17)
1746-2851	0.13	0.70 ± 0.07	2	80	4.22×10^{-9} (2.64×10^{-9})	1.00(1.07)	0.07 ‡ (0.11 ‡)
1800-2338	0.32	1.10 ± 0.10	7	81	1.46×10^{-10} (7.45×10^{-11})	1.40(1.50)	1.91 ‡ (3.73 ‡)
1824-1514	0.52	1.19 ± 0.18	16	86	4.18×10^{-11} (1.24×10^{-11})	1.49(1.67)	12(141)
1826-1302	0.46	1.00 ± 0.11	18	88	2.78×10^{-10} (1.32×10^{-10})	1.30(1.41)	1.00 ‡ (2.11 ‡)
1837-0606	0.19	0.82 ± 0.14	25	97	6.30×10^{-10} (2.40×10^{-10})	1.12(1.26)	0.44 ‡ (1.16 ‡)
1856+0114	0.19	0.93 ± 0.10	32	112	3.33×10^{-10} (1.65×10^{-10})	1.38(1.48)	0.83 ‡ (1.68 ‡)
3EG		HESS I					
0617+2238	0.13	1.01 ± 0.06	46	82	2.21×10^{-10} (1.48×10^{-10})	1.31(1.37)	4.22(9.44)
0631+0642	0.46	1.06 ± 0.15	30	53	1.42×10^{-10} (5.53×10^{-11})	1.36(1.51)	6.69(44)
0634+0521	0.67	1.03 ± 0.26	28	52	1.77×10^{-10} (3.49×10^{-11})	1.33(1.59)	4.17(107)
1410-6147	0.36	1.12 ± 0.14	39	66	1.80×10^{-10} (7.28×10^{-11})	1.42(1.56)	5.11(31)
1714-3857	0.51	1.30 ± 0.20	16	43	7.44×10^{-11} (2.21×10^{-11})	1.60(1.80)	20(224)
1744-3011	0.32	1.17 ± 0.08	7	41	2.63×10^{-10} (1.63×10^{-10})	1.47(1.55)	1.48(3.88)
1746-2851	0.13	0.70 ± 0.07	6	40	8.36×10^{-9} (5.49×10^{-9})	1.00(1.07)	0.03 ‡ (0.05 ‡)
1800-2338	0.32	1.10 ± 0.10	1	40	3.93×10^{-10} (2.16×10^{-10})	1.40(1.50)	0.71 ‡ (2.17)
1824-1514	0.52	1.19 ± 0.18	8	41	1.28×10^{-10} (4.34×10^{-11})	1.49(1.67)	6.28(55)
1856+0114	0.19	0.93 ± 0.10	24	48	9.55×10^{-10} (5.15×10^{-10})	1.23(1.33)	0.29 ‡ (0.54 ‡)
3EG		MAGIC I					
0010+7309	0.24	0.85 ± 0.10	44	58	7.87×10^{-10} (4.16×10^{-10})	1.15(1.25)	0.35 ‡ (0.67 ‡)
0617+2238	0.13	1.01 ± 0.06	6	30	8.11×10^{-10} (5.75×10^{-10})	1.31(1.37)	0.34 ‡ (0.48 ‡)
0631+0642	0.46	1.06 ± 0.15	22	35	2.49×10^{-10} (1.03×10^{-10})	1.36(1.51)	1.12 ‡ (3.15)
0634+0521	0.67	1.03 ± 0.26	24	36	2.89×10^{-10} (6.26×10^{-11})	1.33(1.59)	0.96 ‡ (8.75)
1744-3011	0.32	1.17 ± 0.08	59	114	5.64×10^{-11} (3.21×10^{-11})	1.62(1.70)	35(107)
1746-2851	0.13	0.70 ± 0.07	58	106	3.16×10^{-9} (1.94×10^{-9})	1.15(1.22)	0.09 ‡ (0.14 ‡)
1800-2338	0.32	1.10 ± 0.10	53	82	1.45×10^{-10} (7.42×10^{-11})	1.40(1.50)	3.71(14)
1824-1514	0.52	1.19 ± 0.18	44	58	7.48×10^{-11} (2.38×10^{-11})	1.49(1.67)	10(99)
1837-0423	0.52	1.71 ± 0.44	33	43	4.44×10^{-11} (3.08×10^{-12})	2.01(2.45)	21(> 500)
1856+0114	0.19	0.93 ± 0.10	28	38	1.26×10^{-9} (6.97×10^{-10})	1.23(1.33)	0.22 ‡ (0.40 ‡)
1903+0550	0.64	1.38 ± 0.17	23	35	9.10×10^{-11} (3.35×10^{-11})	1.68(1.85)	4.12(30)
2016+3657	0.55	1.09 ± 0.11	8	31	3.43×10^{-10} (1.83×10^{-10})	1.39(1.50)	0.81 ‡ (1.52 ‡)
2020+4017	0.16	1.08 ± 0.04	11	31	1.26×10^{-9} (1.00×10^{-9})	1.38(1.42)	0.22 ‡ (0.28 ‡)
3EG		VERITAS					
0010+7309	0.24	0.85 ± 0.10	41	141	2.70×10^{-10} (1.31×10^{-10})	1.30(1.40)	1.03 ‡ (2.12 ‡)
0617+2238	0.13	1.01 ± 0.06	9	82	2.20×10^{-10} (1.47×10^{-10})	1.31(1.37)	1.26 ‡ (1.89 ‡)
0631+0642	0.46	1.06 ± 0.15	25	98	6.16×10^{-11} (2.19×10^{-11})	1.36(1.51)	4.51 ‡ (13)
0634+0521	0.67	1.03 ± 0.26	27	100	7.34×10^{-11} (1.22×10^{-11})	1.48(1.74)	3.78 ‡ (42)
1800-2338	0.32	1.10 ± 0.10	56	251	2.61×10^{-11} (1.19×10^{-11})	1.55(1.65)	23(110)
1856+0114	0.19	0.93 ± 0.10	31	108	3.48×10^{-10} (1.73×10^{-10})	1.38(1.48)	0.80 ‡ (1.61 ‡)
1903+0550	0.64	1.38 ± 0.17	26	99	1.62×10^{-11} (5.00×10^{-12})	1.68(1.85)	24(249)
2016+3657	0.55	1.09 ± 0.11	5	81	8.92×10^{-11} (4.27×10^{-11})	1.39(1.50)	3.11 ‡ (6.50 ‡)
2020+4017	0.16	1.08 ± 0.04	8	82	3.34×10^{-10} (2.55×10^{-10})	1.38(1.42)	0.83 ‡ (1.09 ‡)

Table 10: Instrumental parameters of some of the forthcoming satellite missions in the MeV-GeV range. EGRET data (first panel) is shown for comparison. The second panel corresponds to AGILE-GRID and the third to GLAST-LAT.

Energy range	Energy resolution $\Delta E/E$	Effective area cm^2	Field of view sr	Angular resolution	Minimum flux $\text{ph cm}^{-2} \text{ s}^{-1}$	Source location arcmin	Bremsstrahlung	Life yr
20 MeV	~ 0.1	1500	0.5	100 MeV: 5.8° 1 GeV: 1.7°	$\sim 10^{-7}$	~ 30	91-96	
30 GeV								
30 MeV	~ 1	540	3.0	1 GeV: 0.6°	$\geq 6 \times 10^{-8}$	5-20	03-06	
50 GeV								
20 MeV	~ 0.1	8000	2.5	100 MeV: $\sim 3.5^\circ$ 10 GeV: $\sim 0.1^\circ$	$\sim 4 \times 10^{-9}$	< 1	06-11	
300 GeV								

Kilometer-scale neutrino telescopes have also proposed as viable detectors of hadronic cosmic ray sources (Halzen & Hooper 2002), and will be a welcomed addition to the arsenal of space- and ground-based detectors that ought to be lined up by the time the large-scale neutrino telescopes are functional. Surely, with all this instrumentation focused on the problem we will finally be able to test Shklovskii's suspicion that "it is possible that ionized interstellar atoms are accelerated in the moving magnetic fields connected with an expanding [SNR] nebula." (Shklovskii, 1953).

14 Appendix: Reviewing the prospects for the forthcoming GeV satellites

14.1 INTEGRAL

The International Gamma-ray Astrophysics Laboratory (INTEGRAL) will be launched by the end of 2002. It will have two main scientific instruments, named SPI (Spectrometer of INTEGRAL) and IBIS (Imager onBoard the Integral Satellite). SPI will work in the range 20 KeV – 8 MeV and will perform high resolution spectroscopy; it can measure γ -ray line profiles with an accuracy of 2 keV. The sensitivity of IBIS lies in the range 10 keV – 10 MeV, and it will focus on achieving good angular resolution (12 arcmin). INTEGRAL will also have three monitors, the twin JEM-X's (3 keV – 35 keV) and a OMC in the optical band (500-600 nm). The JEM-X's will have an angular resolution of 3 arcmin and a 4.8° fields of view. The OMC will have a pixel resolution of 16.6 arcsec and a $5^\circ \times 5^\circ$ field of view (Schönfelder 2001).

INTEGRAL could identify compact objects with good spatial resolution that are likely counterparts of EGRET sources, and will help confirm or reject interpretations based, for instance, on microquasars and γ -ray blazars. The INTEGRAL galactic plane exposure will help to clarify the confused region near Vela. Another 1 Ms exposure, part of the satellite Open Program, will focus on the Carina region. That part of the sky is populated with five EGRET sources, two of which were analyzed above in the case-by-case study: 3EG J1102-6103 and 3EG J1013-5915. As an example of its potential, we will briefly discuss what

INTEGRAL can do in establishing the nature of these sources.

The former case, 3EG J1102-6103, was briefly mentioned in the corresponding section above. Although a hadronic origin for the γ -ray emission is possible for this source, it could also be the result of inverse Compton up-scattering of UV photons by electrons accelerated in the winds of one or several Wolf-Rayet stars (particularly in the region where the winds of W39 and WR38B collide). If the latter explanation is correct, INTEGRAL should see a source where the winds collide.

In the latter case, the source 3EG J1013-5915 is likely mostly produced by PSR J1013-5915 (Camilo et al. 2001). The JEM-X monitor, in particular, could then probe the putative non-thermal emission from this region, especially the tail of the synchrotron spectrum and, in this way, help to determine the high-energy cutoff of the electron population in the source.

In addition, there have been suggestions that INTEGRAL could detect the 0.511 MeV line from giant molecular clouds (see e.g. Guessoum et al. 2001). Giant molecular clouds are typically surrounded by HII regions, ionized in an uncertain fraction. If cosmic-rays are diffusing into the cloud, the cores, too, may be ionized. If a sufficient density of cosmic-rays is present, they could excite CNO nuclei as well as lead to the production of nuclear gamma-rays lines and positron-production, the latter being emitted by radioactive nuclei. The fluxes and line separations predicted are on the verge of detectability by INTEGRAL (Guessoum et al. 2001), but it will be an interesting arena to explore with forthcoming observations, particularly for those giant molecular clouds closer to Earth (regrettably not the ones we find superposed with the SNRs in Table 1).

Thus, although it is expected that no direct observations with INTEGRAL can prove that cosmic-rays are accelerated in SNR shocks (the energy range of the relevant phenomena, around 100 MeV and beyond, is out of the INTEGRAL energy band), they can be used to explore alternative explanations for the unidentified EGRET sources, and so are important to get an overall picture of the SNR-EGRET source connection. Nuclear gamma-ray line signatures in the 0.1-10 MeV band will certainly also provide important hints regarding the CR acceleration processes in the Galaxy.

14.2 AGILE

AGILE (Astro-rivelatore Gamma a Immagini Leggero), is expected to be launched in 2003 (for a recent review see Tavani et al. 2001). AGILE will have a very large field of view, covering at one time approximately 1/5 of the sky at energies between 30 MeV and 50 GeV. The angular resolution will be a factor of two better than that of EGRET, specifically due to the GRID instrument, whose parameters are given in Table 10. However, the sensitivity for point-like sources will remain comparable to that of EGRET. AGILE will also have detection and imaging capabilities in the hard X-ray range provided by the Super-AGILE detector. The main goals of Super-AGILE are the simultaneous γ -ray and hard X-ray detection of astrophysical sources (which was never achieved by previous γ -ray instruments), improved source positioning (1-3 arcmins, depending on intensity), fast burst alert, and on-board triggering capability.

AGILE is thus very well suited for studying compact objects, particularly those presenting γ -ray variability or pulsed emission. AGILE will search for pulsed γ -ray emission from all recently discovered Parkes pulsars coincident with EGRET sources (D'amico et al. 2001, Torres et al. 2001d, Camilo et al. 2001), so establishing their contribution to the EGRET γ -ray flux. Unpulsed γ -ray emission from plerionic SNRs, and search for time variability in pulsar-wind nebula interactions will also be possible targets for AGILE. Finally, AGILE will be essential in assessing the possible existence of new populations of variable

Please see the jpg file attached.

Figure 31: Models of the neutral pion decay, non-thermal Bremsstrahlung (NB), inverse Compton (IC), and pulsar (PSR) γ -ray spectra associated with W66. The sum of the three cosmic-ray components ($\pi^0 + \text{NB} + \text{IC}$) of the shell and the sum of all four components ($\pi^0 + \text{NB} + \text{IC} + \text{pulsar emission}$) are shown. EGRET spectral data is also included. From Allen et al. (1999). Astro-ph arXiv file: allen-spe.jpg

γ -ray sources in the galaxy, such as non-pulsating black holes, X-ray binaries, and microquasars. In the case of 3EG J0542+2610, for instance, AGILE could test the hypothesis that the γ -ray emission is produced in A0535+26 (Romero et al. 2001). The key prediction of this model is anti-correlation of the X-ray and γ -ray emissions.

14.3 GLAST

The Large Area Telescope (LAT) on the upcoming Gamma-ray Large Area Space Telescope (GLAST) mission will be suitable for studying the relationship between γ -ray sources and SNRs. The instrument's parameters are given in Table 10 (Michelson 2001). GLAST, expected to be launched in 2006, will explore the energy range from 30 MeV to greater than 100 GeV with 10% energy resolution between 100 MeV and 10 GeV. GLAST uniquely combines high angular resolution with superb sensitivity, and has a moderate effective area. Sources below the EGRET threshold ($\sim 6 \times 10^{-8}$ photons $\text{cm}^{-2} \text{ s}^{-1}$) will be localized to arcmin scales. This clearly will improve our understanding of the SNR shock acceleration of cosmic-rays and hadronic γ -ray production.

In what follows, we provide a brief example of GLAST capabilities as applied to the SNR γ -cygni (W66), courtesy of Seth Digel and NASA (see also, Ormes et al. 2000 astro-ph/0003270 from which this example is adapted). Allen et al. (1999) studied what information could be obtained from GLAST observations based on a 1-year all-sky survey assuming that 60% of the γ -ray flux was produced by a pulsar at the location proposed by Brazier et al. (1996). This pulsar was assumed to have a differential photon index of 2.08, that of the coincident source, 3EG J2020+4017. The remainder of the photon flux was assumed to

Please see the jpg file attached.

Figure 32: Comparison between the observed EGRET data and a GLAST simulation for the W66 SNR region. The large circle shows the position and extent of the radio shell of the SNR. GLAST will be able to localize distinctively the position of the putative γ -ray pulsar (marked here as the X-ray source) proposed by Brazier et al. as well as the SNR shock interacting with the molecular cloud, should both contribute as assumed to the γ -ray flux observed. Courtesy of S. Digel and NASA; adapted from Ormes et al. 2000 astro-ph/0003270. Astro-ph arXiv file: glast.jpg.

come from relativistically accelerated particles through both leptonic and hadronic processes – the large dominance of the latter in agreement with what we found in the corresponding section above. The position of the molecular cloud assumed in the simulations corresponds well with the CO clouds actually found – see Figure 28).

Allen et al. additionally assumed that the electron and proton spectra of W66 have the shape specified by Bell (1978, see their Eq. 5), with a common relativistic spectral index of $\Gamma = 2.08$. The normalization of the electron spectrum was determined from the radio data, by assuming that the magnetic field strength is $100 \mu\text{G}$. The normalization of the proton spectrum, instead, was determined by assuming that the total number of non-thermal electrons is a factor of 1.2 larger than the number of non-thermal protons.

The spectral results of the simulations are shown in Figure 31. It shows the γ -ray spectra produced by the putative pulsar, by the decay of neutral pions, as well as by the leptonic processes: Bremsstrahlung radiation of the electrons, and inverse Compton scattering of electrons on the cosmic microwave background radiation. The latter three of these four spectra were obtained using the γ -ray emissivity results of Gaisser, Protheroe, & Stanev (1998), and Baring et al. (1999). The non-thermal Bremsstrahlung and neutral pion spectra were obtained assuming that the average density of the material with which the cosmic-rays interact was $n_0 = 190 \text{ atoms cm}^{-3}$, which should be compared with the actual density we found, of $188 \text{ atoms cm}^{-3}$ (see Section 10.17. Perhaps most illustrative is Figure 32, which demonstrates that the resolution of

GLAST will allow one to distinguish the contribution of the pulsar from that of the interacting molecular cloud. Should a picture like Figure 32 be the result of an actual GLAST observation the proposed composite origin for 3EG J2020+4017 would be proved.

Acknowledgments

We thank Fumio Yamamoto, Masumichi Seta, Toshihiro Handa, and Tetsuo Hasegawa for providing CO(2-1) survey data toward the SNRs IC443, W44, and W66. We acknowledge F. Aharonian, M. Mori, F. Bocchino, J. Paredes and S. Digel for their kind permission to reproduce Figures 5 and 6, 3, 11, 23, and 32, respectively. We further acknowledge Felix Aharonian, Seth Digel, Dave Thompson, Don Ellison, Paula Benaglia, and Isabelle Grenier for useful comments. We thank D. Petry for his permission to adapt part of his work (Petry 2001) in Section 12.1.

D.F.T. was supported by Princeton University, CONICET, and Fundación Antorchas during different stages of this research. Also, part of his work was performed under the auspices of the U.S. Department of Energy by University of California Lawrence Livermore National Laboratory under contract No. W-7405-Eng-48. G.E.R. and J.A.C. were supported by CONICET (under grant PIP N° 0430/98), ANPCT (PICT 03-04881), as well as by Fundación Antorchas. He also thanks the Max Planck Association for additional support at the MPIfK, Heidelberg, as well as the University of Paris VII and the Service d’Astrophysique, Saclay, for kind hospitality. Y.M.B. acknowledges the support of the High Energy Astrophysics division at the CfA and the *Chandra* project through NASA contract NAS8-39073.

This research would have been impossible without the effort of D. A. Green at the Mullard Radio Astronomy Observatory, Cambridge (UK) in providing a web-based SNR catalog. NASA Goddard’s EGRET archive and MPE’s ROSAT All-Sky Survey were also invaluable to this study. The optical (and part of the radio) data is from the Digitized Sky Survey, accessible through <http://skyview.gsfc.nasa.gov/> Parts of this work were based on photographic data obtained using The UK Schmidt Telescope. The UK Schmidt Telescope was operated by the Royal Observatory Edinburgh, with funding from the UK Science and Engineering Research Council, until 1988 June, and thereafter by the Anglo-Australian Observatory. Original plate material is copyright (c) the Royal Observatory Edinburgh and the Anglo-Australian Observatory. The plates were processed into the present compressed digital form with their permission. The Digitized Sky Survey was produced at the Space Telescope Science Institute under US Government grant NAG W-2166.

References

- [1] Aharonian F.A., Drury L.O’C., & Völk H.J. 1994, A&A 285, 645
- [2] Aharonian F.A., & Atoyan, A.M. 1996, A&A 309, 91
- [3] Aharonian F.A., et al. 1999, A&A 346, 913
- [4] Aharonian F.A. et al. 2000, ApJ 539, 317
- [5] Aharonian F.A. 2001, Space Sci. Rev. 99, 187
- [6] Aharonian F.A. et al. 2001, A&A 375, 1008
- [7] Aharonian F.A., Konopelko A.K., Völk H.J., & Quintana H., 2001b, Astrop. Phys. 15, 335

- [8] Aharonian F.A., et al. 2002, astro-ph/0209360, *A&A*, in press.
- [9] Aharonian F.A., et al. 2002b, *A&A* 390, 39
- [10] Allen G.E., Digel S.W., & Ormes J.F. 1999a, Proc. Int. Cosmic Ray Conf., Utah, 5, 515
- [11] Allen G.E., Gotthelf E.V., & Petre R. 1999b, Proc. Int. Cosmic Ray Conf., Utah, 5, 480
- [12] Amenomori M., et al. 1999, *ApJ* 525, L93
- [13] Anderson S.B., et al. 1996, *ApJ* 468, L55
- [14] Arikawa Y., Tatematsu, K., Sekimoto Y., & Takahashi, T. 1999, *PASJ* 51, L7
- [15] Arqueros F. et al. 1999, Proc. Int. Cosmic Ray Conf., Utah, 5, 211
- [16] Asaoka I., Aschenbach B. 1994, *A&A* 284, 573
- [17] Aschenbach B. 1998, *Nature* 396, 141
- [18] Atoyan A.M., Aharonian F.A., & Voelk H.J. 1995, *Phys. Rev. D* 52, 3265
- [19] Atoyan A.M., Aharonian F.A., Tuffs R.J., Völk H.J. 2000a, *A&A* 355, 211
- [20] Atoyan A.M., Tuffs R.J., Aharonian F.A., Völk H.J. 2000b, *A&A* 354, 915
- [21] Bamba A., Yokogawa J., Sakano M., & Koyama K. 2000, *PASJ* 52, 259
- [22] Baring, M.G. et al. 1999, *ApJ* 513, 311
- [23] Becker R.H., & Helfand D.J. 1987, *AJ* 94, 1629
- [24] Bednarek W. 1993, *A&A* 278, 307
- [25] Bell A.R. 1978, *MNRAS* 182, 147
- [26] Benaglia P., Romero G.E., Stevens I. & Torres D.F. 2001, *A&A* 366, 605
- [27] Bignami G.F., & Hermsen W. 1983, *ARA&A* 21, 67
- [28] Bignami G.F., Bennet K., Buccheri R., Caraveo P., & Hermsen W. 1981, *A&A* 93, 71
- [29] Bildsten L. 1997, *ApJS* 113, 367
- [30] Bloemen H., et al. 1997, *ApJ* 475, L25
- [31] Bocchino F., & Bykov A.M. 2000, *A&A* 362, L29
- [32] Bocchino F., & Bykov A.M. 2001, *A&A* 376, 248
- [33] Brazier K.T.S., Kanbach G., Carramiñana A., Guichard J., & Merck M. 1996, *MNRAS* 281, 1033
- [34] Brazier K.T.S., Reimer O., Kanbach G., & Carramiñana A. 1998, *MNRAS* 295, 819
- [35] Buckley J.H., et al. 1997, Proc. 25th Int. Cosmic Ray Conf., Durban, 3, 237
- [36] Buckley J.H., et al. 1998, *A&A* 329, 639

[37] Burdett A., et al. 1999, Proc. Int. Cosmic Ray Conf., Utah, 5, 448

[38] Butt Y., Torres D.F., Combi J.A., Dame T., & Romero G.E. 2001, ApJ 562, L167

[39] Butt Y., Torres D.F., Romero G.E., Dame T., & Combi J.A. 2002a, Nature 418, 499

[40] Butt Y., Torres D.F., Combi J.A., Dame T., & Romero G.E. 2002b, To appear in the proceedings of 22nd Moriond Astrophysics Meeting: The Gamma Ray Universe, Les Arcs, Savoie, France, 9-16 Mar 2002. astro-ph/0206132

[41] Bykov A.M., Chevalier R.A., Ellison D.C., & Uvarov Y.A. 2000, ApJ 538, 203

[42] Camilo F., et al. 2001, ApJ 557, L51

[43] Caraveo P.A., De Luca A., Mignani R.P., & Bignami G.F. 2001, ApJ 561, 930

[44] Carramiñana A. 2001, in Proc. Int. Workshop on The Nature of Galactic Unidentified Gamma-ray Sources, O. Carramiñana, O. Reimer, D. Thomson Eds., Kluwer Academic Press, p.107

[45] Case G., & Bhattacharya D. 1998, ApJ 504, 761

[46] Case G., & Bhattacharya D. 1999, ApJ 521, 246

[47] Caswell J.L., & Barnes P.J. 1985, MNRAS, 216, 753

[48] Caswell J.L., Murray J.D., Roger R.S., Cole D.J., & Cooke D.J. 1975, A&A 45, 239

[49] Chadwick P.M. et al. 1997, Proc. 25th Int. Cosmic Ray Conf. Durban, 3, 189

[50] Chantell M.C., et al. 1998, Nucl. Instrum. Methods A408, 468

[51] Chapman J.M., Leitherer C., Koribalski B., Bouter R., & Storey M. 1999, ApJ 518, 890

[52] Chen W. & White R. 1991, ApJ 381, L63

[53] Cheng K.S., & Ruderman M. 1989, ApJ 337, L77

[54] Cheng K.S., & Ruderman M. 1991, ApJ 373, 187

[55] Chevalier R.A. 1999, ApJ 511, 798

[56] Clark D.H., & Caswell J.L. 1976, MNRAS 174, 267

[57] Clark G.W., Garmire G.P. & Kraushaar W.L. 1968 ApJ 153, L203

[58] Claussen M.J., Frail D.A., Goss W.M., & Gaume R.A. 1997, ApJ 489, 143

[59] Clemens D.P. 1985, ApJ 295, 422

[60] Combi J.A., & Romero G.E. 1995, A&A 303, 872

[61] Combi J.A., Romero G.E., & Azacárate I. 1997, Ap&SS, 250, 1

[62] Combi J.A., Romero G.E., & Benaglia P. 1998, A&A 333, L91

[63] Combi J.A., Romero G.E., & Benaglia P. 1999, ApJ 519, L177

[64] Combi J.A., Romero G.E., Benaglia P., & Jonas J. 2001, A&A 366, 1047

[65] Condon, J.J., Broderick, J.J., & Seielstad, G.A. 1991, AJ 102, 2041

[66] Contreras M.E., et al. 1997, ApJ 488, L153

[67] Corbel S., Chapuis C., Dame T.M., & Durouchoux P. 1999, ApJ 526, L29

[68] Cornett R.H., Chin G., & Knapp G.R. 1977, A&A 54, 889

[69] Crovisier J., Fillit R., & Kazes I. 1973, A&A 27, 417

[70] Crutcher R.M. 1988, in “Molecular Clouds, Milky-Way & External Galaxies”, R. Dickman, R. Snell, & J. Young Eds., New York, Springer, p.105

[71] Crutcher R.M. 1994, “Clouds, cores and low mass stars”, Astronomical Society of the Pacific Conference Series, volume 65; Proceedings of the 4th Haystack Observatory, edited by D. P. Clemens and R. Barvainis, p.87

[72] Crutcher, R.M. 1999, ApJ 520, 706

[73] Cusumano G., Maccarone M.C., Nicastro L., Sacco B., & Kaaret P. 2000, ApJ 528, L25

[74] Dame T.M., Elmegreen B.G., Cohen R.S., & Thaddeus P. 1986, ApJ 305, 892

[75] Dame T.M., Hartmann D., & Thaddeus P. 2001, ApJ 547, 792

[76] D’Amico N., et al. 2001, ApJ 552, L45

[77] De Jager O.C., & Mastichiadis A. 1997, ApJ 482, 874

[78] De Naurois M., et al. 2001, Proc. Int. Symp. on High Energy Gamma-Ray Astro. (Heidelberg), F. Aharonian and H.J. Völk (Eds.), AIP, New York, p.540

[79] Dermer C.D. 1986, A&A 157, 223

[80] Dermer C.D., et al. 1997, AJ 113, 1379

[81] Dermer C.D. 1997, in Proceedings of the Fourth Compton Symposium, Editors Charles D. Dermer, Mark S. Strickman, and James D. Kurfess, Williamsburg, VA April 1997: AIP Conference Proceedings 410, p. 1275.

[82] Dickman R.L., Snell R.L., Ziurys L.M., & Huang Y.-L. 1992, ApJ 400, 203

[83] Doherty et al. 2002, MNRAS, submitted.

[84] Dorfi E.A. 1991, A&A 251, 597

[85] Dorfi E.A. 2000, Ap&SS. 272, 227

[86] Downes A.J.B., Pauls T., & Salter C.J. 1980, A&A 92, 47

[87] Drury L.O’C., Aharonian F., & Völk H.J. 1994, A&A 287, 959

[88] Drury L.O’C. et al. 2001. Report of working group number four at the ISSI workshop on Astrophysics of Galactic Cosmic Rays: astro-ph/0106046

[89] Dubner G.M., Velázquez P.F., Goss W.M., & Holdaway M. A. 2000, AJ 120, 1933

[90] Duncan A.R., Stewart R.T., Haynes R.F., & Jones K.L. 1995, MNRAS 277, 36

[91] Duncan A.R., Stewart R.T., Haynes R.F., & Jones K.L. 1997, MNRAS 287, 722

[92] Eichler D., & Usov V.V. 1993, ApJ 402, 271

[93] Ellison D.C., Slane P., & Gaensler B.M. 2001, ApJ 563, 191

[94] Enomoto R., et al. 2002, Nature 416, 823

[95] Esposito J.A., Hunter S.D., Kanbach G., & Sreekumar P. 1996, ApJ 461, 820

[96] Falcke H., Cotera A., Duschl W.J., Melia F., & Rieke M.J. 1999, “The Central Parsecs of the Galaxy”, ASP Conference Series, Vol. 186.

[97] Fegan S. 2001, Proc. Int. Workshop on The Nature of Galactic Unidentified Gamma-ray Sources, O. Carramiñana, O. Reimer, D. Thomson Eds., Kluwer Academic Press, p.285

[98] Fesen R.A. 1984, ApJ 281, 658

[99] Fierro J.M., et al. 1993, ApJ 413, L27

[100] Frail D.A., Kulkarni S.R., & Vasisht G. 1993, Nature 365, 136

[101] Frail D.A., Giacani E.B., Goss W.M., & Dubner G. 1996, ApJ 464, L165

[102] Fürst E., Reich W., Reich P., & Reif K. 1990, ApJS 85, 691

[103] Gaisser T.K., Protheroe R.J., & Stanev T. 1998 ApJ 492, 219

[104] Gehrels N., Macomb D.J., Bertsch D.L., Thompson D.J., & Hartman R.C. 2000, Nature 404, 363

[105] Gehrels N., & Shrader C.R. 2001, in 2001, in Gamma 2001, edited by S. Ritz, N. Gehrels, & C. R. Schader, AIP Conference Proceedings, New York, p.3

[106] Georganopoulos M., Aharonian F. A., & Kirk J. 2002, A&A 388, L25

[107] Georgelin Y.P. & Georgelin Y.M. 1970, A&A 7, 133

[108] Georgelin Y.P. & Georgelin Y.M. 1976, A&A 49, 57

[109] Giacani E.B., et al. 1997, AJ 113, 1379

[110] Gillanders G., et al. 1997, Proc. 25th Int. Cosmic Ray Conf. Durban, 3, 185

[111] Ginzburg V.L., Syrovatskii S.I. 1964, “The Origin of Cosmic Rays”, Pergamon Press, London

[112] Goldwurm A. 2001, In “Exploring the gamma-ray universe”, Proceedings of the Fourth INTEGRAL Workshop, Eds. B. Battrick, A. Gimenez, V. Reglero & C. Winkler. ESA SP-459, Noordwijk: ESA Publications Division, p.455

[113] Grabelsky D.A., Cohen R.S., Bronfman L., & Thaddeus P. 1988, ApJ 331, 181

[114] Gray A.D. 1994, MNRAS 270, 847

- [115] Goren A.J., Frail D.A., Goss W.M., & Otrupcek R. 1997, AJ 114, 2058
- [116] Green A.J., Cram L.E., Large M.I., & Ye T. 1999, ApJS 122, 207.
- [117] Green D.A. 1997, PASA 14, 73
- [118] Green D.A. 2000, A Catalogue of Galactic Supernova Remnants, Mullard Radio Astronomy Observatory, Cambridge, UK (available at <http://www.mrao.cam.ac.uk/surveys/snrs/>)
- [119] Grenier I.A. 1995, Advances in Space Research 15, 73
- [120] Grenier I.A. 2000, A&A 364, L93
- [121] Grenier I.A. 2001, in The Nature of Unidentified Galactic Gamma-Ray Sources, eds. A. Carramiñana, O. Reimer & D. Thompson, Kluwer Academic Publishers, Dordrecht, p.51
- [122] Guessoum N., Von Ballmoos P., Knodleseder J., & Vedrenne G., 2001, in Gamma 2001, edited by S. Ritz, N. Gehrels, & C. R. Schader, AIP Conference Proceedings, New York, p.16
- [123] Halpern J.P., Eracleous M., Mukherjee R., & Gotthelf E.V. 2001a, ApJ 551, 1016
- [124] Halpern J.P., et al. 2001, ApJ 552, L125
- [125] Halpern J.P., Gotthelf E.V., Mirabal N., & Camilo F. 2002, ApJ 573, L41
- [126] Halzen F. & Hooper D. 2002, Rept. Prog. Phys. 65, 1025
- [127] Hartman R.C., et al. 1999, ApJS 123, 79
- [128] Harrus I.M., Hughes J.P., & Helfand D.J. 1996, ApJ 464, L161
- [129] Harrus I.M. & Slane P.O. 1999, ApJ 516, 811
- [130] Haslam C.G.T., Salter C.J., Stoffel H., & Wilson W.E. 1982, ApJS 47, 1
- [131] Hensberge H., Pavlovski K., & Verschueren W. 2000, A&A 258, 553
- [132] Hermans W., et al. 1981, in Proc. Int. Cosmic Ray Conf. 17th, Paris, 1, 320
- [133] Hillas A.M., et al. 1998, ApJ 503, 774
- [134] Hnatyk B., & Petruk O. 1998, Condensed Matter Physics 1, 655
- [135] Huang Y.-L., Dame T.M., & Thaddeus P. 1983, ApJ, 272, 609
- [136] Huang Y.-L., & Thaddeus P. 1986, ApJ, 309, 804
- [137] Hunter, et al. 1997, ApJ 481, 205
- [138] Jaffe T.R., Bhattacharya D., Dixon D.D., & Zych A.D. 1997, ApJ 484, L129
- [139] Jonas J.L. 1999, PhD Thesis, Rhodes University
- [140] Jones L.R., Smith A., & Angellini L. 1993, MNRAS 265, 631
- [141] Jones T.W. 2001, in Proc. of the 7th Taipei Astrophysics Workshop on Cosmic Rays in the Universe, ASP Conference Proceedings, Vol. 241. Edited by Chung-Ming Ko. San Francisco: Astronomical Society of the Pacific, astro-ph/0012483

- [142] Kaaret P., & Cottam J. 1996, *ApJ* 492, L35
- [143] Kaaret P., Piraino S., Halpern J., & Eracleous M. 1999, *ApJ* 523, 197
- [144] Kaaret P., Cusumano G., & Sacco B. 2000, *ApJ* 542, L41
- [145] Kaspi V.M., et al. 1997, *ApJ* 485, 820
- [146] Kaspi V.M., et al. 2000, *ApJ* 528, 445
- [147] Kassim N.E., & Frail D.A. 1996, *MNRAS* 283, L51
- [148] Kaufman-Bernadó M.M., Romero G.E., Mirabel I.F. 2002, *A&A* 385, L10
- [149] Keohane J.W., Petre R., Gotthelf E.V., Ozaki M., & Koyama K. 1997, *ApJ* 484, 350
- [150] Kifune T., et al. 1995, *ApJ* 438, L91
- [151] Kirk J.G., & Dendy R.O. 2001, *J. Phys. G27*, 1589
- [152] Kirshner R.P., & Winkler P.F. 1979, *ApJ* 227, 853
- [153] Kniffen D.A., et al. 1974, *Nature* 25, 397
- [154] Koralesky B., Frail D.A., Goss W.M., Claussen M.J., & Green A.J. 1998, *AJ*, 116, 1323
- [155] Konopelko A.K. 2001, in: *High Energy Gamma-Ray Astronomy*, F.A. Aharonian & H.J. Völk (eds.), AIP, Melville, p. 568
- [156] Kraushaar W.L., et al. 1972, *ApJ* 177, 341
- [157] Klothes R., Landecker T.L., Foster T., & Leahy D.A. 2001, *A&A* 376, 641
- [158] Lamb R.C., & Macomb D.J. 1997, *ApJ* 488, 872
- [159] Lasker B.M., et al. 1990, *AJ* 99, 2019
- [160] Leahy D.A., Naranan S., & Singh K.P. 1986, *MNRAS* 220, L501
- [161] Leslard R.W. et al. 1995, *Proc. Int. Cosmic Ray Conference*, Rome, 2, 475
- [162] Longair M.S. 1994, “*High Energy Astrophysics*, Vol.2: Stars, the Galaxy and the Interstellar Medium”, Cambridge University Press, 2nd ed.
- [163] Lozinskaya T.A. 1974, *Soviet Astronomy* 17, 603
- [164] Lozinskaya T.A. 1992, “*Supernovae and stellar wind in the interstellar medium*”, AIP, New York
- [165] Lozinskaya T.A., Pravdikova V.V., & Finoguenov A.V. 2000, *AstL* 26, 77
- [166] Lucarelli F., Konopelko A., Rowell G., Fonseca V. & the HEGRA collaboration, 2001, in *High-energy gamma-ray astronomy*, edited by F. Aharonian and H. Völk, AIP Conference Proceedings, New York, p.779
- [167] Manchester R.N., et al. 2001, *MNRAS* 328, 17
- [168] Markiewicz W. J., Drury L. O’C., & Völk H J. 1990, *A&A* 236, 487

- [169] Markoff S., Melia F., & Sarcevic I. 1997, *ApJ* 489, L47
- [170] Markoff S., Melia F., & Sarcevic I. 1999, *ApJ* 522, 870
- [171] Mastichiadis A. 1996, *A&A* 305, L53
- [172] Mastichiadis A., & Ozernoy L.M. 1994, *ApJ* 426, 599
- [173] Mayer-Hasselwander H.A., et al. 1998, *A&A* 335, 161
- [174] McLaughlin M.A., Mattox J.R., Cordes J.M., & Thompson D.J. 1996, *ApJ* 473, 763
- [175] Melia F. 1992, *ApJ* 387, L25
- [176] Melia F., & Falcke H. 2001, *ARA&A* 39, 309
- [177] Merck M., et al. 1996, *A&AS* 120, 465
- [178] Michelson P.F. 2001, in *Gamma 2001*, edited by S. Ritz, N. Gehrels, & C. R. Schader, AIP Conference Proceedings, New York, p.713
- [179] Milne D. K. 1979, *Aust. J. Phys.*, 32, 83
- [180] Mirabal N., & Halpern J.P. 2001, *ApJ* 547, L137
- [181] Mirabal N., & Halpern J.P., Eracleous M., & Becker R.H. 2000, *ApJ* 541, 180
Ray Conf., Paris, 1, 17
- [182] Montmerle T. 1979, *ApJ* 231, 95
- [183] Morfill G.E., Forman M., & Bignami G. 1984, *ApJ* 284, 856
- [184] Morfill G. E., & Tenorio-Tagle G. 1983, *Space Sci. Rev.* 36, 93
- [185] Mori M. 2001, *J. Phys. Soc. Japan Suppl.* B70, 22
- [186] Mukherjee R., Gotthelf E.V., Halpern J., & Tavani M. 2000, *ApJ* 542, 740
- [187] Muraishi H., et al. 2000, *A&A* 354, 57L
- [188] Naito T. & Takahara F. 1994, *J. Phys. G* 20, 477
- [189] Nicastro L., Gaensler B.M., & McLaughlin M.A. 2000, *A&A* 362, L5
- [190] Nolan P.L., et al. 1996, *ApJ* 459, 100
- [191] Odegard N. 1986, *ApJ* 301, 813
- [192] Ögelman H., & Finley J.P. 1993, *ApJ* 413, L31
- [193] Olbert C., Clearfield R.C., Williams N., Keohane J., & Frail D.A. 2001, *ApJ* 554, L205
- [194] Oliver R.J., Masheder M.R.W., & Thaddeus P. 1996, *A&A* 315, 578
- [195] Ong R.A. 1998, *Phys. Rep.* 305, 93
- [196] Oser S., et al. 2000, *ApJ* 547, 949

- [197] Paredes J.M., Martí J., Ribó M., Massi M., 2000, *Science* 288, 2341
- [198] Petre R., Keohane J., Hwang U., Allen G., & Gotthelf E. 1998 in “The Hot Universe”, Proceedings of IAU Symposium 188. Edited by Katsushi Koyama, Shunji Kitamoto, & Masayuki Itoh. Dordrecht: Kluwer Academic Press, 1998., p.117
- [199] Petry D., & Reimer O. 2001, in *Proceedings Gamma 2001 Workshop*, edited by S. Ritz, N. Gehrels, & C. R. Schader, AIP Conference Proceedings, New York, p.696
- [200] Petry D. 2001, *Proc. Int. Workshop on The Nature of Galactic Unidentified Gamma-ray Sources*, O. Carramiñana, O. Reimer, D. Thomson Eds., Kluwer Academic Press, p.299
- [201] Pineault S., et al. 1993, *AJ* 105, 1060
- [202] Pineault S., et al. 1997, *A&A* 324, 1152
- [203] Plaga R. 2001, *astro-ph/0111555*, submitted to *New Astronomy Reviews*
- [204] Plaga R. 2002, *New Astron.* 7, 317
- [205] Pohl M. 1996, *A&A* 307, 57
- [206] Pohl M. 1997, *A&A* 317, 441
- [207] Pollock A.M.T. 1985, *A&A* 150, 339
- [208] Preite-Martinez A., Feroci M., Strom R.G., Mineo T. 2000, in *Proceedings of the Fifth Compton Symposium*, American Institute of Physics (AIP), edited by Mark L. McConnell and James M. Ryan, AIP Conference Proceedings, Vol. 510., p.73
- [209] Pühlhofer G., et al. 2001, *Proc. Int. Symp. on High Energy Gamma-Ray Astro.* (Heidelberg), F. Aharonian and H.J. Völk Eds., AIP New York, p.749
- [210] Punsly B. 1998a, *ApJ* 498, 640
- [211] Punsly B. 1998b, *ApJ* 498, 660
- [212] Punsly B., Romero G.E., Torres D.F., & Combi J.A. 2000, *A&A* 364, 556
- [213] Radhakrishnan V., Goss W.M., Murray J.D., & Brooks J.W. 1972, *ApJS* 24, 49
- [214] Ribó M., et al. 2002, *A&A* 384, 954
- [215] Reich W., Fürst E., & Sofue Y. 1984, *A&A* 133, L4
- [216] Reimer O., & Bertsch D.L. 2001, *Proc. of Int. Cosmic Ray Conf.*, Hamburg, to appear.
- [217] Reimer O., & Pohl M. 2002, *A&A* 390, L43
- [218] Reynoso, E. & Mangum J.G. 2000, *ApJ* 545, 874
- [219] Reynolds S.P. 1996, *ApJ* 459, L13
- [220] Reynolds S.P. 1998, *ApJ* 493, 375
- [221] Rho J., & Petre R. 1998, *ApJ* 503, L167

[222] Rho J., Petre R., Schlegel E.M., & Hester J.J. 1994, *ApJ* 430, 757
1999, *ApJ* 515, 712

[223] Roberts M.S.E., Romani R.W., & Kawai N. 2001, *ApJS* 133, 451

[224] Rodgers A.W., Campbell C.T., & Whiteoak J.B. 1960, *MNRAS* 121, 103

[225] Romero G.E., Combi J.A., & Colomb F.R. 1994, *A&A* 288, 731

[226] Romero G.E. 1998, *Rev. Mex. A&A* 34, 29

[227] Romero G.E., Benaglia P., & Torres D.F. 1999a, *A&A* 348, 868

[228] Romero G.E., Torres D.F., Andruhov I., Anchordoqui L.A., & Link B. 1999b, *MNRAS* 308, 799

[229] Romero G.E., Kaufman-Bernadó M., Combi J., & Torres D.F. 2001, *A&A* 376, 599

[230] Romero, G. E. 2001, in *The Nature of Unidentified Galactic Gamma-Ray Sources*, eds. A. Carraminana, O. Reimer & D. Thompson, Kluwer Academic Press, p.65

[231] Rowell G.P., et al. 2000, *A&A* 359, 337

[232] Ruiz M.T., & May J. 1986, *ApJ* 309, 667

[233] Sakamoto S., Hasegawa T., Hayashi M., Handa T., & Oka T. 1995, *ApJS*, 100, 125

[234] Seta M., et al. 1998, *ApJ* 505, 286

[235] Seward F.D., Schmidt B., & Slane P. 1995, *ApJ* 453, 284

[236] Schönfelder V. 2001, in *Gamma 2001*, edited by S. Ritz, N. Gehrels, & C. R. Schader, AIP Conference Proceedings, New York, p.809

[237] Scoville N.Z., Irvine W.M., Wannier P.G., & Predmore C.R. 1977, *ApJ* 216, 320

[238] Sedov L.I. 1959, “Similarities and dimensional methods in mechanics”, Academic Press, New York

[239] Stecker F.W. 1977, *ApJ* 212, 60

[240] Shklovskii I. S. 1953, *Dokl. Akad. Nauk SSSR* 91, No. 3, 475

[241] Sigl G., Torres D.F., Anchordoqui L.A., & Romero G.E. 2001, *Phys. Rev. D* 63, 081302

[242] Sinnis G., et al. 1995, *Nucl. Phys. B (Proc. Suppl.)* 43, 141

[243] Slane P., et al. 1997, *ApJ* 485, 221

[244] Slane P., et al. 1999, *ApJ* 525, 357

[245] Smith D.A., et al. 1997, *Nucl. Phys. (Proc. Suppl.)* 54, 362

[246] Sofue Y., & Reich W. 1979, *A&AS* 38, 251

[247] Sturner S.J., & Dermer C.D. 1995, *A&A* 293, L17

[248] Sturner S.J., Dermer C.D., & Mattox J.R. 1996, *A&AS* 120, 445

- [249] Sturner S.J., Skibo J. G., Dermer C. D., & Mattox J. R. 1997, *ApJ* 490, 617
- [250] Sugizaki M., et al. 2001, *ApJS* 134, 77
- [251] Swanenburg, et al. 1981, *ApJ* 243, L69
- [252] Swanenburg, et al. 1978, *Nature* 275, 298
- [253] Tanimori T., et al. 1998, *ApJ* 497, L25
- [254] Tavani M., et al. 2001, in *Gamma 2001*, edited by S. Ritz, N. Gehrels, & C. R. Schader, AIP Conference Proceedings, New York, p.729
- [255] Taylor J.H., et al. 1993, *ApJS* 88, 529 (updated at <ftp://pulsar.princeton.edu>)
- [256] Thompson D.J., et al. 1975, *ApJ* 200, L79
- [257] Thompson D.J., et al. 1995, *ApJS* 101, 259
- [258] Thompson D.J., et al. 1996, *ApJS* 107, 227
- [259] Thompson D.J., et al. 1999, *ApJ* 516, 297
- [260] Thompson D.J. 2001, Proc. Int. Symp. on High Energy Gamma-Ray Astro. (Heidelberg), F. Aharonian and H.J. Völk (Eds.), AIP, New York, p.103
- [261] Thompson D.J., Digel S.W., Nolan P.L., & Reimer O. 2001, in Proc. Neutron Stars in Supernova Remnants, ASP Conference Series, Vol. 9999, 2002, P. O. Slane and B. M. Gaensler Eds., in press. [astro-ph/0112518](http://arxiv.org/abs/astro-ph/0112518)
- [262] Tompkins W. 1999, Ph.D. Thesis, Stanford University.
- [263] Torres D.F., et al. 2001a, *A&A* 370, 468
- [264] Torres D.F., Combi J.A., Romero G.E., & Benaglia P. 2001b, Proc. Int. Workshop on The Nature of Galactic Unidentified Gamma-ray Sources, O. Carramiñana, O. Reimer, D. Thomson Eds., Kluwer Academic Press, p.97
- [265] Torres D.F., Pessah M.E., & Romero G.E. 2001c, *Astronomische Nachrichten*, 322, 223
- [266] Torres D.F., Butt Y.M. & Camilo F. 2001d, *ApJ* 560, L155
- [267] Torres D.F., Romero G.E., & Eiroa E.F. 2002a, *ApJ* 560, 600
- [268] Torres D.F., Romero G.E., Eiroa E.F., Wambsganss J., & Pessah M.E. 2002b, *MNRAS*. Submitted. [astro-ph/0205441](http://arxiv.org/abs/astro-ph/0205441)
- [269] Tümer, T., et al. (1999), *Astropart. Phys.* 11, 271
- [270] Uchida K., Morris M., & Yusef-Zadeh F. 1992, *AJ* 104, 1533
- [271] Uchiyama Y., Takahashi T., & Aharonian F.A. 2002a, *PASJ*, in press.
- [272] Uchiyama Y., Takahashi T., Aharonian F.A., & Mattox J.R. 2002b, *ApJ* 571, 866
- [273] Usov V.V. 1994, *ApJ* 427, 394

- [274] van den Ancker M.E., Thé P.S., & de Winter D. 2000, A&A 362, 580
- [275] Vargas M. et al. 1996, A&A 313, 828
- [276] Velázquez P.F., Dubner G.M., Goss W.M., & Green A. 2002. astro-ph/0207530
- [277] Völk H.J. 2001, To appear in the proceedings of 21st Moriond Astrophysics Meeting: High energy astrophysical phenomena, Les Arcs, Savoie, France, 20-27 Jan 2001. astro-ph/0105356
- [278] Völk H.J. 2002, in Proc. Int. Cosmic Ray Conf., Hamburg, to appear. astro-ph/0202421
- [279] Wallace P.M., et al. 2000, ApJ 540, 184
- [280] Wallace P.M., Halpern J.P., Magalhaes A.M., & Thompson D.J. 2002, ApJ 569, 36
- [281] Wang Z.R., Asaoka I., Hayakawa S. & Koyama K. 1992, PASJ 44, 303
- [282] Whiteoak J.B.Z. & Green A.J 1996 A&AS 118, 329
- [283] Wootten, A. 1981, ApJ 245, 105
- [284] Yadigaroglu I.-A., & Romani R.W. 1997, ApJ 476, 356
- [285] Yamamoto F., Hasegawa T., Morino J., Handa T., Sawada T., & Dame T. M 1999, in Proc. of Star Formation 1999, T. Nakamoto Ed., Nobeyama Radio Observatory, p.110
- [286] Yusef-Zadeh F., Melia F., & Wardle M. 2000, Science 287, 85
- [287] Yusef-Zadeh F., Law C., & Wardle M. 2002, ApJ 568, L121
- [288] Zhang L., & Cheng K.S. 1998, A&A 335, 234
- [289] Zhang L., Zhang Y.J., & Cheng K.S. 2000, A&A 357, 957

This figure "3EG.jpg" is available in "jpg" format from:

<http://arxiv.org/ps/astro-ph/0209565v1>

This figure "G338-1.jpg" is available in "jpg" format from:

<http://arxiv.org/ps/astro-ph/0209565v1>

This figure "GMon1.jpg" is available in "jpg" format from:

<http://arxiv.org/ps/astro-ph/0209565v1>

This figure "G39-2.jpg" is available in "jpg" format from:

<http://arxiv.org/ps/astro-ph/0209565v1>

This figure "GMon2.jpg" is available in "jpg" format from:

<http://arxiv.org/ps/astro-ph/0209565v1>

This figure "ic443-2.jpg" is available in "jpg" format from:

<http://arxiv.org/ps/astro-ph/0209565v1>

This figure "G6-4.jpg" is available in "jpg" format from:

<http://arxiv.org/ps/astro-ph/0209565v1>

This figure "GW28.jpg" is available in "jpg" format from:

<http://arxiv.org/ps/astro-ph/0209565v1>

This figure "G39.jpg" is available in "jpg" format from:

<http://arxiv.org/ps/astro-ph/0209565v1>

This figure "GW44.jpg" is available in "jpg" format from:

<http://arxiv.org/ps/astro-ph/0209565v1>

This figure "GW66.jpg" is available in "jpg" format from:

<http://arxiv.org/ps/astro-ph/0209565v1>

This figure "GCTB87.jpg" is available in "jpg" format from:

<http://arxiv.org/ps/astro-ph/0209565v1>

This figure "G284.jpg" is available in "jpg" format from:

<http://arxiv.org/ps/astro-ph/0209565v1>

This figure "G290.jpg" is available in "jpg" format from:

<http://arxiv.org/ps/astro-ph/0209565v1>

This figure "G312.jpg" is available in "jpg" format from:

<http://arxiv.org/ps/astro-ph/0209565v1>

This figure "G338.jpg" is available in "jpg" format from:

<http://arxiv.org/ps/astro-ph/0209565v1>

This figure "G347.jpg" is available in "jpg" format from:

<http://arxiv.org/ps/astro-ph/0209565v1>

This figure "GIC433.jpg" is available in "jpg" format from:

<http://arxiv.org/ps/astro-ph/0209565v1>

This figure "allen-spe.jpg" is available in "jpg" format from:

<http://arxiv.org/ps/astro-ph/0209565v1>

This figure "cosb.jpg" is available in "jpg" format from:

<http://arxiv.org/ps/astro-ph/0209565v1>

This figure "glast.jpg" is available in "jpg" format from:

<http://arxiv.org/ps/astro-ph/0209565v1>

This figure "lat.jpg" is available in "jpg" format from:

<http://arxiv.org/ps/astro-ph/0209565v1>

This figure "ls5039.jpg" is available in "jpg" format from:

<http://arxiv.org/ps/astro-ph/0209565v1>